Superconductor-based passive shielding and screening systems

TOPICAL REVIEW • OPEN ACCESS

Superconductor-based passive shielding and screening systems

OPEN ACCESS
IOP Publishing
Superconductor Science and Technology
Supercond. Sci. Technol. **38** (2025) 043002 (41pp)
https://doi.org/10.1088/1361-6668/adb7cc

Topical Review

Superconductor-based passive shielding and screening systems

Nicolas Rotheudt[1,3], **Michela Fracasso**[2,3], **Philippe Vanderbemden**[1] and **Laura Gozzelino**[2,*]

[1] Department of Electrical Engineering and Computer Science, Montefiore Institute B28, University of Liège, Liège, B-4000, Belgium
[2] Department of Applied Science and Technology, Politecnico di Torino, 10129 Torino, Italy

E-mail: laura.gozzelino@polito.it

Received 29 November 2024, revised 6 February 2025
Accepted for publication 17 February 2025
Published 17 March 2025

Abstract

The attenuation of magnetic fields is crucial for various application fields, including health, space exploration, and fundamental physics, to name just a few. Superconductors are key materials for addressing this challenge. In this review, we mainly focus on the shielding and screening of quasi-static magnetic fields using superconductor-based passive layouts. After providing a brief overview of the principles of magnetic shielding and screening using superconductors, we outline commonly used procedures for measuring the field attenuation. Next, we give an insight into analytical and numerical models able to reproduce experimental results and predict the performances of new designs. Key challenges and achievements in employing low temperature or high temperature superconducting bulk and tape-based structures for reducing a given applied field are then discussed. Additionally, hybrid designs combining superconducting and ferromagnetic materials, aimed at enhancing the shielding ability or fabricating magnetic cloaks, are described. Finally, we highlight future challenges and potential advancements in this technology.

Keywords: magnetic shielding, magnetic field distribution, bulk superconductors, coated conductors, REBCO, BSCCO, MgB_2

Contents

[3] These authors contributed equally to this work and are joint first authors.
[*] Author to whom any correspondence should be addressed.

Main acronyms-expansions and symbols, as they appear in the article

2D	two-dimensional
3D	three-dimensional
2G	second generation
A	magnetic vector potential
AC	alternating current
AR	aspect ratio for tubular structure ($= h/R_{\rm in}$)
B	magnetic flux density
$B_{\rm in}$	magnetic flux density value in a given position inside the shield (or behind the screen)
$B_{\rm lim}$	magnetic flux density for which SF decreases below a threshold value
Bi-2212	$Bi_2Sr_2CaCu_2O_{8+x}$
Bi-2223	$Bi_2Sr_2Ca_2Cu_3O_{10+x}$
BSCCO	$Bi_2Sr_2Ca_{m-1}Cu_mO_{2m+4+x}$ ($m = 2, 3$)
CC	coated conductor
CSM	critical state model
d	wall thickness in hollow cylinder layout
DC	direct current
e.m.f.	electromotive force
E	electric field
FC	field cooling
FEM	finite element method
FM	ferromagnetic
h	height
H	magnetic field
$\mathbf{H}_{\rm app}$	external applied field
H_c	critical field
H_{c1}	lower critical field
H_{c2}	upper critical field
$h_{\rm FM}$	height (ferromagnetic sample)
HTS	high-temperature superconductor
HY	hybrid (i.e. superimposed FM/SC structures)
J	current density
J_c	critical current density
LTS	low-temperature superconductor
MRI	magneto-resonance imaging
n	creep factor
NMR	nuclear magnetic resonance
RF	radio frequency
$R_{\rm in}$	inner radius
$R_{\rm in,FM}$	inner radius (ferromagnetic sample)
$R_{\rm out}$	outer radius
$R_{\rm out,FM}$	outer radius (ferromagnetic sample)
REBCO	$(RE)Ba_2Cu_3O_{7-\delta}$ (RE = rare earth)
SC	superconducting
SF	shielding or screening factor
SQUID	superconducting quantum interference device
T_c	critical temperature
TES	transition edge sensor
$\hat{u}$	unit vector
ZFC	zero field cooling
μ_0	permeability of space/vacuum permeability ($4\pi \times 10^{-7}$ H/m)
μ_r	relative magnetic permeability

1. Introduction

Electromagnetic shielding is one of the great challenges in today's world. For example, the shielding of low-frequency/quasi–static magnetic field is a fundamental requirement for the proper functioning of SQUID-based detectors or other magnetic-field sensitive devices [1–6] and magnetic mitigation is crucial to solving problems of electromagnetic compatibility between instruments, as well as to protect the safety of workers operating near strong magnetic field sources [7–10]. Magnetic shields can be applied in various applications including biomedical engineering, space missions, automotive devices, quantum computing and high-energy physics experiments, and magnetic focusing, to name a few [4, 11–15].

According to the magnetic field characteristics and the design requirements, both active and passive shielding systems were developed. Active shielding is based on current injection in additional coils in order to generate a magnetic field opposite to the field to be shielded. Applications using active shielding include, for example, the protection of spacecraft against space radiation [16–20], most MRI systems [21–26], magneto-encephalography [27] or wireless power transfer systems [28, 29].

Passive shielding exploits the intrinsic properties of metallic, FM and/or SC materials; no external current source is used. As an example, a grounded metal shell can be used to

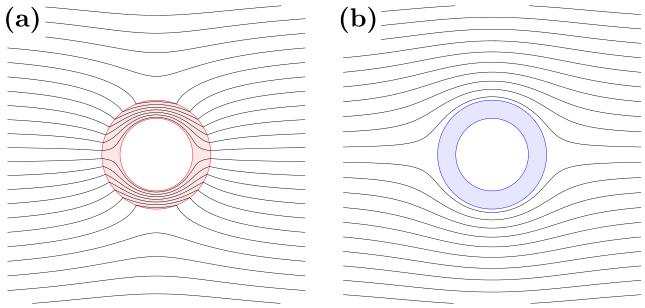

Figure 1. Schematic distribution of the magnetic flux line in the cross-section of (a) a ferromagnetic and (b) a superconducting shield shaped as an infinite hollow cylinder subjected to a uniform magnetic field perpendicular to its axis.

protect a region from external electric field penetration [30], while high frequency electromagnetic fields can be mitigated by employing metal- and carbon-based materials as well as conductive polymer composites [30–32].

A metallic material subjected to an alternating magnetic field can act as a shield thanks to the appearance of eddy currents, which in turn create a magnetic field with orientation opposite to the applied field. However, this shielding effect decreases with decreasing frequency of the AC field. This renders the mitigation of power frequency (50/60 Hz) or quasi-static magnetic fields quite difficult with conductors of decent thickness (< 1 cm).

FM materials are characterized by a high magnetic permeability and can therefore concentrate magnetic flux lines [30]. Figure 1(a) shows schematically how a hollow FM cylinder is able to shield a given region of space from a uniform transverse applied field. However, the use of FM materials is limited by their saturation magnetization (e.g. $\mu_0 M_{\text{sat}} \approx 0.7$ T for μ-metal [33]) that can compromise their shielding properties in strong external magnetic fields [34].

Alternatively, a SC shell can provide effective shielding for quasi–static magnetic fields. Such a shielding effect owes to the onset of macroscopic current loops arising in the material and producing a magnetic field opposite to the applied one [35–37]. Hence, superconductors divert the flux lines as shown schematically in figure 1(b). Shielding in superconductors is mostly limited by two penetration mechanisms. First, the induced current density cannot be larger than the critical current density J_c. Consequently, as the magnitude of the applied field becomes larger, the flux front penetrates deeper in the superconductor until it reaches the region to be shielded. Second, every practical shield has some openings through which flux lines can penetrate, therefore reaching the region to be shielded. By contrast with FM materials, these limitations can be overcome and passive SC shielding has been demonstrated for applied fields well above 1 T [38–41]. Hence, superconductors are ideal candidates for large-scale and power applications [42–44]. Also, superconductors bring advantages for ultra-low magnetic field applications since they generate significantly fewer losses and noise compared to metals [45].

In this review, we aim to provide a wide, although certainly not exhaustive, review on passive magnetic shielding and screening via superconductor-based systems. This review is organized as follows.

- Section 2 gives an overview of the basics of magnetic shielding and screening. To do so, the problem of attenuating a given applied field is formalized, the characteristics of the applied field are described and metrics are defined.
- In section 3, experimental set-ups used to assess the quality of a shield are described. These set-ups consists of an appropriate source of applied field with a well-chosen measurement technique.
- Section 4 summarizes analytical and numerical techniques used to model SC materials and employed to predict the behaviour of both SC and hybrid SC/FM shields. Analytical models are usually easier to apply but limited to simplified geometries and assumptions. Numerical models allow investigating more complex shielding configurations, at the cost of increased computing time. Although alternative numerical approaches have been proposed [46, 47], the FEM [48] is the most widely used for magnetic shielding studies, with a variety of formulations briefly presented in this review.
- The performances of HTS bulk shields or screens are then discussed in section 5. High temperature superconducting cuprates [40, 49–51] have successfully been employed for passive shields for more than 3 decades. (RE)$Ba_2Cu_3O_{7-\delta}$ (REBCO, where RE denotes a rare earth ion), $Bi_2Sr_2Ca_{m-1}Cu_mO_{2m+4+x}$ (BSCCO, m being 2 or 3) and MgB_2 shields and screens are described.
- Section 6 focuses on shields or screens built using second-generation HTS CCs alone or combined with bulks.
- The performances of LTS shields or screens are described in section 7.
- The benefits of building hybrid SC/FM structures are discussed in section 8. Enhancements of the shielding capability thanks to the hybridization as well as cloaking structures are described.
- Concluding remarks and future challenges are summed up in section 9.

2. Definitions

2.1. Emission or immunity?

Protecting a device from a magnetic field source can be achieved in two different ways.

First, the magnetic field source itself can be placed in a magnetic shield in order to reduce its stray field in the neighbouring environment. Such a situation is referred to as an *emission* problem. Typical emission problems are found in naval applications where the magnetic field signature of ships has to be attenuated [52] or in high-field applications where the influence of the magnetic source on a device or on the environment should be reduced [53, 54].

Second, the magnetic shield is used to generate a low-field region in which the device to be protected can be placed. Such

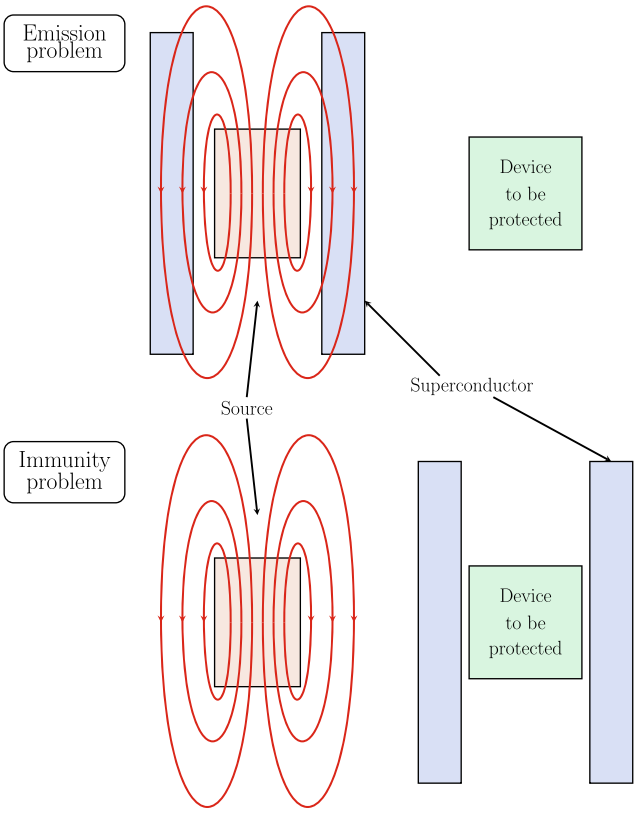

Figure 2. Schematic representation (cross-section) of the two possible problems to consider with a superconducting tube. Above: emission. Below: immunity.

a configuration is called an *immunity* problem. Typical applications include devices requiring a low magnetic background such as cryogenic current comparators [55–57], DC current transformers [58], some space applications [59, 60] or devices measuring very low magnetic fields, e.g. SQUIDs [61–72]. Both emission and immunity problems are illustrated schematically in figure 2.

2.2. Shielding, screening or cloaking?

Different SC systems can be used to reduce a given applied field. Depending on how these systems are operated, different terms exist.

The term *shielding* refers to closed or partly closed geometries (e.g. a long tube or a vessel) that can protect a small volume from the applied field. These shields can provide a strong field attenuation, reducing the applied field by a factor, which can exceed 10^4 [41, 50, 73].

The term *screen* is used for open geometries whose goal is typically to protect large volumes from the stray field of a magnetic source, e.g. a SC magnet or a rotating machine operating at a few teslas. These screens reduce the amplitude of the field by a factor usually less than 100 at a reasonable distance (i.e. a few mm) from the screen. Such a reduction might be sufficient for equipment sensitive to the magnetic field such as cryocoolers. The term 'screening' used for attenuating fields should be distinguished from the terms 'screening currents' and 'screening current-induced field' described in the literature on high-T_c SC magnets [74–82]. From the definitions above, it can be understood that for semi-open geometries such as a wide, short SC cup, the difference between shielding and screening blurs.

The term *cloaking* refers to closed or partly closed geometries that can protect a small volume from the applied field. The main difference between a shield and a cloak is that a cloak is able to attenuate the field inside a volume without any distortion of the applied field outside this volume, therefore making the device 'invisible' to the applied field. Practical cloaks are made of metamaterials combining FM and SC layers [83–91] as described in section 8.2.

Shielding, screening and cloaking configurations are schematically shown in figure 3. Note that, unless otherwise indicated, hereafter in reporting shield/screen/cloak shapes the words 'tube' and 'hollow cylinder' will be used as synonyms for each other as well as the words 'semi-closed tube', 'semi-closed hollow cylinder' and 'cup'.

2.3. Characterization of the applied field

In order to determine the shielding or screening properties of a given SC system, the characteristics of the applied field should be defined. A distinction should be made between *homogeneous* (or uniform) and *inhomogeneous* (or non-uniform) applied fields.

Homogeneous fields are, stricto sensu, theoretical. A homogeneous field is never met in practice except if the volume to be shielded is much smaller than the length scale over which the non-uniformity of the field is visible. The advantage of considering homogeneous fields is that useful analytical expressions can be obtained (see section 4.2) and several physical conclusions can be drawn. Another advantage of homogeneous fields is that they provide easily reproducible conditions since they are defined by three parameters: the magnitude of the field, its direction and its frequency content (or time evolution). As an example, axial and transverse shielding properties of SC hollow cylinders are often compared with each other [41, 58, 72, 92–98].

All practical applications (larger than a few mm) deal with inhomogeneous fields. Although inhomogeneous fields are more realistic, the properties of SC shields under these fields are rarely explored in the literature [51, 99–102]. The main reason is that the local magnitude and orientation of the applied field with respect to the superconductor may vary significantly even along the material itself. Hence, the current distribution is complex and may strongly be affected by the anisotropy, the field dependence and the angular dependence of J_c. In order to work with inhomogeneous fields and obtain reproducible results, a mathematical framework characterizing the applied field should be defined [100]. An example of such a mathematical framework is as follows.

The magnetic flux density is a 3D vector field. Hence, the flux density at a given position $\boldsymbol{r}$ writes

$$\mathbf{B}(\boldsymbol{r}) = B(\boldsymbol{r})\,\hat{\boldsymbol{u}}_{\boldsymbol{B}}(\boldsymbol{r}), \tag{1}$$

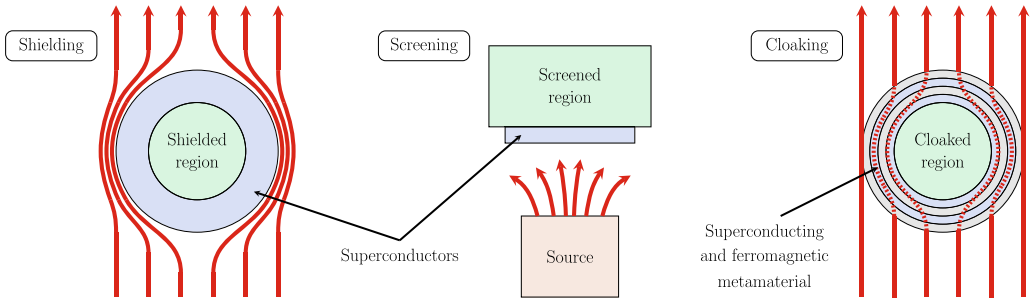

Figure 3. Schematic representation of three ways to attenuate an applied field (in red). From left to right: top view of a tube used for shielding, front view of a plate used for screening and top view a tube used for cloaking.

where $B(\boldsymbol{r})$ is the local magnitude of the flux density and $\hat{\boldsymbol{u}}_{\boldsymbol{B}}(\boldsymbol{r})$ is a unit vector giving the local direction of the flux density. From Maxwell's equation $\nabla \cdot \mathbf{B} = 0$, (1) becomes

$$\nabla B(\boldsymbol{r}) \cdot \hat{\boldsymbol{u}}_{\boldsymbol{B}}(\boldsymbol{r}) + B(\boldsymbol{r}) \nabla \cdot \hat{\boldsymbol{u}}_{\boldsymbol{B}}(\boldsymbol{r}) = 0, \tag{2}$$

where $\nabla B(\boldsymbol{r})$ is the gradient of B and $\nabla \cdot \hat{\boldsymbol{u}}_{\boldsymbol{B}}(\boldsymbol{r})$ is the divergence of $\hat{\boldsymbol{u}}_{\boldsymbol{B}}$. Equation (2) highlights that if the magnitude of the flux density varies along a flux line ($\nabla B(\boldsymbol{r}) \neq 0$), this flux line is necessarily curved ($\nabla \cdot \hat{\boldsymbol{u}}_{\boldsymbol{B}}(\boldsymbol{r}) \neq 0$). Hence, in addition to the metrics already existing for a homogeneous applied field, a complete description of an inhomogeneous applied field should include the spatial variation of the magnitude B as well as the local direction of $\hat{\boldsymbol{u}}_{\boldsymbol{B}}$. Taking inspiration from the methods used in plasma physics [103–106], the curvature and the torsion of the flux lines can be defined. For a geometry having a revolution symmetry, the torsion is not relevant and can therefore be neglected here. The curvature vector is always perpendicular to $\hat{\boldsymbol{u}}_{\boldsymbol{B}}$ and is defined as

$$\boldsymbol{\kappa}(\boldsymbol{r}) = -\hat{\boldsymbol{u}}_{\boldsymbol{B}}(\boldsymbol{r}) \times (\nabla \times \hat{\boldsymbol{u}}_{\boldsymbol{B}}(\boldsymbol{r})), \tag{3}$$

$$= (\hat{\boldsymbol{u}}_{\boldsymbol{B}}(\boldsymbol{r}) \cdot \nabla) \hat{\boldsymbol{u}}_{\boldsymbol{B}}(\boldsymbol{r}). \tag{4}$$

Instead of using ∇B and $\boldsymbol{\kappa}$, it is possible to describe inhomogeneous magnetic field sources with two more practical metrics:

- The characteristic length $l_{\mathrm{c}}(\boldsymbol{r})$ over which the flux density varies by a certain percentage. For a homogeneous field, $l_{\mathrm{c}} \to \infty$. Mathematically, it is defined by

$$l_{\mathrm{c}}(\boldsymbol{r}) = \frac{B(\boldsymbol{r})}{|\nabla B(\boldsymbol{r})|}. \tag{5}$$

- The local radius of curvature of the flux lines $R_{\mathrm{c}}(\boldsymbol{r})$. For a homogeneous field, $R_{\mathrm{c}} \to \infty$. Mathematically, it simply writes

$$R_{\mathrm{c}}(\boldsymbol{r}) = (|\boldsymbol{\kappa}(\boldsymbol{r})|)^{-1}. \tag{6}$$

2.4. Time-dependence of the applied field

In addition to the spatial dependence of the applied field, its time dependence should be specified. As discussed in section 1, superconductors have several advantages over metals depending on the frequency content of the applied field. Depending on the frequency range, the following classification can be considered.

First, superconductors are very useful in the quasi–static regime. Very often, this regime is referred to as DC shielding or DC screening in the literature [39, 40, 89, 101, 102, 107–111]. Strictly speaking, however, the magnetic field applied to the superconductors varies from zero to the final value at a finite rate, and this variation is required for the supercurrents to be induced. The term 'DC' is thus somewhat equivocal. Hence, even in the case of 'DC' excitation, the way (e.g. staircase or linear ramp) and the rate at which the applied field is modified should ideally be specified. Such precisions are especially relevant for some HTSs because the sweep rate of the applied field may affect the shielding behaviour (e.g. BSCCO shields at 77 K) [96, 97, 107, 110]. This relates to the fact that, for a given geometry, a faster variation of the applied field induces a higher electric field and larger currents.

Another regime of importance is the steady state AC regime. The frequency of the applied field extends typically up to a few kHz and down to a few mHz. At such low frequencies, the distinction between DC and AC fades away. The effect of increasing the frequency is similar as increasing the sweep rate as mentioned above [50, 110]. Other considerations might be relevant in the AC regime:

- AC losses are generated, which induce a local temperature rise. This may affect the shield behaviour if the cooling power is not sufficient to drain out the heat rapidly.
- If the frequency is such that the equivalent resistance R of shielding current loops can be neglected with respect to their equivalent reactance ωL (ω being the angular frequency and L the inductance of the current loops), metallic soldering can be used to join SC parts without detrimental effect on the shielding effect, by contrast with the DC regime.
- For non-sinusoidal or parasite applied fields, the influence of harmonics on the shielding properties should be considered.

- At medium frequencies, eddy currents can be induced in some metallic parts of the experimental set-up and can affect the shielding behaviour.

The transient behaviour, i.e. under a non-periodic excitation, of SC shields or screens is also useful to consider. Examples include the ramping losses also induced in the shield during the charging process of a magnet [112–118] or the response of the shield to a quench of the magnetic field source. The sweep rate of the applied field should be defined to study the transient behaviour. Again, the difference between the DC and transient regimes blurs if the considered sweep rate is very low.

Finally, the behaviour of the shield under a continuous frequency spectrum is often considered when an ultra-low-field environment needs to be achieved. Typical applications are in biomagnetism, where SQUIDs are used and the signals of interest are often at frequencies below 1 kHz and of very small amplitude lower than 1 pT [119]. Hence, the focus is to reduce the magnetic noise spectral density below 1 fT/$\sqrt{\text{Hz}}$ (order of magnitude) [5]. At these magnetic field magnitudes, the different sources of noise might be the thermal (Johnson) noise, mostly in metallic (e.g. cryostat [120, 121], cryocooler [4], walls of a magnetically shielded room [122] or substrate of the CCs [123]) or FM parts (e.g. magnetization fluctuations [124]), the noise of the measuring instrument itself [125] or the noise from mechanical vibrations [126].

2.5. Performance metrics

In order to assess the quality of a shield, a screen or a cloak, the corresponding performance metrics should be mathematically defined. The most common ones are summarized below.

(a) Ideally, the superconductors should reduce the applied field by a very large factor. This field attenuation can be measured by the shielding or the screening factor (henceforth both shortened to SF). A general definition of this quantity is

$$\text{SF}\left(\boldsymbol{r}, \mu_0 \mathbf{H}_{\text{app}}\right) = \frac{\mu_0 H_{\text{app}}\left(\boldsymbol{r}\right)}{B\left(\boldsymbol{r}, \mu_0 \mathbf{H}_{\text{app}}\right)}, \tag{7}$$

where $\mu_0 \mathbf{H}_{\text{app}}$ is the vector applied field (without the shield/screen), $\mu_0 H_{\text{app}}$ its magnitude (root mean square value in AC), B the magnitude of the flux density measured with the shield/screen and $\boldsymbol{r}$ the position. With this definition, the applied field is reduced when $\text{SF} > 1$, and a larger SF indicates better shielding or screening effect.
Note that other expressions exist in the literature, such as

$$\text{SF}_{\text{bis}} = 100 \times \frac{\mu_0 H_{\text{app}} - B}{\mu_0 H_{\text{app}}}\ [\%], \tag{8}$$

which is sometimes called shielding/screening efficiency and is expressed between 0 (no shielding/screening) and 100 % (ideal shielding/screening). The following definition can also be found:

$$\text{SF}_{\text{ter}} = 100 \times \frac{B}{\mu_0 H_{\text{app}}}\ [\%]. \tag{9}$$

In this case, SF_{ter} varies from 0 (ideal shielding/screening) to 100 % (no shielding/screening). Additionally, (7) is sometimes expressed in dB, i.e.

$$\text{SF}_{\text{quater}}[\text{dB}] = 20 \log\left(\text{SF}\right). \tag{10}$$

It is worth mentioning that the SF defined by (7) will be used in this review.

(b) In many applications, it is desirable to maximize the volume over which the field attenuation is effective. Therefore, the shielded volume or the screened volume should be maximized. It can be defined as the region for which $\text{SF} > \text{SF}^*$, where SF^* is a certain threshold that is defined depending on the application (considering (7)).

(c) When the magnitude of the applied field increases, the shielding or screening effect degrades due to the penetration of the flux lines. Hence, a threshold field, often called B_{lim} in the literature, should be defined. In theory (e.g. infinite tube analysed using the CSM, see section 4.2), B_{lim} could be defined as soon as the field in the shielded region is non-zero. Such a definition corresponds to the threshold field for which SF becomes finite (considering (7)). In practical systems, however, SF is always finite. Hence, in practice, the threshold field B_{lim} is defined as the field for which SF at a certain position is reduced to a user-defined threshold value SF_{lim}, where SF_{lim} depends on the application (e.g. 2, 10, 100 or 1000) but is always smaller than the maximal SF at low applied fields. Ideally, B_{lim} should be as large as possible.

Other metrics can also be defined in some specific cases. For example, the uniformity of the field outside a cloak can be described by giving the percentage distortion of the applied field at a given position after the addition of the cloak, but, generally, no specific parameter is used.

3. Experimental systems

The experimental characterization of SC magnetic shields and screens can be done in a number of ways. They differ basically in the type of magnetic field source and of probe used to measure the magnetic flux density attenuated by the superconductor.

3.1. Magnetic field sources

We first consider the source of magnetic field. Various possible geometric configurations are illustrated schematically in figure 4. The most common experimental set-ups reported in the literature investigate magnetic shielding in the immunity configuration (see section 2.1), i.e. an external field is applied to the SC shield and the low-field region is located inside the shield. In the schematic drawings shown in figure 4(a)–(g), the SC shield is always shown as a grey cylinder with a vertical axis for simplicity. In practice, the shield itself could be of any shape and oriented along any direction with respect to the applied field. The coils illustrated in figure 4 can be fed either

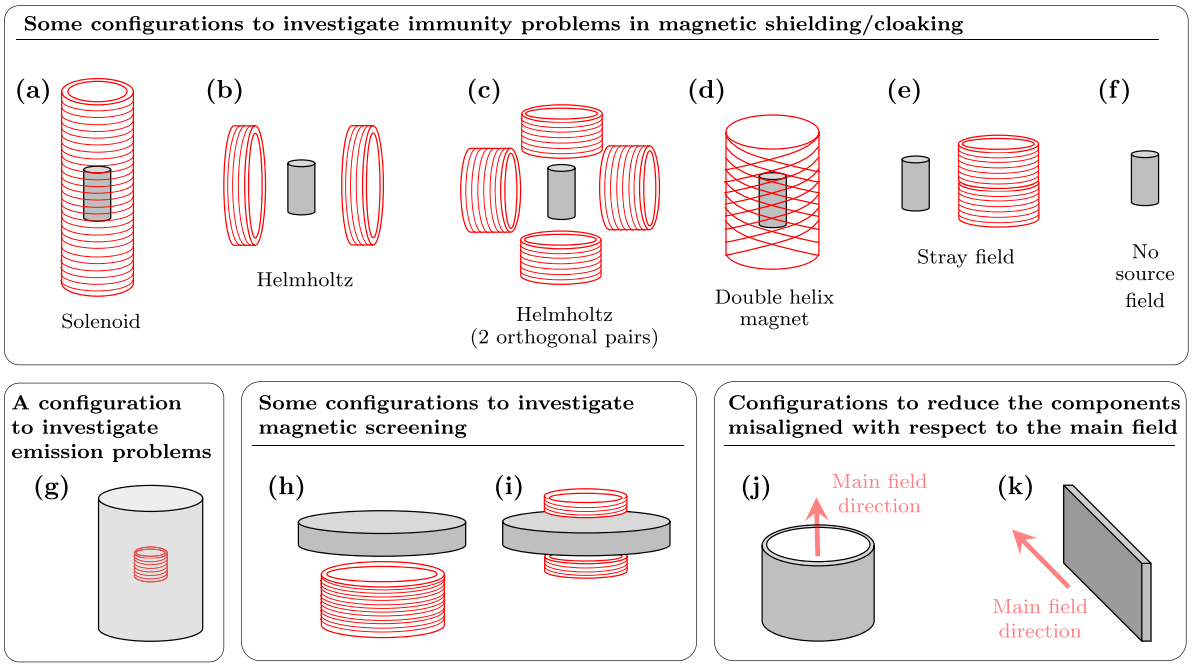

Figure 4. Schematic illustration of several possible geometric configurations. For simplicity, the grey cylinders represent the superconducting shield/screen, irrespective of the real shape and orientation. Panels (a)–(f) show examples of various configurations for studying immunity problems. The magnetic field source can be (a) a long solenoid, (b) one Helmholtz coil, (c) a pair of Helmholtz coils, (d) a double helix magnet, (e) the inhomogeneous stray field of a solenoid, or (f) no source coil (only the ambient noise). (g) Emission problem with the coil inside the shield. (h) Screening problem with the screen on one side of the source coil. (i) Screening problem with the screen between the coils of a transformer. (j) Cylindrical configuration or (k) planar configuration for reducing the field components not aligned with the main direction.

with a DC current, a slowly ramping current or an AC current. In the latter case, shielding properties are often measured within the range ~ 0.1 Hz to a few kHz. The amplitude of the applied field can be as low as a few μT (to assess the ability of the shield to generate ultra-low field environments) or several teslas (to investigate SC shields at field levels exceeding the saturation magnetization of conventional FM shields).

The basic configurations include a long solenoid (figure 4(a)), one (figure 4(b)) or several (figure 4(c)) pairs of Helmholtz coils. In order to produce a transverse field without Helmholtz coils, a variant consists in using a double helix magnet (figure 4(d)) consisting of two sets of tilted coils [127, 128]: the coils are fed in series in order to cancel out the axial field and produce a purely transverse field. In all the geometries shown in figure 4(a)–(d), the applied field is (theoretically) uniform. Experimental data can therefore be easily compared to the results given by theoretical or numerical models. In order to improve the field uniformity, compensation windings may be used [129]. In addition to air coils illustrated in figure 4, the magnetic shields can also be placed in the gap of electromagnets based on a large iron yoke and two [92] or four [85] coils.

For practical purposes, it is relevant to investigate the magnetic shielding properties in conditions encountered in applications, e.g. the inhomogeneous stray field of a solenoid (figure 4(e)). Such a configuration was studied for example in [51]. When the magnetic shield is used to reduce the magnetic noise, the set-up itself may rely solely on the ambient noise and require no external source coil (figure 4(f)) [130]. Up to now very few works have investigated SC shields in the emission configuration, i.e. when the source field is located inside the shield (figure 4(g)). In this case, the measurements of the attenuated flux density should be carried out outside the shield [99].

When considering magnetic screens, i.e. open or semi-open geometries, the main magnetic field source is located on one side of the screen and the attenuated field is measured on the other side. This is illustrated in figure 4(h), where the SC screen is shown as a flat grey disk for simplicity but could consist of any of the SC screen systems discussed in the paragraphs below. This configuration was studied for example in [101, 102]. A variant consists in using a pair of coils acting as a transformer, the source coil is the primary and the pick-up coil is the secondary (figure 4(i)); obviously, this last configuration can only be used in AC. The useful signal might be directly the voltage across the secondary coil [131] or can be expressed as a function of the mutual inductance between the two coils separated by the screen [132, 133].

Finally, some experimental configurations aim at reducing not the whole field but only the components of the field that are not aligned with the main direction, as further discussed in section 6.1. This can be done in a cylindrical configuration (figure 4(j)) or using planar SC screens (figure 4(k)) [134–136].

3.2. Measurement methods

We now consider the various types of probes to measure the flux density shielded or screened by the superconductor depending on the nature of this flux density. When ultra-low-field environments need to be characterized, e.g. in the nT range or lower, SQUIDs are the obvious choice [137–139]. In this case, particular attention should be paid to the cooling procedure of the superconductor, since it is mandatory to minimize the amount of magnetic flux that can be trapped (or 'frozen') in the SC shield during the cooling process [60]. Similar precautions should also be applied when the source coil is made of SC wire: appropriate procedures need to be applied to demagnetize the SC magnet and minimize its remnant field [39]. Flux-gate magnetometers offer an excellent sensitivity to detect flux densities in the μT range; their operating range is usually below 1 mT. Such sensors were used e.g. in [6, 140, 141].

For applied fields above $\sim 100\,\mu$T, the use of Hall probes is the most common choice; they can be sensitive to axial fields, transverse fields or measure simultaneously the three components of the field. To obtain easily a 3-axis Hall probe operating in cryogenic environment, a reliable and cost-effective solution is to insert a commercial 3-axis Hall sensor designed for room temperature operation in a small (garolite or G10) insert acting as reverse cryostat: the inside is kept at room temperature while the outside can be placed at cryogenic temperature to probe the fields of interest [142]. In order to obtain field mappings, Hall probes can be attached to a micro-positioning stage that can be operated in a liquid nitrogen bath or in a sealed chamber with thermally controlled environment [143]. Hall probes can be used in AC and DC. Note that when the Hall probe is used for measuring a DC field, an AC control current can be used (e.g. at 2 kHz) so that the Hall voltage is measured with a lock-in amplifier and the sensitivity of the measurement is increased [144]. An elegant way to ensure that the Hall probe operates correctly is to measure small and known values of the magnetic flux density during the experiment by adding a small coil acting as a 'zero-field magnet' [145].

Finally, several experimental systems are based on measuring the electromotive force e.m.f. across a sensing or pick-up coil. When the coil is stationary, this method is applicable only for probing a time-varying flux density; most of the time, it is used in the AC regime. The pick-up coil is usually made of thin (e.g. 50–60 μm-diameter) Cu wire and the e.m.f. is measured through a lock-in amplifier [110, 129, 146]. To obtain the three components of **B**, three orthogonal pick-up coils can be used [147]. The sensing coil can also be moved, e.g. along the axis of a hollow cylindrical shield [50], to obtain the distribution of the magnetic flux density. It is of interest to note that a pick-up coil can be used in DC if the coil moves. As an example, when characterizing the amplitude of small components misaligned with respect to the main direction of the field (section 4(k)), the use of rotating coils directly provides the small deviations from a pure 'dipole' field [136]. In this case, the magnetic flux density is usually expressed in terms of field harmonics.

4. Theoretical and numerical approaches for modelling magnetic shielding

This section summarizes the theoretical and numerical frameworks used for modelling the SC magnetic shielding. The section first includes the various constitutive laws of increasing complexity. Next, the analytical approaches are summarized with the emphasis on how they can be used to understand the influence of geometric effects on the shielding properties. Finally, numerical models are introduced, with particular attention paid to the choice of the formulation depending on the type of magnetic shielding problem considered.

4.1. Constitutive laws

The reduction of an external field by a SC material can be analysed by modelling the superconductor in different ways:

(i) A perfect diamagnetic material without induced currents,
(ii) A type-I superconductor following the London equations,
(iii) An irreversible type-II SC material satisfying the CSM with constant critical current density J_c, or with a field-dependent critical current density $J_c(B)$.
(iv) An irreversible type-II SC material obeying the electric field–current density ($E-J$) constitutive law.

These models are considered below.

4.1.1. Perfect diamagnetic material. Considering the superconductor as a perfect diamagnetic material is the most straightforward approach. The perfect diamagnetism is introduced by assuming that the normal component of the magnetic field vanishes at the external surface of the superconductor. The model ignores the existence of shielding currents flowing in the superconductor and assumes that the superconductor can never be penetrated, achieving therefore perfect shielding [63, 148]. It should be noted that the perfect diamagnetic material model is inherently a non-physical, idealised system that limits the application of this approach to real world shielding solutions.

4.1.2. Type-I superconductor. The next approach considers a type-I superconductor or a type-II superconductor below the critical field H_c and H_{c1} respectively. In this analysis, it is assumed that the magnetic flux is expelled from the material and that shielding is provided by induced shielding (or 'Meissner') currents flowing over a typical length scale λ (namely, the London penetration depth) according to London equations [47, 149]. This state will also be referred to as 'Meissner state' in the following. If the wall thickness is much larger than λ, the results should be consistent with some of the results obtained for a perfectly diamagnetic material, as will be discussed in section 4.2.2.

4.1.3. CSM. For irreversible type-II superconductors, the penetration of the magnetic flux can be described by the

CSM [150]. The simplest approach is given by the Bean's model according to which the current density within the superconductor can only take two values: either the constant maximum value $|J| = J_c$ or zero. Since the Bean's model neglects magnetic relaxation processes, the results predicted by this approach are frequency independent. In the frequent case where a $J_c(B)$ dependence needs to be included, various laws can be considered. For REBCO (see section 5.2) and BSCCO (see section 5.3) magnetic shields, experimental results can be reproduced successfully using Kim's model [151] i.e.

$$J_c(B) = J_{c0}\left(1 + \frac{B}{B_1}\right)^{-1}. \tag{11}$$

For MgB_2 shields (see section 5.4), the exponential decay

$$J_c(B) = J_{c0}\exp\left(-\left(\frac{B}{B_1}\right)^{\gamma}\right) \tag{12}$$

was found to provide a good agreement between computed and experimental outcomes [152–154]. In MgB_2 shields produced by reactive liquid magnesium infiltration technique [155], an analogous remarkable agreement between computation and experiments was achieved assuming the simplified exponential dependence:

$$J_c(B) = J_{c0}\exp(-\gamma B). \tag{13}$$

In equations (11)–(13), J_{c0}, B_1 and γ are constant parameters generally determined by fits on the experimental data [96, 155, 156].

4.1.4. $E-J$ constitutive law. Most numerical models use a continuous and smooth relationship between E and J. The advantage of using a continuous E–J law is that it can be incorporated into a suitable 2D or 3D model to investigate more complex magnetic shield geometries. The most common approach derives from the flux creep theory proposed by Anderson in 1960, which considers the thermal activation as the cause of the hopping of fluxons [157], and provides the following power law dependence:

$$E = E_c\left(\frac{J}{J_c}\right)^n \tag{14}$$

where E_c is an arbitrary electric field value (usually set to 10^{-4} V m^{-1}) chosen to identify the value of the critical current density, J_c, and n is called the 'creep factor'. It defines the steepness of the transition between the SC state and the normal state. If $n = 1$, (14) describes a normal conducting material (linear Ohm's law), whereas for $n \to \infty$ it reduces to the Bean's model. Figure 5 shows several E–J curves obtained from (14) for different n values. In addition to be used in the numerical approaches developed in section 4.3, the E–J law can also be used in the semi-analytical approach developed by Brandt [158, 159]. This semi-analytical approach was applied to magnetic shielding problems in [50, 160].

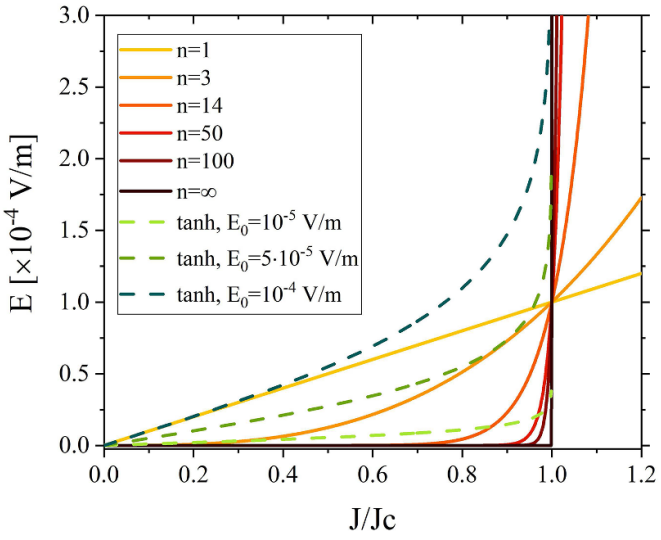

Figure 5. Comparison of the E–J power law given by (14) in the main text for different values of the exponent n and the E–J hyperbolic tangent law given by (15) for different values of the parameter E_0.

Even though the power law equation can be implemented easily in finite element codes, for MgB_2 the creep factor n usually takes a huge value ($n \approx 100$) [154] that can lead to numerical difficulties. As a consequence, to better address the case of superconductors with $n \gg 1$ alternative approaches were developed. In particular, assuming that the current density is locally collinear with the electric field, the relation

$$\mathbf{J} = J_c\tanh\left(\frac{|\mathbf{E}|}{E_0}\right)\left(\frac{E_x}{|\mathbf{E}|}\hat{\boldsymbol{u}}_x + \frac{E_y}{|\mathbf{E}|}\hat{\boldsymbol{u}}_y + \frac{E_z}{|\mathbf{E}|}\hat{\boldsymbol{u}}_z\right) \tag{15}$$

can be considered as a suitable smooth approximation of the stepwise function predicted in the CSM [161] and was successfully applied to solve 3D shielding problems [93]. In this equation, the parameter E_0 controls the sharpness of the transition just as the n-factor in the E–J power law, E_x, E_y and E_z represent the three components of the local value of the electric field and $\hat{\boldsymbol{u}}_x$, $\hat{\boldsymbol{u}}_y$, $\hat{\boldsymbol{u}}_z$ are the unit vectors along the x, y and z directions, respectively. The use of this E–J relationship, developed starting from the microscopic analysis by Campbell [162], was generally coupled with the application of the magnetic vector potential, $\mathbf{A}$, formulation (see section 4.3) to describe the superconductor flux dynamics [161, 163]. Both in (14) and (15) the most suitable $J_c(B)$ law is then included according to the investigated material.

Other E–J relationships have also been proposed, e.g. in [164, 165]. However, these relationships will not further be discussed here because to our best knowledge they have never been applied to model magnetic shielding and screening problems.

4.2. Analytical approaches for modelling magnetic shields

Analytical approaches are very helpful to estimate the efficiency of SC shields and screens and to investigate the influence of geometric or physical parameters on their performances. In this section, we summarize the analytical results obtained for simple geometries, together with considerations regarding how the analytical formulas can be used. Unless otherwise stated, the analytical approaches reported below consider the superconductor first cooled in zero field (ZFC procedure) and then subjected to a uniform magnetic field H_{app}. Frequency effects are ignored, i.e. the applied field is assumed to be DC or such that its time dependence has no effect on the properties of the shield or screen. The section focuses only on superconductors and will not cover the comparison with the analytical formulas obtained for their high-permeability counterparts. Detailed comparisons can be found in the reviews by Pavese [36] and Claycomb [166].

Typical problems benefiting from analytical solutions include the magnetic shielding by a hollow cylinder with the applied field either parallel (axial field) or perpendicular (transverse field) to its axis, the magnetic shielding by a hollow sphere, the magnetic field penetration in long cylindrical holes drilled in semi-infinite volumes or the magnetic screening of an infinitely thin SC disk with the field parallel to its axis. These geometries are illustrated schematically in figure 6 together with the definition of the geometric parameters.

4.2.1. Perfect diamagnetic material. The model assuming a perfect diamagnetic material ignores the penetration of magnetic flux in the body of the superconductor. Such a model is not useful to find the shielding factor of closed geometries with no 'entry gate' for the flux lines, such as a hollow sphere or an infinite hollow cylinder under a transverse field. The reason is that the perfect diamagnetism simply yields a zero internal flux density B_{in} and an infinite shielding factor $\text{SF} = \infty$, i.e. a trivial result. More relevant information, however, can be found regarding how the magnetic flux lines penetrate through open ends (figures 6(c) and (d)). The analysis was done for a semi-infinite hollow cylinder in the pioneering works of Cabrera [148] and Claycomb [63]. The flux density can be expressed as a series of decaying exponential functions of the normalized distance z/R_{in} from the opening of the tube. Along the axis and far enough from the opening, one has the following approximation

$$B \approx K\mu_0 H_{\text{app}} \exp\left(-k\left(z/R_{\text{in}}\right)\right). \tag{16}$$

As such, equation (16) gives information on how B changes with the distance z. This equation, however, cannot be used to find the value of B since the factor K is unknown. For an axial field, one has $k = k_{\parallel} = 3.83$; for a transverse field, $k = k_{\perp} = 1.84$. These two numbers correspond to the first root of the Bessel function J_1 and of its derivative J_1', respectively [63, 148]. The fact that $k_{\parallel} > k_{\perp}$ emphasizes that openings have less detrimental effect for axial fields than for transverse fields, in contrast with FM shields [166, 167]. The analysis above refers to a semi-infinite hollow cylinder but can be extended in a fairly good approximation to a finite semi-closed tube of height h. Fagnard *et al* [98] showed that, under an axial field, the entry of magnetic flux lines through the opening, hence their distribution in the plane $z = 0$, is strongly sensitive to the shape of the superconductor around the opening and its general aspect ratio of height to radius. Consequently, K may differ significantly from one geometry to another. On the opposite, for short semi-closed tubes ($h \sim 2R_{\text{out}}$) in transverse fields, it was shown that the coarse approximation $K \approx 1$ leads to analytical results that are in fair agreement with those obtained by finite element modelling. While this analysis holds for semi-infinite or semi-closed tubes, it can be used to model a tube with two openings (figure 6(e)). The fields entering from both sides of such an open tube simply add, and each of them can be roughly approximated by the field that would enter in a semi-infinite tube.

Analytical expressions of the flux density can also be obtained for holes or grooves in perfectly diamagnetic superconductors. For a small circular hole of radius R in a SC thin sheet with the applied field parallel to the sheet (figure 6(g)), the flux density along the axis of the hole and far enough from the opening decays as $(R/z)^3$ [148]. Approximations were derived to estimate the penetration of magnetic flux in a SC plate containing numerous holes [138]. Analytical formulas were also established for a narrow slit in a SC thin sheet (figure 6(h)) or an infinitely deep groove in a semi-infinite superconductor (figure 6(i)) [36, 168].

A perfectly diamagnetic disk (figure 6(j)) diverts the flux lines and therefore offers a given amount of magnetic screening. For an infinitely thin disk of radius R subjected to a uniform field parallel to z, the magnetic field along the axis of the disk was calculated analytically [63] by solving Laplace's equation for the magnetic scalar potential in oblate spheroidal coordinates. The result for $r = 0$ is given by

$$H_z = H_{\text{app}}\left[1 - \frac{2}{\pi}\left(\tan^{-1}\left(\frac{R}{z}\right) - \frac{Rz}{R^2 + z^2}\right)\right], \tag{17}$$

where z is the distance to the disk. Along the axis ($r = 0$) the radial component of the magnetic field H_r is zero by symmetry. It is of interest to notice that this mathematical analysis can be extended to any value of r to find the analytical expressions of H_r and H_z around the disk. The corresponding mathematical developments, unpublished so far, are provided in appendix A of this review. The results can be used to find the shape of the flux lines at any point around the disk, as illustrated in figure 7.

In the models considered in this section, the magnetic flux lines do not penetrate the body of the superconductor but are located in free space. Therefore, the flux density in the region of interest is only related to flux lines meandering around the superconductor through openings and is proportional to the applied field. The corresponding shielding factor, referred to as 'SF_{open}', is a constant. The consequence is that, strictly speaking, the use of SF_{open} alone does not allow a threshold B_{lim} to be estimated. This is not the case when considering also the shielding factor through the walls 'SF_{wall}' which is

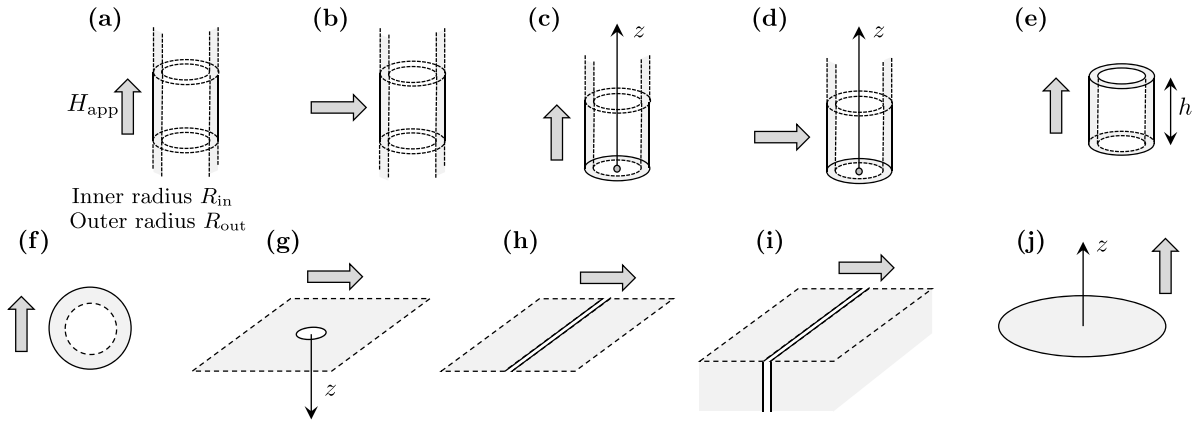

Figure 6. Schematic illustration of several geometries of superconductors for which some analytical expressions (exact or approximate) of the magnetic flux density modified by the superconductor or the threshold magnetic flux density B_{lim} can be found. (a) infinite hollow cylinder with applied field parallel to the axis (axial field), (b) same with applied field perpendicular to the axis (transverse field), (c) semi-infinite hollow cylinder under an axial field, (d) same under a transverse field, (e) finite hollow cylinder under an axial field, (f) hollow sphere, (g) small circular hole in an infinite superconducting thin sheet, (h) narrow slit in an infinite superconducting thin sheet, (i) infinitely deep groove in a semi-infinite superconductor, (j) thin superconducting disk under an axial field.

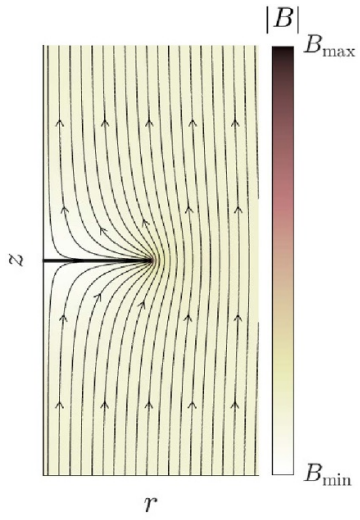

Figure 7. Magnetic flux density lines around an infinitely thin superconducting disk (perfect diamagnetism assumption) subjected to a uniform axial field as calculated by the formulas in A. The background colour shows $|\mathbf{B}|$. The units are arbitrary.

generally a function of the applied field. The effective shielding factor $SF_{eff}(H_{app})$ is then given [167] by $1/SF_{eff}(H_{app}) = 1/SF_{open} + 1/SF_{wall}(H_{app})$.

By increasing the applied magnetic field, the ultimate limit of the 'perfect diamagnetic' model is the disappearance of perfect diamagnetism that occurs when the local magnetic field at the surface of the superconductor exceeds the critical field H_c (for a type-I superconductor) or H_{c1} (for a type-II superconductor). When there are no demagnetization effects, i.e. when the applied field is directed along the supposedly infinite direction, the field at the surface is simply equal to the applied field H_{app}, hence the 'perfect diamagnetic' model is valid until $H_{app} = H_c$ (or H_{c1}). In all other situations, the local field may exceed H_c at some places while being below H_c at some others, leading to the 'intermediate' state [169]. In simple geometries, the onset of the intermediate state can be estimated using the demagnetization factor N in the direction of the applied field. For an infinite hollow cylinder subjected to a transverse field, one has $N = 1/2$ and the material enters the intermediate state as soon as H_{app} exceeds $H_c/2$. It should be kept in mind that this reasoning is true when the field is applied after a ZFC procedure and is not valid when the magnetic flux expulsion occurs in FC. As an example, for a hollow cylinder cooled in a transverse field (in FC), it can be shown [148] that the Meissner effect occurs until $H_{app} = H_c\sqrt{(1-(R_{out}/R_{in})^2)/2}$. This formula emphasizes that in the FC regime, physical phenomena happen in the volume of the superconductor; hence the limit field is not only dictated by the shape of the outer surface of the superconductor, but is a function of both R_{out} and R_{in}.

It is also of interest to note that the 'perfect diamagnetic material' model was also used in an original way to calculate the influence of a closed, cylindrical SC shield placed coaxially around a cylindrical solenoid. The corresponding flux density distribution can be found in [170].

4.2.2. Type-I superconductor. We now consider the material as a type-I superconductor following the London equations, as defined in section 4.1.2. For an infinite hollow cylinder (inner and outer radii R_{in} and R_{out}), analytical expressions were determined more than 6 decades ago by Ginzburg [171] as well as Lung-Tao and Zharkov [172]. Using the dimensionless parameters $\xi_1 = R_{in}/\lambda$ and $\xi_2 = R_{out}/\lambda$, the internal field H_{in} inside the cylinder subjected to an axial field H_{app} (figure 6(a)) is given by

$$H_{in} = \left(\frac{2H_{app}}{\xi_1^2\left[K_0(\xi_1)I_0(\xi_2) - I_0(\xi_1)K_0(\xi_2)\right]}\right) \times \left(1 + \frac{2}{\xi_1}\frac{K_0(\xi_2)I_1(\xi_1) + I_0(\xi_2)K_1(\xi_1)}{K_0(\xi_1)I_0(\xi_2) - I_0(\xi_1)K_0(\xi_2)}\right)^{-1}, \quad (18)$$

where I_n and K_n denote the modified Bessel functions of the first and second kind, respectively. If the radii and the wall thickness $d = R_{out} - R_{in}$ of the cylinder are all much larger than λ, one can use the asymptotic expressions of the Bessel functions for large arguments. This yields

$$H_{in} \approx 4H_{app}\frac{\lambda}{R_{in}}\sqrt{\frac{R_{out}}{R_{in}}}\exp\left(-d/\lambda\right). \tag{19}$$

A similar analysis for an applied field H_{app} perpendicular to the axis of the cylinder (transverse field, figure 6(b)) gives [172]

$$H_{in} = \frac{2H_{app}}{\xi_1^2\left[K_2\left(\xi_1\right)I_0\left(\xi_2\right) - I_2\left(\xi_1\right)K_0\left(\xi_2\right)\right]} \tag{20}$$

and, for R_{in}, R_{out} and $d \gg \lambda$,

$$H_{in} \approx 4H_{app}\frac{\lambda}{R_{in}}\sqrt{\frac{R_{out}}{R_{in}}}\exp\left(-d/\lambda\right). \tag{21}$$

Interestingly, equations (19) and (21) lead to the same asymptotic result. They also show that the internal field decays exponentially with d/λ. For $d \gg \lambda$, the internal field is zero as expected for a perfectly diamagnetic material with no opening. Analytical formulas were also determined for a hollow sphere [172] (figure 6(f)) and lead to a similar asymptotic exponential behaviour. It is recalled here that the analysis above is only valid in ZFC. For a hollow superconductor in the FC regime, flux quantization may occur [171].

It is of interest to stress that analytical formulas derived for the shielding factor of *linear* magnetic materials with constant permeability in the limit $\mu_r \to 0$ *cannot* be used to approximate the Meissner state. As an example, the SF predicted for an infinite hollow cylinder made of linear material subjected to a transverse field reads [173–175]

$$SF = 1 + \frac{\left(1-\mu_r\right)^2}{4\mu_r}\left[1 - \left(\frac{R_{in}}{R_{out}}\right)^2\right]. \tag{22}$$

In the limit $\mu_r \to 0$, SF becomes infinite as intuitively expected. However, if one considers a small, but finite value of μ_r in (22), the dependence of SF on the geometric parameters differs significantly from the SF that can be deduced from (21). Unlike conventional diamagnetic materials for which diamagnetism is due to phenomena at the microscopic scale, the attenuation of magnetic flux by superconductors is due to macroscopic shielding currents. As a consequence the distribution of the magnetic flux density in the SC walls differs significantly from what would be expected for a linear material.

The model of a type-I superconductor can also be used to estimate the flux screening by a thin SC disk (radius $\gg$ thickness) in axial field. Analytical expressions of the screening current density flowing in the disk are available in [159, 176–178]. This current density can be incorporated in Biot–Savart's law to obtain the field along the axis of the disk. Doing so, it can be checked readily that one recovers (17) which is valid for a perfect diamagnetic material.

4.2.3. Irreversible type-II superconductor. For type-II superconductors, we consider below 4 cases of increasing complexity, outlining the types of analytical expressions that are available and how they can be used. In a type-II superconductor with no entry gate for the flux lines such as an infinite hollow cylinder, the penetration of the magnetic flux occurs through the walls of the superconductor. As long as the flux front does not reach the inner surface of the wall, the Bean's CSM [150] predicts that the flux density inside the cylinder $B_{in} = 0$, i.e. $SF = \infty$.

We first consider an infinite hollow cylinder with constant J_c, subjected to a magnetic field parallel to its axis (figure 8(a)), B_{lim} is given by the full-penetration field $B_p = \mu_0 J_c d$, where d is the wall thickness. For $\mu_0 H_{app} \leqslant B_p$, $B_{in} = 0$, for $\mu_0 H_{app} \geqslant B_p$, $B_{in} = \mu_0 H_{app} - B_p$, as illustrated in figure 8(a). Knowing J_c, it is then straightforward to predict B_{lim} or, conversely, by a measurement of B_{in} vs $\mu_0 H_{app}$, the abrupt change in the curve occurring at $H_{app} = J_c d$ enables J_c to be determined experimentally.

The second considered case deals with the same geometry, i.e. an infinite hollow cylinder, with a field dependent $J_c(B)$. The radial distribution of B in the cylinder walls can still be found easily since there are no demagnetization effects and all quantities are dependent on the radial distance r only. In the frequent case where the $J_c(B)$ is approximated by Kim's law (11), the value of B_{lim} is given by [179, 180]

$$B_{lim} = -B_1 + \sqrt{B_1^2 + 2\mu_0 J_{c0} B_1 d}. \tag{23}$$

The corresponding B_{in} vs $\mu_0 H_{app}$ curve is illustrated schematically in figure 8(b). Detailed calculations are summarized in [97]. In figure 8(b), it is assumed that B_{lim} is the same as in (a). This situation often occurs in practice, when a certain B_{lim} is measured experimentally and an appropriate model such as constant J_c or $J_c(B)$ should be chosen to explain the experimental results.

A signature of the $J_c(B)$ dependence is the concave downward curvature of this plot. Knowing the parameters J_{c0} and B_1 of Kim's law, B_{lim} can be estimated by (23). The measurement of B_{lim} only, however, does not allow J_{c0} and B_1 to be determined with one equation. A practical solution is to increase the applied field up to a user-defined value $\mu_0 H_{max}$ and measure the corresponding flux density inside the cylinder $B_{in,max}$ (figure 8(b)). The parameters from Kim's law can be found as follows [110]

$$B_1 = \frac{1}{2}\frac{\left(B_{lim}^2 + B_{in,max}^2 - B_{max}^2\right)}{\left(B_{max} - B_{lim} - B_{in,max}\right)}, \tag{24}$$

$$J_{c0} = \frac{B_{lim}}{\mu_0 d}\left(1 + \frac{B_{lim}}{2B_1}\right), \tag{25}$$

where $B_{max} = \mu_0 H_{max}$.

The next case is to consider an infinite hollow cylinder with constant J_c, subjected to a transverse magnetic field, i.e. perpendicular to its axis (figure 8(c)). At very low field, the cylinder can be considered as a nearly perfect diamagnetic material. The local field at a point α can be estimated from the transverse demagnetization factor for cylinders ($N = 1/2$), i.e.

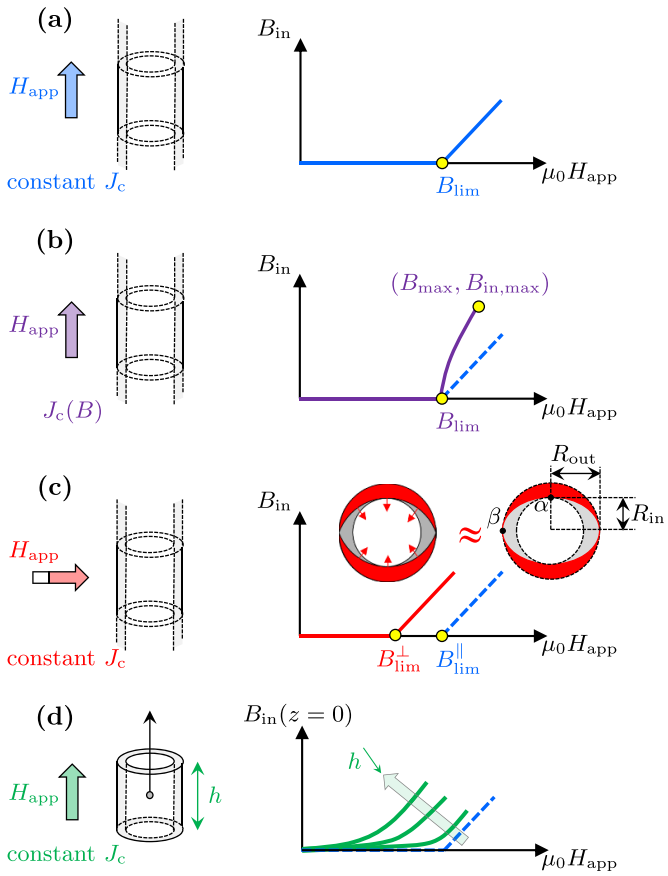

Figure 8. Schematic illustration of the internal magnetic flux density B_{in} as a function of the applied field $\mu_0 H_{app}$ in different cases, along with a representation of the considered superconducting geometry. (a) infinite hollow cylinder with constant J_c subjected to an axial field, the curve serves as a reference and is shown as a dashed line for the three other panels, (b) infinite hollow cylinder with field-dependent J_c subjected to an axial field, (c) infinite hollow cylinder with constant J_c subjected to a transverse field, the cross-section of the cylinder schematically shows the nearly elliptical flux front reaching the inner wall of the cylinder, (d) finite hollow cylinder with constant J_c subjected to an axial field.

$H_\alpha = 2H_{app}$. By increasing the applied field, flux fronts penetrate in the walls of the cylinder, as illustrated in figure 8(c). These flux fronts have a nearly elliptical shape [181]; approximate analytical expressions of these flux fronts can be found in [182, 183]. The consequence is that, for a given applied field, the flux fronts in the transverse field reach the inner wall of the cylinder before they would do so for an axial field (figure 8(c)). The transverse threshold induction $B_{lim}^{\perp}$ is therefore smaller than the axial one, $B_{lim}^{\parallel}$. Interestingly, the relation between $B_{lim}^{\perp}$ and $B_{lim}^{\parallel}$ can be estimated from a simple analysis explained in [96]. When the transverse flux front reaches the inner wall of the cylinder, the flux-free zone can be approximated by an ellipse whose small axis is R_{in} and large axis R_{out}. The local field at a point β can therefore be estimated from the transverse demagnetization factor N for an infinitely long cylinder with a plain elliptical cross-section. Along the direction of the applied field, one has $N = R_{in}/(R_{in} + R_{out})$ [184]. This leads to the following approximate relation [96]:

$$\frac{B_{lim}^{\parallel}}{B_{lim}^{\perp}} \approx 1 + \frac{R_{in}}{R_{out}}. \tag{26}$$

This approximate relation was found to be in good agreement with experimental data [96]. For a cylinder with a very thin wall ($R_{in} \sim R_{out}$), a factor ~ 2 between the two threshold fields is expected, i.e. $B_{lim}^{\perp} \approx \mu_0 J_c d/2$. Remarkably, in the 'thin wall limit' ($d \ll R_{in}$), the magnetic flux distribution inside the cylinder can be calculated analytically using conformal mapping and the complex-field approach; this was done by Mawatari [185].

Finally, the fourth case is a SC cylinder with constant J_c but of finite height h subjected to an axial field (figure 8(d)). With this geometry, the magnetic flux penetration through both open ends yields a finite B_{in}, even at the smallest applied field. This is illustrated schematically in figure 8(d). In this case, fully analytical expressions do not exist for B_{in} vs $\mu_0 H_{app}$ and a semi-analytical approach has to be followed [50], e.g. using the Brandt algorithm [186]. The threshold magnetic flux density B_{lim} can be approximated using the analytical expression of the full-penetration field given by Navau *et al* for finite type-II SC rings [187]. Defining $\gamma = h/R_{out}$ and $\delta = R_{in}/R_{out}$, one has

$$B_{lim} = \mu_0 J_c R_{out} \frac{\gamma}{2} \frac{(1-\delta)}{(1+\delta)} \times \ln\left(\frac{2(1+\delta)}{\gamma} + \sqrt{1 + \left(\frac{2(1+\delta)}{\gamma} \right)^2} \right). \tag{27}$$

4.3. Numerical approaches for modelling magnetic shields

To address magnetic shielding problems, with more complex geometry (e.g. non-basic shape or non-homogeneous applied field) or when a continuous E–J relation—such as the power law (14) or the hyperbolic tangent (15) law—is employed, the use of numerical methods is necessary. In recent years, various numerical methods have been exploited such as fast Fourier transform (FFT) [188] or spectral methods [189]. To date, the most widely used method is the FEM also thanks to the availability of several commercial software packages that employ it. FEM allows investigating the electromagnetic response of a SC material, solving time-dependent Maxwell's equations in differential form and using nonlinear resistivity (or conductivity) to represent the superconductor electrical behaviour.

To highlight the interest of using numerical models, one can, for example, study the shielding properties of a SC tube of finite height using analytical models for the infinite tube (see section 4.2.3) and numerical methods for the actual height. Hence, we consider here an infinite tube and a finite tube having a small aspect ratio (hereafter referred to as height over inner radius, AR $= h/R_{in}$ for tubular structure) with inner radius $R_{in} = 8$ mm, height $h = 16$ mm and wall thickness $d = 5$ mm. The results obtained with the analytical and numerical approaches are compared in figure 9, which shows the flux density B_{in} at the centre ($z = 0$ mm) and at the extremity of

the finite tube ($z = 8$ mm) as a function of the uniform axial applied field : (i) in violet, the analytical results for the infinite tube with constant J_c (solid line), i.e. applying the Bean's model, and with a $J_c(B)$ law given by (11) (symbols); (ii) in green, the numerical results for a finite tube with constant J_c (solid line) and with a $J_c(B)$ law given by (11) (symbols) calculated at $z = 0$ mm; (iii) in orange, the numerical results for a finite tube with constant J_c (solid line) and with a $J_c(B)$ law given by (11) (symbols) calculated at $z = 8$ mm (i.e. in correspondence to an opening). Similarly to what was done in section 4.2.3, it is assumed that B_{lim} is known (e.g. by experiments) and that the parameters such as constant J_c, J_{c0} or B_1 are chosen to model this B_{lim}. Here, it corresponds to equating B_{lim} from the Bean's model (section 4.2.3) with (23). The degree of freedom in choosing B_1 is here fixed arbitrarily, but in practice determined by the shape of the B_{in} vs $\mu_0 H_{app}$ curve. Once fixed to give the same B_{lim}, the values of constant J_c, J_{c0} and B_1 are the same for the three pairs of curves.

Focusing on the curves computed at position $z = 0$ with the numerical method and its approximation using the analytical approach for an infinite tube, the comparison highlights that the analytical expressions always overestimate the threshold field B_{lim} predicted by the FEM. This is due to the small AR of the tube: the flux lines can penetrate through the open ends and reduce the shielding ability, which is not captured by the analytical expressions. Furthermore, the numerical approach provides the additional advantage of calculating the magnetic flux density near the tube's extremities, such as at $z = 8$ mm, which is not possible using the analytical approach for a type-II superconductor.

Another benefit from FEMs is that both the magnetic flux density magnitude and the magnetic flux lines distribution can be observed, which helps understand the penetration through the open ends and the influence of the chosen J_c law. This is illustrated in figure 10, which presents the magnetic flux lines distribution and the magnetic flux density magnitude in the sample obtained assuming a constant J_c (a, c) and a $J_c(B)$ dependence (Kim's law (11), for (b) and (d)) for a tube with a small AR ($R_{in} = 8$ mm, $h = 16$ mm) and wall thickness either $d = 5$ mm (a, b) or $d = 10$ mm (c, d). The comparison reveals that assuming a constant J_c may underestimate the penetration of the external magnetic field, highlighting the necessity of using a current density model dependent on B, especially when the parameter B_1 in the Kim's law is not much larger than B_{lim}.

Remarkably, as shown in figure 11, a non-negligible $J_c(B)$ dependence strongly affects the flux penetration rate in the shield wall. Indeed, increasing the wall thickness brings a rather limited improvement in B_{lim}, as also reported in [49, 156] and suggested by (23). In particular, assuming a constant J_c and doubling the wall thickness results in a 44% increase in the B_{lim}, compared to only 31% when considering the above-mentioned $J_c(B)$.

4.3.1. Electromagnetic formulations. Depending on the investigated shielding problems, different electromagnetic formulations of the Maxwell's equations have been employed.

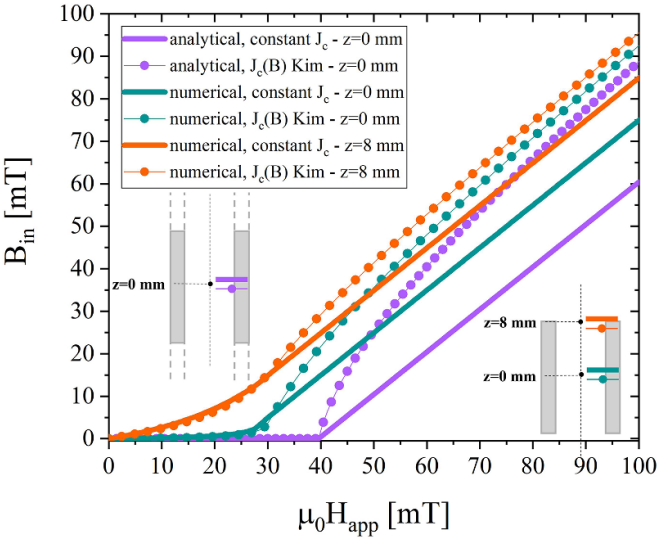

Figure 9. Predicted magnetic flux density inside a superconducting tube as a function of a uniform axial applied field. The curves are: (i) in violet, the analytical results for an infinite tube with constant J_c (solid line) and with a $J_c(B)$ law given by (11) (symbols); (ii) in green, the numerical results for a finite tube with constant J_c (solid line) and with a $J_c(B)$ law given by (11) (symbols) calculated at $z = 0$ mm; (iii) in orange, the numerical results for a finite tube with constant J_c (solid line) and with a $J_c(B)$ law given by (11) (symbols) calculated at $z = 8$ mm. For the sake of comparison, the analytical results are referred to as '$z = 0$' mm, even if the results are position-independent (infinite tube). Parameters of the tube are $R_{in} = 8$ mm, $h = 16$ mm and wall thickness $d = 5$ mm. Other parameters are 6.3 MA m^{-2} for the constant J_c value and $J_{c,0} = 18.9$ MA m^{-2} and $B_1 = 9.9$ mT (see (11)). Here, the finite element model uses the **A**–V formulation (see section 4.3.1).

Among them, the **A**–V [190] and the **H** [191, 192] formulations were often applied. By using the **A**–V formulation, the Maxwell's equations are written in terms of the magnetic vector potential **A** and the electrostatic potential V [193]. Remembering that $\mathbf{B} = \nabla \times \mathbf{A}$ and $\mathbf{E} = -\partial \mathbf{A}/\partial t - \nabla V$, Ampere's equation becomes:

$$\sigma(E)\frac{\partial \mathbf{A}}{\partial t} + \nabla \times \left(\frac{1}{\mu_0 \mu_r}\nabla \times \mathbf{A}\right) = -\sigma(E)\nabla V \qquad (28)$$

where μ_r is the relative magnetic permeability (set to 1 in the SC domain) and $\sigma(E) = J(E)/E$ the electric conductivity taking a form depending on the selected E–J relation (see section 4.1.4). In the Coulomb gauge ($\nabla \cdot \mathbf{A} = 0$), under suitable conditions, V can be set to zero [93, 194]. This formulation was successfully employed to predict the shielding efficiency of REBCO [195, 196], BSCCO [99, 196], and MgB_2 [93, 197] shields or screens and extended to model the shielding properties of hybrid structures combining superconductors and other magnetic materials [93, 198, 199].

The **H**-formulation solves the Faraday's equation, which in terms of the magnetic field strength **H** takes the form [192]:

$$\frac{\partial \mu_0 \mu_r \mathbf{H}}{\partial t} + \nabla \times (\rho(J)\nabla \times \mathbf{H}) = 0 \qquad (29)$$

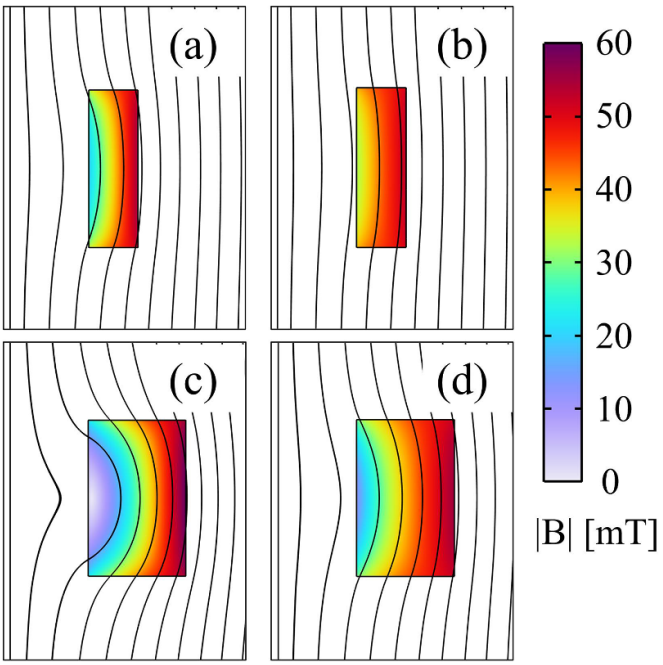

Figure 10. Magnitude of the magnetic flux density in the sample (colour maps) and distribution of the magnetic flux lines obtained for tube-shaped shields whose dimensions are $R_{in} = 8$ mm, $h = 16$ mm and $d = 5$ mm (a), (b) or $d = 10$ mm (c), (d) when a $\mu_0 H_{app} = 50$ mT is applied. A constant $J_c = 6.3$ MA m^{-2} was assumed for (a) and (c), while a $J_c(B)$ dependence (Kim's law (11)) with $J_{c0} = 18.9$ MA m^{-2} and $B_1 = 9.9$ mT was used for (b) and (d). Here, the finite element model used the **A**–V formulation (see section 4.3.1).

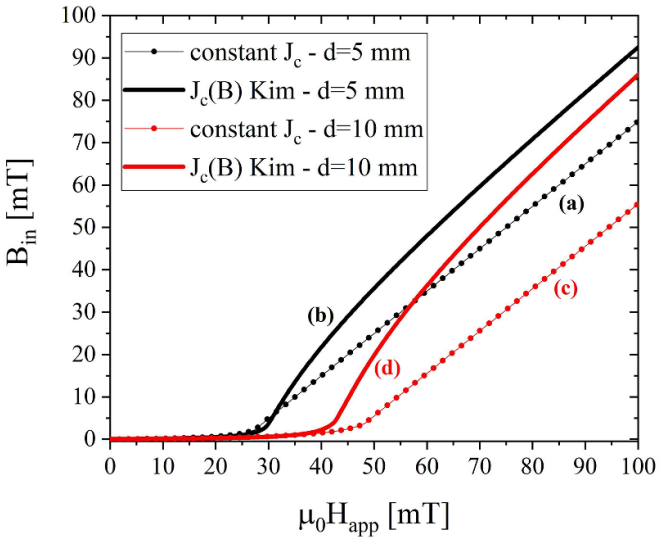

Figure 11. Internal magnetic flux density B_{in} as a function of the applied field $\mu_0 H_{app}$ for tube-shaped shields whose dimensions are $R_{in} = 8$ mm, $h = 16$ mm and $d = 5$ mm (a), (b) or $d = 10$ mm (c), (d). A constant $J_c = 6.3$ MA m^{-2} was assumed for (a) and (c), while a $J_c(B)$ dependence (Kim's law (11)) with $J_{c0} = 18.9$ MA m^{-2} and $B_1 = 9.9$ mT was used for (b) and (d). Here, the finite element model uses the **A**-V formulation (see section 4.3.1). The magnetic flux density distributions for these geometries are shown in figure 10.

where $\rho(J) = E(J)/J$ is the resistivity. Just as with the electric conductivity, the selected E–J relation provides the resistivity dependence of the current density. Remarkably, the **H**-formulation implementation is quite simple, since no gauging or post-processing is required [163, 200]. This formulation was successfully employed to predict the shielding efficiency of REBCO [44, 201, 202], BSCCO or Pb-doped BSCCO [203] and MgB_2 [155, 163] shields and screens as well.

However, despite their wide use, the **A**- and **H**-formulations are not always the optimal choice. For instance, using the **A**-formulation can lead to numerical instability due to the vanishing resistivity of the superconductor [204]. Similarly, the **H**-formulation presents challenges, such as a higher number of degrees of freedom that increases the computational time [200]. Furthermore, since an artificial resistivity is required even in non-conducting domains, a degradation of the matrix conditioning can occur [200]. In the case of shielding problems, other difficulties in the choice of the formulation may arise from the geometry of the sample (e.g. very thin tapes), or from the combination of different materials (bulk, tapes, FM parts, etc). In particular, for hybrid configurations involving both SC and FM domains (see section 8), the choice between the **A**- and **H**-formulations is not straightforward [205]: as an example, in [206], the use of the **H**-formulation in the SC domain and the use of the **A**-formulation in the other domains (included possible permanent magnets) was proposed.

In order to simulate realistic shields combining SC bulks, tapes and/or FM materials, alternative formulations have been implemented in electromagnetic-focused FEM software, often tailored to specific applications [198, 200, 204, 207–211].

In the last few years, the use of 2nd generation (2G) CC tapes for fabricating magnetic shields has become more and more extensive (see section 6). The high aspect ratio (in this case, width over thickness) of these structures is a challenge that has to be tackled numerically, yielding the introduction of new formulations. An example is the $\mathbf{T} - \mathbf{A}$ formulation, which is considered as a promising formulation for predicting the shielding properties of tape-based structures [212]. In this formulation, the problem is solved using the current vector potential $\mathbf{T}$ ($\mathbf{J} = \nabla \times \mathbf{T}$) in the SC domain and the magnetic vector potential $\mathbf{A}$ in all the domains [208, 213, 214], thus reducing the number of mesh elements.

Other challenges occur when FM parts are involved in the shield. In this regard, Bortot *et al* [136] used a coupled **A**–**H** field formulation [204] to model HTS tapes-based screens in a complex scenario where there are also FM elements. The problem was solved under magneto-quasistatic assumptions for the magnetic field **H** in the SC tapes and for magnetic vector potential **A** in the other domains.

Another example is the modelling of CC with a FM substrate. Such a substrate turns the entire structure into an SC-FM multilayered hybrid shields with field-dependent resistivity and permeability [215]. Dular *et al* [212] investigated the shielding properties of stacks of such tapes with three different formulations: $\mathbf{H} - \phi$, $\mathbf{H} - \phi - \mathbf{B}$ and $\mathbf{A} - \mathbf{J}$. In the first formulation, zero current density is imposed in non-conducting

regions: the Ampere's law becomes $\nabla \times \mathbf{H} = 0$ and a magnetic scalar potential ϕ can be defined as $\mathbf{H} = -\nabla\phi$ and used to solve the problem with a consequent reduction of the degrees of freedom compared to the **H**-formulation. The second one is similar to the first one except that in the non-linear magnetic domains the problem is solved in **B**. The last one is a variation of the **A**-formulation using the **J** variable for the non-linear conducting domains [216]. Therefore, the first two formulations allow overcoming the imposition of an artificial resistivity in non-(super)conducting domains that could affect **H**-formulation-based models, and the second one also the management of complex permeability. The third formulation gets over the problem of the strong non-linearity of the superconductor conductivity that could affect **A**-formulation-based calculations. Simulations do not provide a clear indication that a formulation prevails on the others in terms of efficiency and accuracy, the result depending on the applied field orientation and on the application of a homogenization procedure (see the next paragraph).

The choice of the formulations is not the only way to deal with such a difficult SC-FM multilayered shield. For stacked tapes, it is impractical to simulate the behaviour of the devices by modelling each layer separately. A possible solution to overcome this numerical limit is to adopt the homogenization method [217, 218]. The layered structure is then considered as a homogeneous hybrid bulk with an anisotropic resistivity and permeability, whose values take into account the different behaviour of the superconductor and the FM material when an external field is applied. Dular *et al* [212] and Brialmont *et al* [92] used the homogenized model to predict the shielding properties of stacks of YBCO tape annuli. In Brialmont *et al* [92] the comparison between the experimental data and the corresponding computational results obtained with the homogenized model and the $\mathbf{H} - \phi$ formulation reveals a good agreement, demonstrating the reliability of this approach. In [212], the authors compared the performances of the formulations $\mathbf{H} - \phi$, $\mathbf{H} - \phi - \mathbf{B}$ and $\mathbf{A} - \mathbf{J}$ in reproducing the experimental results in both axial and transverse applied fields when a layered model (assuming a limited number of tapes with a fictitious thickness so that the total height of the stack corresponds to the effective one) and a homogenized model are employed. If comparable results were obtained with all the approaches for the 2D axial field configuration, they highlighted that in the transverse field orientation, even though comparable results were achieved, the layered model involving a limited number of tapes was found to be faster than the homogenized model.

4.3.2. Modelling the magneto-thermal instabilities. When the superconductor is in the critical state, some uncontrolled instabilities can arise, such as quench phenomena or other thermo-magnetic instabilities. Among the latter, the flux jump phenomenon can totally compromise the SC properties of the samples. In fact, when a flux-jumping process starts, it causes a flux lines motion followed by a strong heating of the superconductor—even above the transition temperature—that in turn contributes to the magnetic flux redistribution towards the equilibrium state [219–222]. Therefore, it is easy to understand how a flux jump phenomenon in a SC shield produces an abrupt decay of the shielding factor, thus representing a serious problem for the device application [41, 43, 223–225]. Besides, this process can also produce cracks in the material, permanently lowering its critical current density [226].

During the last decades, several theories based on the CSM and the local adiabatic assumption were developed to explain flux-avalanche phenomena. Swartz and Bean [220] extended the CSM proposed by Bean [227] to include heating effect, presenting their adiabatic critical-state model. In 1996, Mints proposed an approach based on the Bean's model introducing the instability criterion $\delta W > \delta Q$, where δQ is the heat release due to the fluxon motion and δW is the additional heat flux due to a cryogenic coolant at the sample surface [228].

A lot of efforts have been made in order to reduce the flux-jump occurrence, both improving shield material properties such as grain structure or thermal conductivity [155, 224, 229] and its thermal contact with the coolant [229]. On the basis of computational approaches developed in the past few years [230–234], a numerical approach coupling the electromagnetic equations (Maxwell's equations) and the heat diffusion equation:

$$\nabla\left(\kappa\left(T\right)\cdot\nabla T\right) - C\left(T\right)\cdot\rho_m\cdot\frac{\partial T}{\partial t} + Q = 0 \qquad (30)$$

was successfully employed to predict flux jump occurrence, reproducing the experimental drop in the shielding factor [229]. In (30), $Q = \mathbf{E}\cdot\mathbf{J}$ gives the volumetric heating rate and $\kappa(T)$, $C(T)$ and ρ_m are the thermal conductivity, specific heat and mass density, respectively. However, addressing this topic involves several challenges. Firstly, to properly describe the evolution of this thermo-magnetic instability, the current density dependence on both the magnetic flux density **B** and temperature T should be considered [229], as well as the T-dependence of thermal conductivity and specific heat. This introduces significant non-linearities into the electromagnetic and thermal equations and requires the availability of advanced computation techniques to maintain numerical stability and accuracy. Additionally, accurate modelling requires the collection of extensive inputs on the material properties from experimental characterizations, which often provide incomplete or inconsistent datasheet, especially for complex SC materials [231]. Another critical aspect is the treatment of the thermal boundary conditions, particularly the heat exchange with the cryogenic coolant. Realistic modelling of these boundary conditions, which may include imperfect thermal contact, adds further complexity [235]. Furthermore, the transient and dynamic nature of flux jumps also demands high temporal resolution to capture rapid changes in magnetic flux and temperature distributions, leading to increased computational costs, particularly for 3D or large-scale models. Despite these challenges, recent advancements in computational methods and material characterization techniques hold promise for improving the accuracy and predictive capabilities of flux jump models, even allowing mechanical strain prediction [236], thus aiding in the development of more robust SC devices [237].

5. HTS bulk SC shields and screens

5.1. General considerations on bulk-based systems

HTSs are usually classified as bulks, thick films, thin films and CCs. Although their processing method differs from bulks, thick films are considered in the 'bulk' section (section 5) of this review. One of the reasons is that they can be deposited directly on geometries such as cylinders, cups or large plates, therefore resembling 'quasi-bulks'. In the framework of this review, thick films are defined as SC films obtained by processing methods that allow deposition on large or curved surfaces, i.e. mainly electrophoretic deposition [238], continuation detonation spray [239] or plasma spray [240], irrespective of their thickness. By contrast, thin films are deposited on very small planar substrates. Hence, except for some specific applications, e.g. enhancing the characteristics of an HTS SQUID magnetometer [241], thin films are rarely used as screens or shields; they will not be considered in this review. Finally, CCs are rather produced over long (> 1 m) lengths and narrow widths (typ. 10–12 mm) and will be considered in section 6.

SC bulks used as magnetic shields appear most of the time as hollow cylinders (or tubes) or semi-closed cylinders (or vessels or cups). For thick films, cylindrical substrates are often directly used or the shield can be shaped by deep drawing [242]. Magnetic shielding and screening has been demonstrated for various SC materials. This section summarizes some of the general conclusions which are valid irrespective of the nature of the superconductor, while the next subsections focus on the specificities of each material.

As explained in section 4.2, shielding properties are limited by (i) the field penetrating through the walls of the shield and (ii) the magnetic flux lines entering through the openings of the shield.

Considering only the field penetrating through the walls of the shield, shields with thick walls and high J_c have a larger B_{lim}, according to the Bean's model [150] (see section 4.2.3). More specifically, the important parameter is the *intergranular* J_c since the reduction of the magnetic flux density relies on macroscopic current loops taking place in the material. Hence, polycrystalline (or non-textured) and melt-textured shields have distinct advantages. On the one hand, textured shields are usually characterized by a larger B_{lim} than non-textured shields, for which the intergranular J_c is strongly field-dependent and much smaller than the intragranular J_c. On the other hand, one major advantage of polycrystalline bulks is that they can be significantly larger than a few cm. Regarding thick films, they can form large scalable shields and screens but are often characterized by a small B_{lim} due to their small thickness (typ. $< 200\,\mu$m) and their limited intergranular J_c.

Considering the flux lines entering through the openings of the shield, their influence depends on the AR of the shield: the larger the AR of the cylinder, the stronger the field attenuation around the centre [50] (see section 4.2.3 and figure 8(d)). For a hollow cylinder subjected to a uniform axial applied field, the axial field (resp. SF) along the axis of the cylinder is measured to increase (resp. decrease) roughly exponentially as one approaches the open ends [243], as suggested by (16).

In order to reduce the penetration of the flux lines through one of the openings, the shielding properties of semi-closed tubes have been studied. The shielding factor SF in small axial fields is significantly improved when comparing an open tube with a semi-closed tube. The region inside the shield near the closed extremity is often characterized by very large SF values [40]. The shielded volume is also increased in comparison with an open tube [196]. Also, the thicker the cap closing the tube, the better the shielding [195]. In practice, there are two possibilities for closing one extremity of a tube: a disk-shaped cap can be placed mechanically against the opening ('non-SC joint') or the bulk can be directly processed as a cup or a vessel ('SC joint'). The main impact of this difference appears in DC transverse applied fields. The non-SC joint prevents low-frequency shielding currents from flowing between the cap and the tube. Hence, flux lines can leak through the gap between both SC pieces, therefore decreasing SF by roughly one order of magnitude at the extremity [94]. On the other hand, the absence of non-SC gap allows the penetration of the flux lines through the closed extremity to be avoided but is not always possible depending on the application or processing difficulties.

Finally, several works measured the transverse and axial shielding properties of hollow cylinders and found out that B_{lim}(axial) is larger than B_{lim}(transverse) by a factor smaller than 2 because of demagnetizing effects [96] (see section 4.2.3 and (26)).

5.2. REBCO

Magnetic shielding and screening using (RE)$Ba_2Cu_3O_{7-\delta}$ materials, typically YBCO or GdBCO, has been demonstrated for both polycrystalline (or non-textured) and melt-textured bulks.

While magnetic shielding has been demonstrated in the RF (> 1 MHz) regime [244], most bulk REBCO shields have been studied at low frequency (or DC) and with the applied field parallel to their axis (axial field). In this context, table B1 in appendix B summarizes the main results that can be found in the literature.

The main results of the literature on REBCO highlight that, as expected, polycrystalline and thick film shields are larger and that melt-textured shields have a much higher B_{lim}. Fang *et al* [130] also showed that the noise attenuation is roughly one order or magnitude larger with melt-textured shields than with non-textured ones. Considering melt-textured shields, it should be kept in mind that for the tallest samples, J_c may be non-homogeneous: the closer from the seed, the larger J_c. Consequently, the shielding properties may not be symmetric with respect to the top and bottom ends of the tubular shield and the regions exhibiting the highest SF are located near the high-J_c parts [40, 195].

Due to their higher B_{lim}, using melt-textured REBCO shields is therefore mandatory for fields exceeding a few mT. Shielding at higher field was reported in tiny holes inside bulk superconductors [245] or in small gaps between two bulks, up to 11 T [246]. However, when considering shield sizes suitable for most applications, i.e. at least 1 cm-bore, the current

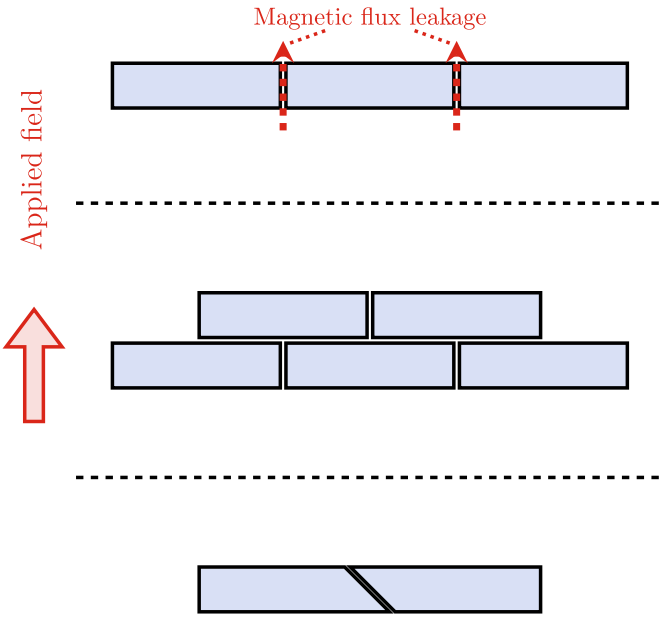

Figure 12. Schematic representation of different configurations studied in the literature to extend the surface area over which magnetic screening is effective.

record threshold field $B_{\rm lim}$ for YBCO cups at 20 K and in axial field orientation is around 1.5 T (considering the SF = 100 limit) [40].

Then, REBCO disks or plates, either bulk pellets or thick films can be used as magnetic screens. Some of the first screening experiments consisted in placing a non-textured YBCO disk between the primary and secondary coils of a transformer at 77 K. The disk therefore strongly reduces the flux density captured by the secondary coil up to applied fields of $\sim$1.7 mT [131] or $\sim$7.5 mT [247]. Similar experiments were reproduced with thick films, attenuating applied fields up to 0.7 mT for a 180 μm-layer deposited on a 45 $\times$ 45 mm stainless steel substrate [248]. SC YBCO disks can also be placed in a uniform applied field in liquid helium in order to evaluate the influence of the disk thickness on the screening [249].

One of the challenges in magnetic screening is to increase the surface area over which the flux density is (uniformly) attenuated. The first idea is to place side-by-side several bulks. The problem in this case is that the magnetic field is concentrated and leaks through the non-SC gaps, as shown schematically in the top panel of figure 12. To mitigate this problem, GdBCO or YBCO plates can be arranged in two [201] or three [250] layers by creating a staggered pattern or a 'brick-wall' arrangement (see middle panel of figure 12). Another solution is to juxtapose plates with trapezoidal cross-sections with a gap at 45° with respect to the applied field [202] (see bottom panel of figure 12). Note that the concentration of magnetic flux lines between two superconductors, depicted as a problem here, may be desired in some applications, e.g. some rotating machines [44, 251].

5.3. BSCCO

Shields or screens made of $Bi_2Sr_2Ca_{n-1}Cu_nO_{2n+4+x}$ materials are polycrystalline. In most cases, at 77 K, they have a smaller $B_{\rm lim}$ than their REBCO counterparts but large magnetic BSCCO shields are currently produced and commercially available [252].

Both Bi-2212 and Bi-2223 (the latter being often doped with lead (Pb) [253]) bulk shields have been characterized at low frequency in the literature. Table B2 in appendix B summarizes the main results for hollow cylinders. Additionally, Fagnard *et al* [254] characterized the penetration of a transverse field into a Bi-2212 hollow cylinder with two longitudinal slits. Magnetic shields were also built based on thick films made of Bi-2212 [138] or Bi-2223 [255]. Ichikawa *et al* [256] compared a Bi-2212 thick film cylinder with a Bi-2223 bulk tube for magnetic fault current limiter applications.

Compared to REBCO, BSCCO shields have two major differences: (i) at 77 K, they have a much stronger $J_{\rm c}(B)$ dependence even at fields smaller than a few tens mT and (ii) the n exponent of the typical E–J power law (14) is smaller. The three main consequences of the $J_{\rm c}(B)$ dependence are as follows.

- Usually, BSCCO shields are not suited for high fields at 77 K.
- The $B_{\rm in}(\mu_0 H_{\rm app})$ curve is measured to have a downward curvature [50, 107, 110, 129, 144, 257, 258], as explained in section 4.2.3, figures 8(b) and 9 or in [50, 107, 110]. Such a measurement gives a simple practical way to extract the $J_{\rm c0}$ and B_1 parameters of Kim's law (11).
- Increasing the wall thickness has a limited influence on $B_{\rm lim}$, which increases as the square root of the thickness (see (23) and figures 10 and 11) and not linearly as it would be the case for a field-independent $J_{\rm c}$.

The fact that the n-value is smaller for BSCCO materials (typ. around 25) than for REBCO has an important impact on the shielding properties, which can be expressed in two ways.

- The constitutive law $E \propto J^n$ gives rise to frequency scaling laws. After calculations [50], it yields that the shielding factor is invariant under scaling, i.e.

$$\mathrm{SF}\left(\mu_0 H_{\rm app}, f\right) = \mathrm{SF}\left(c^{1/(n-1)}\,\mu_0 H_{\rm app}, cf\right) \qquad (31)$$

  for any $c > 0$. In other words, at fixed applied field, SF increases with the frequency f and at fixed frequency, SF decreases with the applied field. For $n \to \infty$, SF is frequency independent (neglecting AC losses).
- Since the average $E \propto J^n$ in the walls of the shield is proportional to the sweep rate $\mu_0 \mathrm{d}H_{\rm app}/\mathrm{d}t$ (Faraday's law) and $B_{\rm lim}$ is proportional to the average J, the larger the sweep rate, the larger $B_{\rm lim}$ [96, 107, 110].

The two points above offer two different ways of determining experimentally n from shielding measurements, either with sinusoidal applied fields at several frequencies or with applied

fields ramped linearly [110]. Caution should be taken that the 'apparent' n-value obtained by these procedures is significantly larger than the real n obtained from flux creep measurement, which can then be retrieved provided that the $J_c(B)$ law is known [96, 110, 259].

Most of the previous conclusions as well as other general factors influencing the magnetic field penetration in BSCCO cylinders are thoroughly summarized in [97].

Even though J_c of BSCCO shields is strongly field-dependent and quite low compared to REBCO at 77 K, Bi-2212 shields can still be used for high fields by lowering the temperature. To our best knowledge, records B_{lim} for hollow cylindrical shields under a uniform axial applied field are around 1 T at 10 K [107] (SF = 1000) and 1.4 T at 4.2 K [145] (SF = 12 000).

Moreover, Hogan *et al* studied the behaviour of Bi-2223 cylindrical shields in an inhomogeneous magnetic field, either as an emission [99] or immunity [51] problem (following the definitions of section 2.1 and section 3). Such studies allow one to highlight the relative contributions of the penetration routes, the influence of the geometry of the shield on the measured properties and the main differences between homogeneous and inhomogeneous applied fields. The main conclusion is that shields subjected to inhomogeneous magnetic fields require additional considerations to be designed. The main reasons are that induced shielding currents cannot be predicted easily (e.g. they do not always flow in an azimuthal manner around the hole) and local magnetic field concentrations might occur and have a profound impact on the shielding properties.

Bi-2223 has also been used to build magnetic screens. The RF (> 1 MHz) screening properties of a plate with a slit were studied [260]. Similarly as what was done for REBCO, a large (40×40 mm^2) screen was built by jointing several plates with a SC paste and showed uniform screening up to 10 mT [261].

5.4. MgB_2

Thanks to its low production costs, non-toxic precursors, low weight, and long coherence length, magnesium diboride (MgB_2) has become a promising choice for bulk applications. Moreover, the improvement of the synthesis methods allows obtaining bulks with high weight density and critical currents, making MgB_2 suitable for high scale applications such as portable MRI, compact magnets or magnetic shielding devices, even for aerospace applications [39, 42, 262]. Focusing on shielding devices, the success of MgB_2 lies in its capability to be shaped into large and complex geometries that can fully enclose the device to be shielded, while ensuring good mechanical strength. Table B3 in appendix B summarizes the main results obtained with MgB_2 bulks.

Two synthesis process was found very promising for shields fabrication. MgB_2 shaped as cylinders or cups were synthesized using the reactive Mg liquid infiltration method [263]. This method was demonstrated to be effective for fabricating shielding devices, further supported by numerical simulations to optimize their design [58, 109]. These shields were successfully tested for protecting SQUID magnetic field sensor, showing significant reduction of ambient magnetic noise and interference [1, 264]. The record values of B_{lim} measured at the centre of a hollow cylinder are 1.1 T [109] and 2 T [39] at 4.2 K under an axial applied magnetic field. Very long hollow cylinders (450 mm long) exhibited B_{lim} values of 2.7 T [42] and 2.75 T [155] at 4.2 K under a transverse applied magnetic field (at our best knowledge no data in axial field are available on these layout).

MgB_2 bulks obtained by spark plasma sintering method also show promising shielding capability [265]. The samples were tested both in axial and transverse field configurations, to study the real working conditions of the shield. Gozzelino *et al* [41, 156] investigated cup- and tube-shaped bulks with AR close to one, highlighting the different shielding behaviour of the bulks with respect to the field orientation. In transverse orientation, shielding abilities are ensured up to 0.8 T at 20 K (SF = 40) and 0.1 T at 25 K (SF = 4.5) for cup- and tube-shaped bulks, respectively [41, 156]. In axial fields, the tube-shaped shield shows shielding ability up to 1 T at 25 K (SF = 160), while the cup-shaped bulk ensures shielding up to 1.8 T at 20 K (SF = 10 000) [156].

An important drawback affecting bulk MgB_2 shields, regardless of their synthesis process, is the thermo-magnetic instability occurrence, such as flux jumps, which degrade their shielding performance. This behaviour is primarily attributed to the specific heat per unit volume of MgB_2 being three orders of magnitude lower, while its thermal conductivity is approximately three times higher, compared to other materials such as REBCO bulks (at typical operating temperature of T = 15 K for MgB_2 and T = 40 K for REBCO). These properties suggest that, under identical heat generation, MgB_2 bulks are expected to experience a greater temperature rise, although the heat dissipates more rapidly [154]. The presence of such flux jumps, was reported in magnetic shielding experiments carried out by various research groups [42, 155, 224]. Nevertheless, experimental results have demonstrated a shielding capability of up to 1 T at 30 K and up to 1.8 T at 20 K in the closed extremity of the cup-shaped shield [41]. Being able to prevent and reduce flux-jump phenomenon is a key aspect of the optimization process of shielding devices. To this aim, a modelling approach allows finding out possible solutions to mitigate or prevent the flux jump occurrence (see section 4.3.2), for instance by improving the thermal properties of the material or the thermal exchange between the sample and the cryogenic environment [229].

Finally, it is worth mentioning that MgB_2 can also be deposited as thick films (6–13 μm). In recent years, promising results were obtained, employing MgB_2 films on different substrates, especially for shielding from low frequency electromagnetic noise [266–268].

6. HTS tape-based shields and screens

This section focuses on the magnetic shielding and screening properties of SC tapes. These can be either first-generation BSCCO tapes, consisting of multi-filament superconductors embedded in, most of the time, an Ag matrix, or 2G REBCO CC tapes. Mostly 2G CCs are used in the literature nowadays.

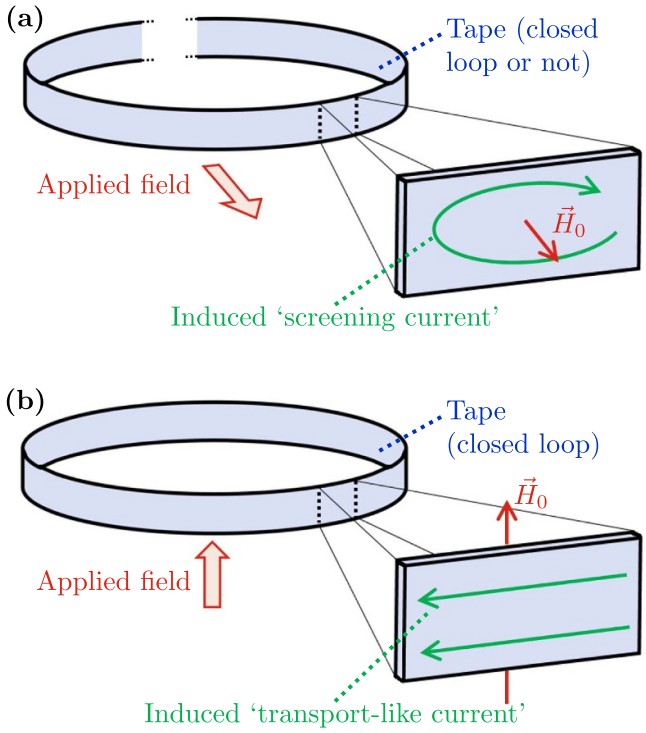

Figure 13. Schematic representation of the two categories of magnetic shields and screens made of 2G coated conductors considered arbitrarily in this review. (a) The applied field has a strong component perpendicular to the tape surface and 'screening currents' appear. (b) The coated conductor is wound into a closed loop embracing a varying flux; hence, a net induced current flows in the loop.

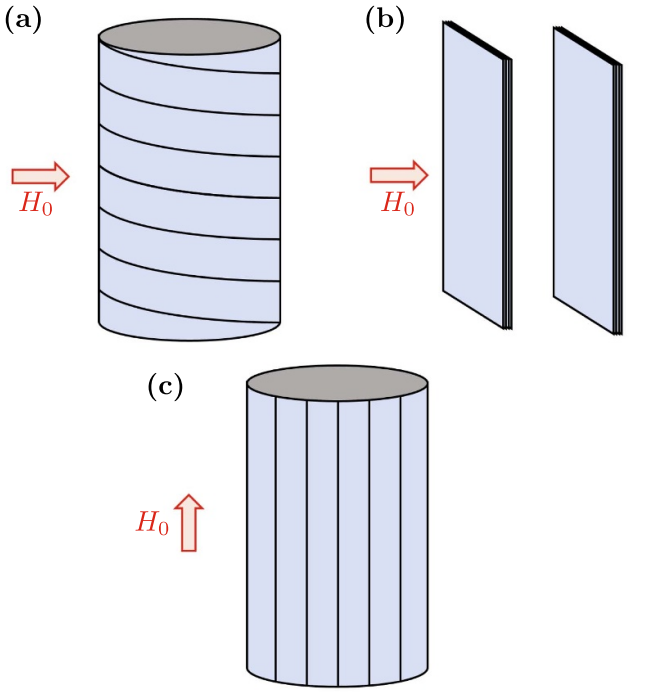

Figure 14. Schematic representation of the three families of tape arrangements to build shields based on screening currents.

By contrast with bulks, 2G CCs have the major advantage of being naturally scalable: they can regularly be processed over tens of meters. The SC layer is extremely thin (a few μm) and the tapes have a limited width, typically between 4 and 12 mm and up to 46 mm in some cases. A single CC, therefore, cannot be used as a large shield or screen in its natural shape: in order to create scalable structures, several tape segments should be arranged stacked or wound. These tape segments should be placed such that macroscopic current loops flowing into the material can oppose the applied field.

In this review, the magnetic shields and screens made of 2G CCs are classified in two categories, depending on the type of current induced in the CCs when subjected to a varying applied field. The two categories are illustrated schematically in figure 13. First (figure 13(a) and section 6.1), current loops may close themselves following a path that is partly along the width of the CC. These current loops are usually called 'screening currents' in magnet applications [74–82]. They typically appear when the main field to be attenuated has an important component perpendicular to the tape surface. In contrast with magnet applications where the term 'screening currents' refers to undesired currents that interfere with the main transport current in the tape, the current loops shown in figure 13(a) can be used advantageously to create magnetic screens, shields and cloaks. Second (figure 13(b) and section 6.2), the induced currents may have the same direction over the entire width of the tape, therefore resembling 'transport currents' even if they are magnetically induced in magnetic shielding and screening applications. Such currents take place when the CC forms a closed loop and a net varying flux is embraced by this closed loop. It should be pointed out that the difference between the two categories illustrated in figure 13 is somewhat arbitrary and may blur in some cases.

In addition, 2G CCs are deposited on a substrate, which is sometimes slightly FM. In this case, the shielding properties are modified, as discussed in section 6.3. Finally, magnetic shields or screens combining CCs and bulks are considered in section 6.4.

6.1. Arrangements based on 'screening currents'

Structures based on screening currents can be subdivided in three families that are schematically shown in figure 14.

The first family of shields (figure 14(a)) consists in surrounding the region to be shielded by several layers of CCs helically wound around a cylindrical former. The tape ends are not electrically connected. Such a structure has been studied in several works for transverse uniform applied fields typically below 100 mT and frequencies below a few hundred Hz. Most of the experiments are carried out in liquid nitrogen (77 K) [147, 269–272], but also at lower temperatures, down to 15 K [111, 128, 273]. Since the field attenuation relies on the appearance of current loops along the tape width, it is very beneficial to use wide tapes (e.g. 46 mm). The reason is that the maximum SF of these structures is primarily limited by the penetration of the flux lines around the structure and between

the tapes. A way to mitigate this problem is to stack the tape segments on several layers and to offset the layers by half the tape width such that the $(i+1)$-th layer covers the gaps of the i-th layer. This method is used in most of the references described below. The main results are summarized as follows.

- Such a shield is intrinsically scalable and can be made very large. Coils with a 50 mm-diameter [111, 128, 269, 273] and up to a 185 mm-height [147] have been investigated. For long coils, the main limiting factor for the shielding behaviour is the penetration of the flux lines from the gaps between each winding of the tape, which highlights the importance of offsetting successive layers.
- At 77 K, typical orders of magnitude for SF values range roughly between 10 and 100 can be obtained up to B_{lim} around a few (tens of) mT.
- At lower temperatures, J_{c} increases, hence B_{lim} increases. Consequently, for a given applied field above a few mT, SF increases with decreasing temperature.
- The higher the number of layers, the better the shield, as intuitively expected.
- The effect of the frequency on the shielding properties, even at a few hundred Hz, might not be negligible. It is, however, more difficult to predict and interpret than for bulks (see section 5.3). There are several reasons that explain why the frequency dependence may vary significantly from one shield to another. First, if the substrate is not too thin or is slightly FM, eddy currents may be induced in the substrate, increasing the screening effect. Second, these eddy currents or other regular AC losses may yield a local temperature increase (depending on the cooling power) that degrades the shielding behaviour. Finally, if the tapes constituting the coils are not insulated, screening currents forming larger loops and coupling several layers may appear depending on the contact resistance and the frequency.
- Such a coil structure has also been combined with FM layers, either to improve the shielding properties [269] or to use the tapes as the SC layer for practical cloaks [84, 86, 274] (see section 8.2). Note that in some cases, the tapes were also placed along the coil height (such as in figure 14(c) but in transverse field) [86, 274].

The second family (figure 14(b)) consists of a pair of planar SC sheets (or stacks) placed around the region to be shielded. The sheets are typically separated by a few cm. They are subjected to a low-frequency (a few Hz at most) uniform applied field perpendicular to their surface. Similarly to the previous family, such a structure was studied for a variable number of layers in each sheet, at different frequencies and at different temperatures [128, 271]. These planar sheets are also intrinsically scalable, i.e. they can be made very large provided that the presence of gaps is mitigated by offsetting successive layers, and can be combined with FM sheets [269]. In addition, the following results have been observed.

- Within each sheet, the influence of the interlayer distance (between 0 and 6 mm) was shown to have a relatively small effect on the shielding [275].
- Increasing the distance between the sheets may reduce significantly SF [272].
- The effect of a circular hole in one of the sheets on the shielding ability has been studied. The smaller the hole, the better the shielding. Also, such a hole can be compensated by the addition of a SC mask [276].
- It is known that stacked tapes are well suited for high fields as they can trap more than 17 T [277]. Similarly, magnetic shielding has been demonstrated at 4.2 K up to 11 T between two stacks of 12 mm-wide tapes [278].
- Sometimes, only part of the structure is used, i.e. one of the two sheets or stacks. For example, the screening properties of a single stack of 45 mm-wide tapes placed in a uniform applied field perpendicular to their surface have been investigated as a function of the number of layers in the stack, the frequency (up to 400 Hz) and the distance between the stack and the position where the measurements are taken [279]. Several 45 mm-wide tapes have also been successfully soldered and arranged as a 250 mm-long paraboloid in order to screen an inhomogeneous field [101].

The third family (figure 14(c)) consists of tape segments aligned with the applied field, e.g. around a cylindrical former. Such a structure is not ideal to reduce a uniform axial field [280] because currents cannot form a closed loop opposing the main field. However, such a structure may be of great interest to reduce one component of the field, e.g. in particle accelerator magnets or in electron cooling systems where the field homogeneity is extremely important. Although these applications are not *stricto sensu* 'shielding' as described in this review, they also rely on the appearance of screening currents. CCs arranged parallel to the main field direction can screen any radial component, therefore improving the field quality of the magnet [135, 136, 281]. Also, the structure shown in figure 14(c) was tested to limit the external magnetic field amplitude to which a cryocooler was subjected. In that case, the tapes were placed parallel to the cold-head axis in an axisymmetric inhomogeneous magnetic field [282].

6.2. Arrangements based on 'transport-like currents'

Creating a closed cylindrical or ring-shaped shield out of 2G CCs is not straightforward. Besides trials to build a continuously coated YBCO cylinder [283], mainly three methods can be used. They are schematically shown in figure 15.

The first method (figure 15(a)) consists in wrapping a tape into a loop and soldering it to create a closed loop, allowing induced 'transport-like' currents to flow. Several layers of these rings can be stacked [271, 284, 285]. Similarly, solenoids can be closed by a joint [108, 280]. In spite of impressive progress in soldering SC tapes [286, 287], the joint always has a finite resistance R at 77 K. Hence, in the AC regime, induced shielding currents are limited by both this resistance R and the self-inductance L of the current loop. Provided that $R \ll \omega L$, an applied magnetic field at a pulsation ω can be attenuated. In case of a sinusoidal applied field, shielding is only possible for frequencies above the cut-off frequency $f_{\mathrm{c}} = R/(2\pi L)$ of the equivalent $R-L$ circuit. Below this threshold, SF decreases

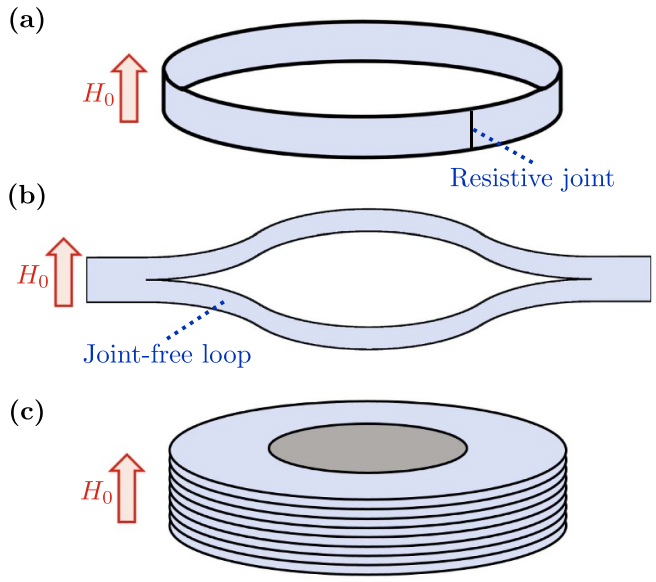

Figure 15. Schematic representation of the three families of tape arrangements to build shields based on transport-like currents.

rapidly [285]. For applied fields ramped up at a sweep rate dB_{app}/dt ($B_{app} = \mu_0 H_{app}$), the resistance of the joint renders magnetic shielding ineffective above a threshold magnetic flux density of the order of $\tau\, dB_{app}/dt$, where $\tau = L/R$ [108].

Consequently, in the DC regime or for very small sweep rates, an effective SC shield requires the existence of persistent current loops, i.e. with no joint, as shown in figure 15(b). Such a closed loop can be created by milling a slit in the middle of a CC segment to form a 'eye-shaped' closed SC loop, allowing persistent currents to flow [288, 289]. Both parts of the CC are extended around a cylindrical holder. This closed-loop structure can be used to create both magnetic shields [108, 290, 291] or permanent magnets [292–296], the latter demonstrating that such a structure is well suited for high fields. For cylindrical shields made of several stacked closed loops, one of the main results is that both SF and B_{lim} increase with increasing AR of the shield, similarly to HTS bulk tubes. At some point, the penetration through the gaps between the loops limits the improvements brought by a larger AR. Also, the higher the number of superimposed layers, the higher B_{lim}. Typical values that can be obtained at 77 K are a maximum SF around 100 and a SF larger than 10 up to $B_{lim} = 56$ mT [291].

Compared with HTS bulk tubes, cylinders made of CCs may have the following advantages: higher current density, good mechanical properties, better thermal stability thanks to the metallic substrate, lower weight, and easier scalability of the structure. However, by contrast with bulks, no 'saddle-shaped' currents can flow across the tapes, along the shield axis. Rather, the loops can only generate an induced opposed field parallel to their own axis. Consequently, cylinders made of closed loops are not suitable to shield transverse applied fields efficiently. Only 'screening currents' appearing along the tape width can reduce the transverse field (see section 6.1). For 'eye-shaped' structures, the distribution of shielding currents as a function of orientation of the applied field is more complex because of the vertical offset between both legs, as explained in [290]. Wéra *et al* [290] proposed a triaxial ('Polywell type') structure able to modestly attenuate the applied field almost independently of the direction.

An interesting trade-off exists in the choice of the coil diameter. If the coil diameter is small, the superconductor is closer to the region to be shielded and contributes more induced magnetic field. However, the induced current of such a small coil is not high, because the enclosed area (hence the flux) is relatively small. The opposite holds for a large coil. To solve the problem, two sets of concentric coils with properly chosen diameters can be connected in series such that the large outer coil provides an extra electric potential (because the surface is larger) to drive the small inner coil, which is closer to the region of interest. Gu *et al* built such a shield and obtained large SF values above 750 at 77 K for frequencies above 1 Hz and applied fields around 1 μT by soldering two BSCCO rings [141]. The shielded zone can be widened using a Helmholtz-like configuration instead of planar coils [297]. These configurations could be reproduced with no joint by specific cutting methods [298]. Also, the shielding ability can be improved by combining the coils with active shielding [6].

The last method to obtain closed current loops around the volume to be shielded is shown in figure 15(c). A disk is removed from the centre of wide square or circular tape segments, forming a set of annuli which are then stacked. This kind of structure has been used in the literature for magnetic shielding [92, 299], levitation [300] and for permanent magnets [301]. Brialmont *et al* [92] measured SF values above 3 up to 670 mT in axial field at 77 K with a stack of circular annuli (outer radius 22.5 mm, inner radius 13 mm, height 14.9 mm, 182 tapes). They also predicted that a 72 mm-high sample would show SF values around 30 000 at low fields and maintain SF > 10 over 0.9 T. The modelling of this shield, including the FM properties of the substrate, can be found in [212].

6.3. *Influence of a FM substrate*

In this section, we consider 2G CCs using Ni-based substrates that are slightly FM. The FM substrate influences the magnetic properties of shields. A few authors have measured the FM properties of the substrate, such as $B(H)$ data and magnetic losses at 77 K [302], the relative permeability μ_r and the AC losses at both room temperature and at 77 K [303], as well as $B(H)$ curves, μ_r, coercitive field and hysteresis losses at different temperatures between 77 K and room temperature [304].

A FM substrate has the following impacts.

- It decreases the reluctance path of magnetic flux lines. Consequently, the magnetic flux density is partly channelled in the FM substrate and magnetic flux concentration may occur in some parts of the shield.
- The skin depth decreases with increasing relative permeability of the substrate, allowing eddy currents to be induced in the FM substrate even at frequencies of a few hundred Hz. These eddy currents may contribute to the screening effect.

- The AC losses increase, both because of the concentration of the flux lines and the additional hysteretic losses. These losses can yield a local temperature increase affecting the critical current of the superconductor.

Brialmont *et al* detailed the effect of the FM substrate on the shielding properties of a stack of annuli [92]. The FM layers were found to have different effects depending on the direction of the applied field. In transverse fields, the FM nature of the substrate is beneficial since the transverse applied field was measured to be attenuated both at room temperature and at 77 K, which would not be the case for a non-magnetic substrate. In axial fields, it was shown that the larger the relative permeability μ_r of the substrate, the smaller the SF values. One of the reasons is that, instead of being fully expelled, the flux lines are attracted inside the sample because of the FM layers. In conclusion, the possible FM properties of the substrate should always be taken into account for a proper interpretation of the results.

6.4. Combination of bulks and tapes

Previous sections have shown that both bulks and CCs can be employed to build efficient magnetic screens and shields. Combining both of them may therefore be useful to benefit from their complementary advantages.

The idea of combining bulk and tape closed loops has already been explored in the literature in the context of trapped field magnet applications. The field trapped in HTS bulks decreases when subjected to crossed fields, i.e. fluctuating fields not aligned with the trapped field [305–307]. Hence, Yamagishi *et al* proposed to surround the bulk by a ring with a joint to use this ring as a shield strongly reducing the AC losses (and the trapped field reduction) in the bulk [134, 308–310]. Another example related to trapped field magnets using 'eye-shaped' closed-loop CCs. These can be combined to either stacked taped [311] or bulks [312] in order to increase the trapped field area, or to improve the uniformity of the magnetic flux density distribution with respect to the 'eye-shaped' loops alone [313].

When combining bulks and tapes to make magnetic shields, Bi-2223 tubes can be surrounded by soldered YBCO rings. In the AC regime, above a certain frequency, such a combination improves significantly B_{lim} in comparison with the bulk tube alone [129]. Regarding magnetic screens, joint-free closed loops surrounding a bulk with a slit have been shown to have the potential of compensating for the presence of this slit [314]. Also, a recent work demonstrated the DC screening ability of GdBCO disks combined with 'eye-shaped' closed GdBCO loops at 77 K and for an inhomogeneous applied field reaching 100 mT at the bottom surface of the bulk [102]. The addition of the loops allows the SF values to be almost doubled and the surface area of the screened region to be multiplied by ~ 4. Such significant improvements are due to the fact that the weakly penetrated bulk deflects the flux lines exactly where the closed loops can oppose them at best, i.e. close to them. Ways to scale-up even further (surface area of the screened region multiplied by ~ 9) is discussed in [315].

7. Low-T_c-based shields and screens

The use of low-T_c superconductors for magnetic shield fabrication has been pursued since the sixties. Although their use was reduced as a consequence of the discovery of high temperature superconducting cuprates and MgB_2, low-T_c superconductors are still used for specific applications thanks to the possibility of fabricating magnetic shields of large dimensions and complex shapes [12, 43, 60, 316, 317].

Type-I superconductors, such as lead (Pb) and tin (Sn) were successfully employed in magnetic shield fabrication. Lead foils exhibit good mechanical properties [148] (e.g. they do not easily tear upon being folded) and their edge can be sealed easily. These properties make Pb a good candidate for applications where a very low magnetic field background is required. Indeed, its bending properties make possible the 'shield expansion process' as described in [148]. Following this procedure, a shield made of a thin Pb foil is cooled tightly folded down below T_c ($T_c = 7.2$ K) under an applied field (FC process). During the cooling process, background magnetic flux lines can get pinned in the superconductors. Once cooled, the shield is opened to a cylinder: the magnetic flux lines pinned in the shield wall remains at the same position and a region with very low background field is then created. To further reduce the ambient field, the procedure can be repeated, unfolding another shield cooled inside the previous one [318]. In such a way, a very low magnetic field region ($B < 10^{-10}$ T) can be achieved. However, more recent investigations [319] evidenced some difficulties in controlling the pinning centre distribution in this material. Also, the use of Pb in Europe must now comply with the Restriction of Hazardous Substances Directive [320].

A Sn-coated copper (Cu) shell ($T_c = 3.7$ K) was used in [316] as a magnetic shield to reduce the AC magnetic noise in the setup employed for the detection of axions in the framework of the ABRACADABRA experiment [316, 317, 321]. To improve the magnetic shielding of the detector, the further addition of μ-metal shields was also proposed [321]. Further designs for the ABRACADABRA SC shield were numerically and analytically investigated in [322], always assuming the use of a type I superconductor and achieving promising results for a layout consisting of two semi-closed tubes inserted in one another.

Another LTS used for magnetic shielding is niobium (Nb) along with its SC alloy niobium-titanium (NbTi) and compound niobium tin (Nb_3Sn).

Nb is a type-I superconductor ($T_c = 9.3$ K) in the clean limit [323]—even though the presence of disorder forces it to become a type-II superconductor—characterized by a very high critical field, H_c [323] (or very high lower critical field, H_{c1}, when it behaves as a type-II superconductor [324]). Moreover, Nb sheets are easy to shear and bend. Screening properties of a Nb disk and ring and shielding properties of a Nb tube were investigated in [325] in the framework of the SAFIRE experiment. The aim was to create a very low magnetic field background for a SQUID-based detector, mitigating the magnetic field generated by the cooling system. In particular, the screens and shields were tested in an

inhomogeneous applied field and the thresholds above which deviations from a perfect diamagnetic behaviour occurred were highlighted [325].

The shielding ability of Nb tubes of different aspect ratios were investigated both experimentally and by computation in [12] in preparation of future precision experiments on atomic and antimatter physics. Particular attention was devoted to the minimization of the field trapped during the cooling process that could induce a non-negligible background field. To this aim, the authors proposed an annealing process of Nb to reduce the grain boundary pinning or the cooling of the shield in a temperature gradient. In addition, an SF improvement of two orders of magnitude was predicted by welding a Nb iris (i.e. a hole disk) at the open front end of the tube. In the same paper, the authors evidenced the better performance of Nb shields compared to Pb shields with similar AR at $T = 4.2$ K.

Thanks to its quite high value of H_{c1}, Nb shields also find applications in equipment for NMR investigations [326, 327]. In such a case, several challenges should be tackled. First, the shield has to solve a somehow 'mixed' emission/immunity problem by avoiding interference among the NMR solenoids and other close apparatuses sensitive to or producing magnetic fields. Second, the shield should not alter the homogeneity of the NMR field, which is ensured only as long as the SC shield works at fields lower than H_{c1}. Indeed, the field penetration inside the shield wall also modifies the NMR field.

NbTi is an alloy where Nb and Ti are in a ratio near 1:1 ($T_c = 9.2$ K). Although NbTi alloy shows lower values of T_c and H_{c2} than Nb_3Sn ($T_c = 18.3$ K), it is widely used because it is easier to manufacture, cost-effective and readily available.

Passive magnetic shields were manufactured by winding NbTi multi-filamentary wires whose critical current was high enough to allow shielding magnetic fields of 4 T [328] at 4.2 K. However, one of the most critical challenges of these structures is to electrically connect the wires so that permanent shielding currents can flow.

Okada *et al* [329] investigated the shielding properties of Nb–Ti–Zr–Ta multi-filamentary wires wound spirally (figure 16(a)) on a bakelite cylinder and impregnated with Wood's metal (e.g. Pb–Bi–Sn–Cd alloy). They found that this solder was more efficient than a Pb–Sn alloy, allowing the attenuation of an axial field of 0.5 T down to less than 10^{-3} T. A similar arrangement of NbTi multi-filamentary wires impregnated with Wood's metal was demonstrated to be able to shield axial fields up to 2 T, while exhibiting poor transverse field shielding ability [95]. Even better shielding results in axial field configuration were reported in [330], where a shield made of spirally wound NbTi wires impregnated with indium and with the same size as in [95] was found to shield magnetic fields up to 3.42 T. Conversely, the mitigation of transverse fields up to 1.1 T was reported by Takahata *et al* [95] using the tilted wound wire configuration sketched in figure 16(b).

More recently, a NbTi/Nb/Cu multilayer-based cylindrical shield was proposed by Barna *et al* [43, 155]. It could shield magnetic fields up to 3 T at 4.2 K, protecting the particle beams in the Future Circular Collider at CERN from the magnetic field of a septum magnet added to improve the beam clearance.

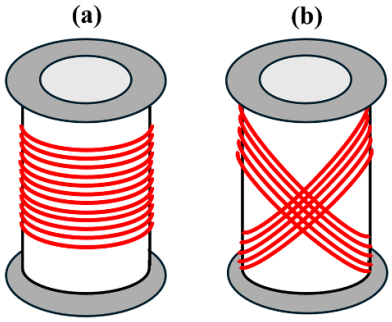

Figure 16. Schematic of the winding configurations compared in [95]: (a) wires wound spirally,(b) wires wound tilted at 45° with respect to the cylindrical support axis.

Notwithstanding its relatively high cost and the need for high-temperature heat treatments to form the SC phase [331], the Nb_3Sn compound is widely employed, thanks to its high critical temperature and upper critical field. However, a critical drawback of Nb_3Sn is the occurrence of flux jumps, which degrade the sample's shielding capability [223, 332, 333].

As shown by Benaroya *et al* [334], who investigated the screening properties of Nb_3Sn plates in transverse field orientation, flux jumps depend on the sweep rate ($\mu_0 dH_{app}/dt$) of the applied field. The authors identified a critical sweep rate with a value depending on the sample's thickness. For example, in the region between a couple of Nb_3Sn plates with a thickness of 0.318 cm, at $T = 4.2$ K the field was reduced by a factor of 11 up to 1.96 T provided that the sweep rate does not exceed $\mu_0 dH_{app}/dt = 2$ mT s^{-1}, above which the flux jumps may degrade the shielding effect. Assembling two cylindrical shells made of Nb_3Sn tapes positioned parallel to the tube axis, as described in [335], the occurrence of flux jumps was mitigated by using solder to bond the layers. This layout ensured shielding capability up to approximately 1.30 T at $T = 4.2$ K in a transverse field orientation.

8. SC-FM hybrid structures

The combined use of SC and FM materials has proven to be a winning strategy for manufacturing high-performance magnetic shields. It is worth mentioning that this is just one of the application areas where it is possible to take advantage of the magnetic properties of both SC and FM materials. Several studies have indeed shown the possibility to enhance SC vortex pinning via FM structure inclusions [336–338], to create magnetic guides and ratchets for SC vortices [339–341], or to reduce the AC losses in SC wires partially covered by FM structures [194, 342–345], among other outcomes. In addition, the exploitation of SC and FM material properties can provide promising results in quasi–static magnetic field trapping [146, 346–349] as well as in concentrating and transferring magnetic energy [350–352].

In this section, we deal with the effect of the superimposition of FM and SC bulk structures (section 8.1) also focusing on the possibility of cloaking DC and AC magnetic fields in suitably shaped SC/FM layouts (section 8.2). The effect of the

FM substrate on the shielding properties of tape-based structure was instead discussed in section 6.3 (except for magnetic cloak configurations, which will be discussed below together with the bulk structures).

For the sake of clarity, in this section the parameters that refer to FM and hybrid structures will have subscripts 'FM' and 'HY', respectively. In the absence of a subscript, the parameter is understood to refer to a SC structure.

8.1. Effects of FM layer and bulk shield addition

Superimposing one or more FM shells on a SC shield can modified the shielding ability of the latter in a non-trivial way. Indeed, FM materials, owing to their capability of concentrating the magnetic flux lines within themselves, should reduce the value of the magnetic field experienced by the superconductor, thus providing a shielding factor of the whole structure greater than that obtained with the SC shield alone [353]. However, attracting the magnetic flux lines within themselves, the FM materials can also induce a greater accumulation of the flux line at the shield open edges, which in turn results in a larger magnetic field entrance [354]. Consequently, the effectiveness of adding a FM layer should always be evaluated carefully.

Several studies focused on experimental and numerical investigations of cylindrical-shaped shields with an AR significantly larger than 1. All of them reported on an improvement of $B_{\rm lim}$ in axial-field orientation after superimposing FM structures on REBCO [355–358] and Pb-doped BSCCO [139, 356, 358–360] hollow cylinders as summarized in tables C1 and C2 in appendix C. Remarkably, depending on the SC and FM composition and size, enhancements of up to a factor of 100 were found [359]. In these papers, the experimental outcomes in correspondence of the shield centre agree well with the value given by the analytical approach:

$$B_{\rm lim,HY} = B'_{\rm lim} \times {\rm SF_{FM}} \tag{32}$$

where $B'_{\rm lim}$ is $B_{\rm lim}$ for the SC shield suitably modified to account for the lateral gap between the SC and FM tube and $\rm SF_{FM}$ is the FM shielding factor. Using the Bean's model to describe the superconductor behaviour, $B'_{\rm lim}$ takes the form

$$B'_{\rm lim} = B_{\rm lim}\frac{3R^2_{\rm in,FM} - \left(R^2_{\rm in} + R_{\rm in}R_{\rm out} + R^2_{\rm out}\right)}{3R^2_{\rm in,FM}}, \tag{33}$$

where $R_{\rm in}$ and $R_{\rm out}$ are the inner and outer radius of SC tube, respectively and $R_{\rm in,FM}$ is the inner radius of the FM tube. With just one superimposed FM tube, $\rm SF_{FM}$ reads as (22) if the end effects in the FM cylinder can be neglected; otherwise the formula was derived by Mager [167]

$${\rm SF_{FM}} = \frac{K}{2.6\sqrt{h_{\rm FM}/\left(2R_{\rm out,FM}\right)}}e^{2.25\frac{h_{\rm FM}}{2R_{\rm in,FM}}} \tag{34}$$

with K a correction factor determined experimentally, $h_{\rm FM}$ and $R_{\rm out,FM}$ the height and the outer radius of the FM tube, respectively. When several FM tubes—identical in height and composition—were superimposed on each other with no gap, (22) and (34) were still applied assuming the outer radius of the largest tube as $R_{\rm out,FM}$ and the inner radius of the smallest tube as $R_{\rm in,FM}$ [358]. Instead, in the case of FM cylinders of different composition or in the presence of an air-gap [139] between the FM shield lateral walls $\rm SF_{FM}$ takes the form:

$${\rm SF_{FM}} = \prod_{i=1}^{N}{\rm SF_{FM},}_i \tag{35}$$

where N is the number of FM layers and $\rm SF_{FM,}{}_i$ the shielding factor of the i-th layer. Note that:

- Keeping constant the height of the FM tube, $B_{\rm lim,HY}$ increases as the gap between the SC and FM lateral walls increases [360];
- $B_{\rm lim,HY}$ shows a non-monotonic behaviour as a function of the FM tube height: indeed, there is an optimal height $h_{\rm FM}$ of the FM tube for which the $B_{\rm lim,HY}$ vs. $h_{\rm FM}$ curve shows a maximum [355–357];
- Superimposing a FM tube on a SC tube is much more effective in increasing $B_{\rm lim}$ than superimposing two SC tubular shields [361];

Lousberg *et al* [353] numerically investigated an analogous structure consisting of two SC and FM coaxial hollow cylinders. They compared two configurations called 'Ferro-In' (with the FM tube placed inside the SC one) and 'Ferro-Out' (with the FM tube placed outside the SC one), keeping the dimension of the SC shield unchanged and focusing on the values of the $\rm SF_{HY}$ and $B_{\rm lim,HY}$ parameters at the shield centre. In both the configurations, they found that:

- The addition of the FM tube always improved the shielding factor, even though the 'Ferro-Out' allows achieving a higher $\rm SF_{HY}$ value, up to seven times greater than that of the single SC tube;
- $B_{\rm lim,HY}$ linearly increases with the thickness of the FM tube wall;
- In agreement with the experimental/analytically computed results reported in [355–357], the height of the FM tube strongly affects $B_{\rm lim,HY}$, which exhibits a maximum at $h_{\rm FM}/h = 0.4$, being h the height of the SC tube.

Remarkably, the shielding factor of the 'Ferro-Out' structure corresponding to the tube centre can be approximated by decomposing the contributions of the two shields:

$$SF_{\rm HY,FM-out} = SF_{\rm FM}\left(\mu_0 H_{\rm app}\right) \times SF\left(B_{\rm interf}\right) \tag{36}$$

where $B_{\rm interf}$ is the magnetic flux density at the interface between the FM and SC tubes. The separate contribution of the two shields can also be appreciated in the $B_{\rm lim,HY}$ equation, as in (32). This does not happen for the 'Ferro-In' configuration: in this case, the authors demonstrated that the FM shield, concentrating the flux lines internally, strongly modifies the magnetic flux distribution in the SC layer, making the separation of the contributions of the two shields impractical.

The same unfeasibility of separating the contributions of two superimposed SC and FM shells was found by Gozzelino *et al* [93, 354] that compared the shielding properties of open and semi-closed MgB_2 tubes alone and placed inside a soft-iron shield of similar shape (i.e. 'Ferro-Out' configuration). In this case, unlike the layouts mentioned above, the AR of both SC and FM shields was close to unity, making significant the magnetic flux penetration through the open end(s). Therefore, in the axial field orientation the addition of the FM shield induced a worsening in the shielding performance at low applied fields (due to a greater flux lines accumulation at the shield opening) and an improvement at high fields (due to the reduction of the magnetic flux density on the external wall of the SC shield). Creating a gap in height between the SC and FM shield open edges was reported to be a solution to reduce the effect of the flux line accumulation at the superconductor open edge and consequently the worsening in the shielding ability at low fields [197] (see also tables C3 and C4 in appendix C). Just splitting the bilayer in a multilayer layout—made up of two SC and two FM alternating semi-closed tubes with lateral wall and base thickness of each shell equal to half of those of the bilayer –, it was found a low-field SF_{HY} comparable to that calculated in the original SC shield without compromising the high-field SF_{HY} improvement [362].

Conversely, owing to the capability of high-permeability materials to more effectively attenuate transverse than axial magnetic fields [63, 166], the superimposition of a FM open or semi-closed tube on a SC one resulted in a significant improvement of the shielding factor in the transverse field orientation, even in layouts with small AR. In particular, placing an MgB_2 semi-closed tube in a soft-iron semi-closed tube was predicted to provide a SF_{HY} higher than 400 near the close extremity and higher than 100 in about half of the innermost volume of the SC shield at $T = 30$ K up to $\mu_0 H_{app} = 0.1$ T (see table C4 in appendix C and [93]). Moreover, since the shielding ability of SC shells with cylindrical symmetry and small AR strongly decreases when the field is not applied parallel to their axis [98], the addition of a FM shell can be an effective method to partially counterbalance this steep reduction, useful even when the external field is tilted by small angles (5–10°) out of the shield axis [163].

For MgB_2 shields, the addition of materials such as soft iron could also be valuable for mitigating the occurrence of magneto-thermal instabilities mentioned in sections 4.3.2 and 5.4. Namely, materials such as soft iron have a low-temperature specific heat higher that MgB_2. Therefore, by placing an MgB_2 semi-closed tube inside a FM shell in a tight thermal contact with each other, it is expected not only to improve the shielding properties of the whole structure but also to prevent flux jump occurrence. For example, in figure 17 we compare the magnetic flux density calculated at 30 K near the extremity of the MgB_2 semi-closed tube investigated in [229], with that predicted when the MgB_2 semi-closed tube is placed inside a FM shell, assuming an indium-layer-mediated thermal coupling between the two shields. A demonstration that flux jump occurrence can be suppressed significantly by a FM layer also comes from experiments carried out on bare

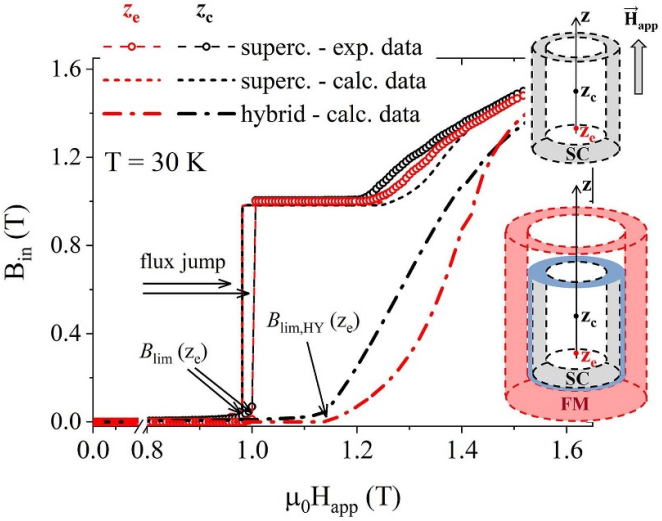

Figure 17. Comparison between the magnetic flux density values B_{in} measured (open symbols) and calculated (dashed lines) at two positions (z_e and z_c) along the axis of an MgB_2 semi-closed cylinder alone (inner radius: 7.0 mm, outer radius: 10.15 mm, inner depth: 18.3 mm, cap thickness: 4.2 mm) and placed inside a soft-iron semi-closed cylinder (inner radius: 11.5 mm, outer radius: 14.0 mm, inner depth: 26 mm, cap thickness: 2.5 mm—only calculated, dot–dashed curves). z_e is near to the closed extremity, z_c corresponds to the shield centre. The thermal contact between the two shields is ensured by an indium layer (turquoise detail in the picture). Details on the procedure followed to model the MgB_2 and soft iron shields are given in [229] and [93], respectively. Details on the modelling of the thermal contact via the indium layer are given in [229], as well.

and hybrid Nb_3Sn wires, the latter wrapped by FM layers of different thicknesses [363].

More complex layouts were investigated in [13, 60, 62, 72, 255, 364], all aimed at specific applications. The first three papers deal with shields for biomagnetic measurements. In [62, 72], the shield consists of two coaxial open-ended cylindrical shells, each of them composed by flexible Fe–Cu–Nb–Si–B nano-crystalline alloy sheets. The addition of two SC rings fabricated by soldering the ends of a BSCCO-2223 tape at each end of the cylindrical shield was proved to significantly reduce the axial field [62] and both the axial and transverse field if the tape is bent to form two double-D-shaped loops still placed at each open end of the cylinder [72]. In [255], the efficiency of differently shaped permalloy structures in improving the shielding properties of a BSCCO-2122 hollow cylinder of large dimensions were investigated to realize a low magnetic noise region ($SF \geqslant 10^7$) to measure the brain's magnetic field and other biomagnetic phenomena. In [60], Bergen *et al* reported on the development of a cryogenic shielding structure for housing TES based detector arrays working in space environment. It consists of an inner Nb shell placed inside a μ-metal (CryoPerm) shield, both made up of two elements suitably joined to avoid magnetic flux penetration, and provides an on-axis shielding factor greater than 10^6. A similar issue was addressed in [364] where the shielding capability of a triple shield consisting of a suitably shaped Nb shell placed inside a two FM shells was investigated in order to achieve a shielding configuration ensuring a homogeneous and low magnetic

field background in a region accommodating x-rays TESs and their read-outs. Another trilayer shielding structure consisting of three coaxial shells, the innermost made of NbTi and the two outermost of permalloy (cryoperm) was investigated in [13] with the aim to reduce the external magnetic field below 50 nT in order to create a magnetic environment suitable for testing a SC single-flux-quantum circuit chip.

8.2. Magnetic cloaks

Cloaking a static or quasi–static magnetic field, i.e. designing an object able to maintain a null interior field and an unperturbed external field, is easier than cloaking electromagnetic waves. For cloaking electromagnetic waves, both the magnetic permeability, μ, and the permittivity, ε, need to be controlled. Cloaking static or quasi–static magnetic fields requires only the control of the magnetic permeability, μ. In addition, it does not require engineering the materials involved down to the sub-wavelength scale of the considered wave. However, the target can only be achieved using metamaterials, i.e. materials with an anisotropic and inhomogeneous magnetic permeability.

In 2007, Wood and Pendry were the first to address the problem of designing a DC magnetic cloak [365]. Their model was based on the use of a metamaterial diamagnetic along one direction and paramagnetic along the perpendicular one. Focusing on the cylindrical geometry, this means the use of a material whose radial $\mu_{r,\rho}$ and angular $\mu_{r,\theta}$ relative permeability satisfy the conditions $\mu_{r,\theta} \gg \mu_{r,\rho}$ and $\mu_{r,\theta}\,\mu_{r,\rho} = 1$ [88]. Since no material with such magnetic properties is currently available, different metamaterials consisting of alternated SC and FM structures have been proposed.

A first approach consists in assembling an arrangement of SC and FM alternated coaxial cylindrical layers (labelled as *R*-type and *A*-type layers, respectively, in figure 18(a)). The former could consist of arrays of SC plates (figure 18(a), inset), which were demonstrated to provide a strong diamagnetic effect when the field is applied normal to the plates and a negligible effect when it is applied parallel to the plates [366], whereas an isotropic and homogeneous FM material could be used for the latter. This approach was adopted in [89] where a hollow cylindrical cloak was manufactured starting from Pb SC films evaporated on polyimide sheets and patterned so as to create rows of SC squares separated by normal channels. On the rear face of each polyimide sheet, multiple permalloy layers spaced by Cr layers were then evaporated. Finally, the sheets were superimposed on each other in such a way that the SC squares were not aligned and rolled to form a hollow cylindrical structure. The flux lines of an external magnetic field applied perpendicular to the cylinder axis expelled from the SC squares penetrate the SC layers through the channels between the SC squares. However, owing to the planes shift, the as-channelled flux lines encounter the second layer in correspondence to a SC square experiencing a distortion. This leads to the fulfilment of the condition $\mu_r \ll 1$ [367, 368]. On the other hand, the FM layers contribute to attracting and guiding the distorted magnetic flux-lines keeping the magnetic field inside the cloak equal to zero (figure 18(b)). This layout

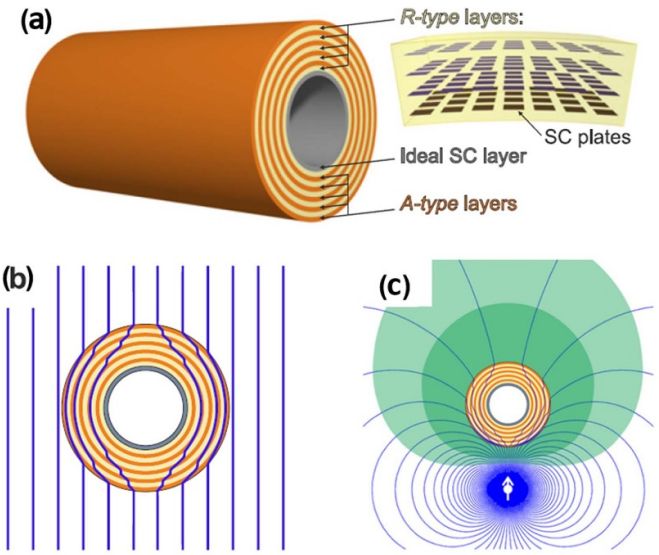

Figure 18. (a) Scheme of a magnetic cloaking device consisting of FM layers (labelled as *A*-type layers) and SC layers (*R*-type layers) patterned as arrays of SC plates (inset). The innermost layer is a homogeneous SC layer. (b) Flux line distribution calculated when a uniform field is applied perpendicularly to the axis of the cloak, which is composed of 5 *R*-type layers ($\mu_{r,\rho} = 0.104$), 5 *A*-type layers ($\mu_r = 6$) and an interior homogeneous SC layer whose permeability was assumed equal to zero. (c) Flux line distribution calculated when a magnetic dipolar source is placed outside the cloak. The device causes a magnetic distortion (evaluated as the difference between the total field and the dipolar source field) lower than 1% except for the light green region (where the distortion is between 1% and 3%) and the dark green region (where the distortion exceeds 3%). Reproduced from [88].

was successfully tested in a field of a few mT. Noteworthy, in such a structure $\mu_{r,\rho}$ can be tuned changing the geometrical arrangement of the SC plates [366–368].

Starting from such a cloak layout and in order to produce a real antimagnet (i.e. not only a magnetic cloak but a system able to fully confine the magnetic field produced by any magnetic element placed inside it—e.g. a permanent magnet), Sanchez *et al* [369] proposed the addition of a coaxial homogeneous SC layer at the inner surface, able to ensure a full magnetic decoupling between the regions inside and outside the cloaking device (labelled as ideal SC layer in figure 18(a)). To this aim, they modelled this additional layer assuming a null value for the permeability [88] and demonstrated that, fixing the number of layers and a relative permeability greater than 1 for the FM layers, it is always possible to find an optimal $\mu_{r,\rho}$ for the patterned SC layers (*R*-type layers, in figure 18(a)) that minimizes the magnetic field distortion [88]. The number of layers is irrelevant when the external field is uniform, whereas for non-uniform fields a higher number of layers provides smaller distortion (figure 18(c)).

However, when a uniform field is applied, even structures with a simplified design where all the SC layers (except the innermost) are replaced with non-magnetic isotropic materials (e.g. a plastic insulator) still work well [369]. In this case, still assuming null the SC permeability and considering the FM sheets as a unique layer, the non-distortion condition for

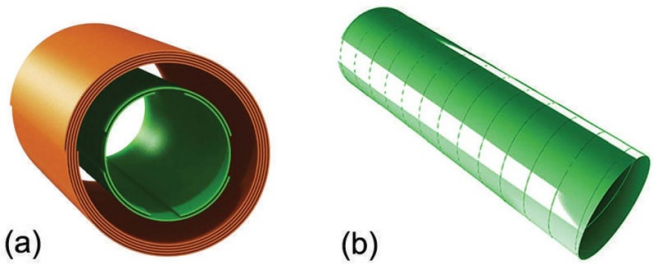

Figure 19. (a) Cross-section of a magnetic cloak consisting of two coaxial cylindrical shells: the inner shell is made of four SC strips oriented along the cylinder axis and assembled in an overlapping configuration, the outer shell is from a FM material. Reproduced from [199]. © IOP Publishing Ltd All rights reserved.; (b) sketch of a SC shell made of a coated conductor tape in double-helix geometry. Reproduced from [161]. © IOP Publishing Ltd All rights reserved.

a cylindrical cloak of infinite length implies that the relative permeability of the FM layer should take the suitable value

$$\mu_r = \frac{R_{\text{out,FM}}^2 + R_{\text{in,FM}}^2}{R_{\text{out,FM}}^2 - R_{\text{in,FM}}^2} \tag{37}$$

where $R_{\text{in,FM}}$ and $R_{\text{out,FM}}$ are the inner and outer radius of the shell. Actually, this structure still works as an antimagnet, provided that the applied field has small spatial variations and the central SC layer is kept in the ideal state [83]. Moreover, starting from a SC/FM bilayer and suitably choosing the value of the relative permeability of the FM layer in relation to the bilayer dimension, a spherical cloak can also be obtained [370]. Remarkably, the dimension of such magneto-static cloaks can be easily scaled up or down as required by the specific applications. The first cylindrical layout was experimentally built by Gomory *et al* [83]: the inner SC layer was obtained by wrapping two turns of REBCO tapes around a central bore while seven FeNiCr alloy layers alternated with Kapton layers constituted the FM shell, with an average relative permeability close to the theoretical value predicted by (37). The authors proved that such a layout properly works as a magnetic cloak at 77 K in an external transverse field of 40 mT, just exhibiting small deviations from the predicted behaviour due to its finite length. Longer layouts to reduce the end effects were successfully fabricated and tested [87, 199], demonstrating the ability to cloak magnetic fields up to 0.45 T [85]. Note that to maximize the shielding ability of the SC layer in transverse field, the SC stripes are oriented along the cylinder axis as sketched in figure 19(a). A bilayer cloaking structure was also proposed by Giunchi *et al* [224] with the use of an MgB_2 bulk tube as SC layer and of a mixture of Mg and Ni powder for the outer FM layer.

Remarkably, in the bilayer cloaking layout discussed above the inner SC layer was always assumed to be an ideal diamagnetic material. However, this assumption is never strictly true because even in the Meissner state the magnetic field partially penetrates the superconductor (e.g. to the London penetration depth in the case of a bulk superconductor) and in type-II superconductors the transition to the mixed state is expected even at low applied fields. Nevertheless, Yampolskii and Genenko demonstrated that a bilayer FM/SC hollow cylinder can still work as a magnetic cloak even though the superconductor is described through the London equations [371] or is already in the critical state [372].

Finally, the possibility of cloaking low-frequency (e.g. up to hundreds of Hz) AC magnetic fields was investigated [84, 86, 87, 199, 274, 373–375]. In this case, the cloaking device can modify both the amplitude and the phase of the external magnetic field. The compensation between the SC and FM permeability values can still ensure the non-distortion condition for what concerns the magnetic field amplitude, but the hysteretic behaviour of the used materials is additive and provides a phase change in the external magnetic field, causing the vanishing of the invisibility condition. Several approaches were proposed to overcome this bottleneck.

Solovyov *et al* [373] suggested choosing a low-loss FM material, such as Fe–Si–C–Cu–Nb polycrystalline ribbon. However, such an alloy has high magnetic permeability values, which means that (37) could not be fulfilled. Therefore, they also wrapped the bilayer cloak with an additional outer SC layer resulting in a reduced magnetic signature although only for very low applied fields [199]. The in-field behaviour of this AC bilayer cloak with and without the additional SC layer was also numerically investigated using the E–J constitutive law (15) to approximate the critical-state model and provided a remarkable agreement with the experiment outputs [199].

Other layouts consisting of a FM tube made of Zn-based ferrite powder in epoxy resin/plastic binder—whose relative permeability lower than 10 can be tuned by changing the ferrite powder concentration—and REBCO CC tapes for the inner SC layer were studied in [86, 274]. Different arrangements of the REBCO tapes were compared, the best one consisting of two tapes helically wound with opposite lay angles on a tubular former (figure 19(b)). This outcome, which would seem to disagree with the previous one obtained under the DC regime [85, 199], was justified by the fact that a SC tape arrangement as that of figure 19(a) requires a stronger tape bending, thus inducing crack formation that affects the AC losses [274]. Magnetic cloaks employing a BSCCO-2212 bulk tube and helically wound REBCO CC tapes are compared in [84]: even though the BSCCO-2212 bulk exhibits better shielding properties, its lower J_c provides much higher losses than tape-based arrangement.

Some of the above-mentioned layouts were also successfully employed in reducing the AC magnetic 'visibility' of copper (with large eddy currents) and iron cylinders placed inside the cloak bore [373, 374]. Demagnetization procedure to remove the Earth magnetic field trapped in the SC component of the cloak during the cooling process was developed as well [375].

9. Conclusions and future challenges

Shielding of low frequency magnetic fields is a key requirement to generate the ultra-low-field environment

needed for SQUIDs or for other magnetic-field sensitive devices used e.g. in biomedical or spatial applications. In addition, the development of high-performance SC applications requires an increase of their operating magnetic field. At fields levels of a few teslas, magnetic flux lines are no longer channelled in the iron yokes and efficient ways to screen the stray field are required. Although active magnetic shields offer suitable solutions, passive magnetic shields require no power supply and no current leads. Machines can therefore strongly benefit from passive shields in order to simplify their design and lower their total weight. The results summarized in this review give evidence that superconductors possess an exceptional ability for passive magnetic shielding or screening. Although the concept of using superconductors for low-frequency magnetic shielding is established for more than 6 decades, continuous progress is made both in terms of performances of the shields and of understanding the magnetic shielding mechanisms.

The first key conclusion from this review is that the ability of SC shields to operate above the saturation magnetization of conventional FM shields (0.7 T for μ-metal) has been demonstrated experimentally, both for low-T_c and high-T_c superconductors. For example, passive high-T_c SC bulk shields of bore size $>$ 1 cm were shown to be effective up to 2.75 T at 4.2 K for MgB_2, 1.4 T at 4.2 K for Bi-2212, 1.5 T at 20 K for YBCO. Second, there is no evidence that the 'record' values mentioned above are close to any sort of limit related to material properties. It is therefore expected that much progress in the threshold induction B_{lim} is possible in the next few years. The third conclusion is that all these compounds are strong candidates for passive shielding of high fields and that no preferred material really emerges. Similarly, 'bulk' materials, 'wires' and 'tapes' (HTS or LTS) all have their own advantages in terms of scalability or high field behaviour, and can be efficiently combined together. This variety of possible materials offers numerous avenues to further increase the performances of SC shields. Last but not least, the shielding mechanisms, including the magnetic field penetration routes and the limiting factors of SC shields, are now much better understood, thanks to the combined development of increasingly efficient numerical modelling tools and sensitive experiments.

In addition to the points above, the development of passive SC shields and screens requires to solve several challenges. The final goal is to increase the shielded volume or surface while sustaining significant field attenuation, and this when the shield experiences possibly high field amplitudes generated by large-scale devices.

In terms of the size of shields and screens, it is important to design shields or screens that are effective over distances of the order of 10–100 cm, in order to be compatible with the typical length of 'large scale' applications. Currently, most of the 'record' B_{lim} values are obtained over relatively small volumes of a few cm^3. Since the field is attenuated by macroscopic current loops, magnetic shielding would strongly be enhanced by developing large pieces of superconductors (large bulks, wide tapes), ideally with SC properties that are uniform over the whole sample. As an example, the development of large Bi-2223 vessels or large diameters REBCO disks goes in the right direction. Similarly, the increase of the shielded or screened volumes would strongly benefit from any method of joining superconductors. In particular, a successful method to join CCs and obtain significant persistent currents over large loops would be very beneficial for low-frequency applications.

In terms of maximum field that can be shielded, increasing J_c (or the critical current I_c for tapes) or lowering the temperature naturally yields higher operating fields, similarly to all engineering applications. In the context of magnetic shielding, however, an increase of B_{lim} may also arise by increasing the thickness of superconductors, as can be done for bulks, or simply stacking them, as can be done for bulks and tapes. There is therefore a need to design, test and validate thicker shields or screens operating at higher fields. These studies require to include thermal effects, to account for losses that arise from the time-changing flux density and to find ways to minimize the occurrence of flux jumps in bulk samples. At high fields, another challenge is the mitigation of the magnetic forces between the different parts of the device. Hence, future studies should also include mechanical aspects.

In view of practical applications, the fabrication of shields of custom-made (possibly complex) shape could be extremely helpful. In the literature, most studies were carried out on well-established geometries (tubes, cups, plates). These geometries are essential to understand as they can form building blocks for more complex ones, e.g. combining shields of different types to benefit of their advantages ('ferromagnetic—superconducting' or 'bulk—tape', amongst others). Another important point is to be able to characterize the shield or screen in conditions that are representative of practical applications, which include most of the time a sequence of inhomogeneous stray magnetic fields. There is therefore a need to investigate how currents are redistributed in the shield when submitted to fields of various directions and with different time dependences. The development of increasingly efficient 3D modelling techniques provides invaluable tools to predict the behaviour of shields of unusual shapes under various experimental solicitations. Finally, SC shields are expected to become the indispensable companion complementing future high-field devices operating at low temperature. Consequently, the shield is expected to rely on the same cryogenic system as the main device and the thermal aspects of the shield should be considered in the design. The design of integrated systems including all these features will be extremely helpful to develop efficient large-scale applications.

Data availability statement

All data that support the findings of this study are included within the article.

Acknowledgment

This manuscript is the result of an international collaboration strengthened by the support of the European Cooperation in Science and Technology (COST) action CA19108.

This work was partly supported by the Fonds de la Recherche Scientifique—FNRS under grant CDR n° J.0184.23. Nicolas Rotheudt is recipient of an FRS-FNRS Research Fellow grant.

Michela Fracasso acknowledges the support of the project Space It Up funded by the Italian Space Agency, ASI, and the Ministry of University and Research, MUR, under Contract No. 2024-5-E.0 - CUP n. I53D24000060005.

Appendix A. Analytical developments for an infinitely thin diamagnetic disk

This appendix details the computation of the magnetic field distribution around a thin SC disk of radius R in an external axial uniform field H_{app}. The computation is carried out assuming a perfectly diamagnetic material as explained in section 4.2.1. To simplify the expressions, oblate spheroidal coordinates are introduced. These coordinates are here $\eta \in [-1,1]$ and $\xi \in [0,+\infty[$. Their relationship with cylindrical coordinates (r,z) writes

$$r = R\sqrt{(1+\xi^2)(1-\eta^2)}, \tag{A.1}$$

$$z = R\xi\eta. \tag{A.2}$$

Taking inspiration from Claycomb and Miller [63], the magnetic field is computed as $\mathbf{H} = -\nabla\Omega$, where Ω is a scalar function. Laplace's equation $\Delta\Omega = 0$ with appropriate boundaries conditions imposing perfect diamagnetism yields

$$\Omega = H_{\text{app}} R\eta \left(\frac{2}{\pi}\left[\xi \cot^{-1}(\xi) - 1\right] - \xi\right). \tag{A.3}$$

The gradient of (A.3) can be calculated as

$$\mathbf{H} = H_{\text{app}}\eta\sqrt{\frac{1+\xi^2}{\eta^2+\xi^2}}\left(1 - \frac{2}{\pi}\cot^{-1}(\xi) + \frac{2}{\pi}\frac{\xi}{1+\xi^2}\right)\hat{\boldsymbol{u}}_{\boldsymbol{\xi}} + H_0\sqrt{\frac{1-\eta^2}{\eta^2+\xi^2}}\left(\xi + \frac{2}{\pi} - \frac{2}{\pi}\xi\cot^{-1}(\xi)\right)\hat{\boldsymbol{u}}_{\boldsymbol{\eta}}, \tag{A.4}$$

where $\hat{\boldsymbol{u}}_{\boldsymbol{\xi}}$ and $\hat{\boldsymbol{u}}_{\boldsymbol{\eta}}$ are the unit vectors in oblate spheroidal coordinates. These can be computed as

$$\hat{\boldsymbol{u}}_{\boldsymbol{\xi}} = \frac{1}{\sqrt{\eta^2+\xi^2}}\left(\xi\sqrt{1-\eta^2}\,\hat{\boldsymbol{u}}_{\boldsymbol{r}} + \eta\sqrt{1+\xi^2}\,\hat{\boldsymbol{u}}_z\right), \tag{A.5}$$

$$\hat{\boldsymbol{u}}_{\boldsymbol{\eta}} = \frac{1}{\sqrt{\eta^2+\xi^2}}\left(-\eta\sqrt{1+\xi^2}\,\hat{\boldsymbol{u}}_{\boldsymbol{r}} + \xi\sqrt{1-\eta^2}\,\hat{\boldsymbol{u}}_z\right), \tag{A.6}$$

where $\hat{\boldsymbol{u}}_{\boldsymbol{r}}$ and $\hat{\boldsymbol{u}}_z$ are the unit vectors of the cylindrical coordinates. By injecting (A.5) and (A.6) into (A.4), the magnetic field can be written in terms of radial and axial components as $\mathbf{H} = H_r\hat{\boldsymbol{u}}_{\boldsymbol{r}} + H_z\hat{\boldsymbol{u}}_z$ with:

$$H_r = \frac{-2H_{\text{app}}\eta}{\pi(\eta^2+\xi^2)}\sqrt{\frac{1-\eta^2}{1+\xi^2}}, \tag{A.7}$$

$$H_z = H_{\text{app}}\left(1 - \frac{2}{\pi}\cot^{-1}(\xi) + \frac{2}{\pi}\frac{\xi}{\eta^2+\xi^2}\right). \tag{A.8}$$

For $r = 0$, one can check easily that (A.7) is zero and (A.8) simplifies into (17).

Appendix B. Properties of HTS bulk shields studied in the literature

This appendix summarizes the shielding properties of bulk samples or thick films with cylindrical shape made of REBCO (axial field only, table B1), BSCCO (table B2) and MgB_2 (table B3).

Table B1. Summary table reporting the threshold field, B_{lim}, for REBCO. The shields are open ('Open': inner radius R_{in}, outer radius R_{out} and height h) or semi-closed tubes ('Semi-closed': inner radius R_{in}, outer radius R_{out} and inner depth h) placed in a uniform axial field. B_{lim} is either given by the authors or estimated from the data. The 'Location' column indicates where the field was measured: at the centre of the tube ('Centre') or close to the inner wall of the closed extremity ('Extremity'). 'NR' stands for 'Not Reported'.

RE	Structure	T (K)	R_{in}—R_{out}—h (mm)	Shape	Location	B_{lim} (mT)	References
Y	Polycrystalline bulk	77	8—10—100	Open	Centre	0.7	[376]
Y	Polycrystalline bulk	77	12.5—15—130	Semi-closed	Centre	1.6	[377]
Y	Polycrystalline bulk	77	2.5—4.4—23	Open	Centre	1.8	[144]
Y	Polycrystalline bulk	77	4.8—6—55	Open	Centre	1.9	[378]
Y	Polycrystalline bulk	77	7.25—9.7—112	Semi-closed	Centre	2.7	[379]
			10.4—13.3—125		Extremity	3.6	
Y	Polycrystalline bulk	5	5—11—87.7	Open	Centre	4	[380]
Y	Polycrystalline bulk	80	4—6.4—6.5	Open	Centre	2.8	[381]
		< 20				8	
Y	Polycrystalline bulk	75	4.5—7.8—50	Open	Centre	2.8	[382]
		4				10	
Y	Polycrystalline bulk	77	4.8—6—100	Open	Centre	2.3	[383]
		4				10.5	
Y	40 μm-thick film on Ag[a]	77	10—NR—100	Open	Centre	0.22[c]	[133, 384, 385]
Y	100 μm-thick film on Ag[a]	77	6.5—8—80	Open	Centre	1.3	[386]
Y	40 μm-thick film on Ag[b]	77	9.5—10—200	Open	Centre	0.1	[387]
		4				1.2	
	75 μm-thick film on Ag[b]	77	9.5—10—200	Open	Centre	0.15	[387]
		4				1.4	
Y	150 μm-thick film on Ag[a]	77	6.5—8—80	Open	Centre	1.9[d]	[388]
		20				8.2[d]	
Y	Melt-textured bulk	77	3.5—8—20	Open	Centre	200	[389]
Gd	Melt-textured bulk	77	3.9—15.6—13.3	Open	Centre	80[c]	[195]
			+8.4 mm-thick cap	Semi-closed	Centre	175[c]	
					Extremity	234[c]	
Gd	Melt-textured bulk	77	5—16—13	Open	Centre	400	[390]
Y	Melt-textured bulk	77	7.4—11.8—30	Semi-closed	Extremity	155[c]	[40]
						225[d]	
		20				1520[c]	
						2400[d]	

[a] using electrophoretic deposition.
[b] using continuation detonation spray.
[c] for SF= 100.
[d] for SF= 10.

Table B2. Summary table reporting the threshold field, B_{lim}, for BSCCO shields. All the shields are open tubes (inner radius R_{in}, outer radius R_{out} and height h) placed in a uniform axial field ('Axial') or transverse field ('Transverse'). B_{lim} is either given by the authors or estimated from the data and the measurements were taken at the shield's centre. 'NR' stands for 'Not Reported'.

Phase	T (K)	R_{in}—R_{out}—h (mm)	Direction	Sweep rate (mT s^{-1})	B_{lim} (mT)	References
2223	77	2.9—5.5—30.4	Axial	NR	1	[391]
2223	77	8.5—11.5—123	Axial	NR	2	[144]
2223	77	15.35—17.4—28.4	Axial	NR	5	[392]
2223	77	5.5—8.5—29	Axial	NR	5.4	[393]
2223	77	13.1—15.3—142	Axial	NR	6	[139]
2223	77	10.5—12.1—80	Axial	0.03	6.4[a]	[51]
2223	77	10.5—12.25—80	Axial	0.1	6.8[a]	[94]
2223	77	5—6.5—80	Axial	NR	8	[257]
			Transverse		5	
2223	77	5—6.6—80	Axial	NR	14	[129]
2223	77	6.5—8—80	Axial	0.2	14	[50]
2223	77	6—7.6—80	Axial	0.01	12.7[b]	[96]
				1	14.1[b]	
			Transverse	0.01	7.8[b]	
				1	8.4[b]	
2223	77	6—7.6—80	Axial	0.02	13.5[a]	[110]
				0.2	14[a]	
				2	14.9[a]	
				20	15.9[a]	
2223	77	2.95—4.75—23	Axial	NR	27	[258]
2212	77	8—13—80	Axial	0.05	18.5[b]	[97]
				0.5	22.5[b]	
				2	27[b]	
			Transverse	0.05	12.5[b]	
				0.5	16[b]	
				2	18.7[b]	
2212	70	8—13—80	Axial	0.125	46[b]	[107]
	40				320[b]	
	10				1000[b]	
2212	4.2	21.5—25—150	Axial	NR	1400	[145]

[a] for SF= 100.
[b] for SF= 1000.

Table B3. Summary table reporting the threshold field, B_{lim}, for MgB_2 shields. The shields are open ('Open': inner radius R_{in}, outer radius R_{out} and height h) or semi-closed tubes ('Semi-closed': inner radius R_{in}, outer radius R_{out} and inner depth h) placed in a uniform axial field ('Axial') or transverse field ('Transverse'). B_{lim} is either given by the authors or estimated from the data. The 'Location' column indicates where the field was measured: at the centre of the tube ('Centre') or close to the inner wall of the closed extremity ('Extremity').

T (K)	R_{in}—R_{out}—h (mm)	Direction	Shape	Location	B_{lim} (T)	References
4.2	7.5—12.5—15	Axial	Open	Centre	1.1	[109]
4.2	9—17.75—70	Axial	Open	Centre	2	[39]
4.2	16.2—24.5—450	Transverse	Open	Centre	2.7	[42]
4.2	16.2—24.5—450	Transverse	Open	Centre	2.75	[155]
15	10.5—18.5—27.9	Axial	Open	Centre	2.05[a]	[225]
25	7—10.15—17.5	Axial	Open	Centre	1	[156]
		Transverse			0.2	
30	7—10.15—18.3+4.2 mm-thick cap	Axial	Semi-closed	Extremity	1[a]	[41]
30	7—10.15—18.3+4.2 mm-thick cap	Transverse	Semi-closed	Extremity	0.8	[41]

[a] the highest treshold field before a flux jump occurrence.

Appendix C. Properties of hybrid shields studied in the literature

The first three tables in this appendix summarizes B_{lim} values measured or calculated in hybrid layouts consisting of SC and FM superimposed bulk shells with cylindrical shape. For the sake of readability, data concerning hybrid layouts with SC component made of REBCO are listed in table C1, data concerning hybrid layouts with SC component made of BSCCO are listed in table C2 and data concerning hybrid layouts with SC component made of MgB_2 are listed in (table C3).

The last table (table C4) sums up some shielding factor values achieved on MgB_2/FM hybrid cylindrical structures.

Table C1. Summary table reporting the threshold field, B_{lim}, for hybrid configurations combining YBCO (SC) with ferromagnetic (FM) shells. All the shields are open tubes (inner radius R_{in}, outer radius R_{out} and height h) placed in a uniform axial field. B_{lim} is either given by the authors or estimated from the data and was measured/calculated at the shield's centre. Letters between parentheses are used to designate a certain layer which is used in different rows. When more than one FM shield is superimposed, the dimensions always refer to the outermost FM shield.

T (K)	SC structure	FM layer	R_{in}—R_{out}—h (mm)	B_{lim} (mT)	References
77.4	Bulk	—	2.5—4.5—19	1.9	[355–358]
		Iron (A)	6—8—35	53	[355, 357]
		Iron (B) + A	10.5—12.5—51	90	[355, 357]
		Iron	10—12—75	12	[356]
		Steel	10—20—75	47.5	[356]
		Permalloy I (C)	12.5—13—100	3.6	[358]
		Permalloy II (D) + C	13—13.5—100	6.2	[358]
		Amorphous metal (E) + D + C	17—21—100	25.0	[358]
		Soft iron I (F) + E + D + C	23.8—24.5—100	41.0	[358]
		Soft iron II (G) + F + E + D + C	28.6—30.2—100	59.0	[358]
77.4	Thick film	—	5.75—5.82—114	0.08	[391]
		Permalloy I (H)	12.5—14.5—100	9.5	[391]
		Permalloy II (J)	12—12.5—100	2.2	[391]
		Amorphous metal (K)	17—20—60	0.12	[391]
		H + J + K	—	12.8	[391]

Table C2. Summary table reporting the threshold field, B_{lim}, for hybrid configurations combining BSCCO (SC) with ferromagnetic (FM) shells. All the shields are open tubes (inner radius R_{in}, outer radius R_{out} and height h) placed in a uniform axial field. B_{lim} is either given by the authors or estimated from the data and was measured/calculated at the shield's centre. Letters between parentheses are used to designate a certain layer which is used in different rows. When more than one FM shield is superimposed, the dimensions always refer to the outermost FM shield.

T (K)	Phase	FM layer	R_{in}—R_{out}—h (mm)	B_{lim} (mT)	References
77.4	2223	—	2.9—10.5—30.4	0.98	[358, 359, 391]
		Permalloy I (A)	12.5—14.5—100	10.8	[391]
		Amorphous metal (B)	17—20—60	2.9	[391]
		A + B	—	12.3	[391]
		2°Soft iron	6.8—9.6—60	30.4	[359]
		6°Soft iron	6.8—15.5—60	30.4	[359]
		Permalloy I (C)	12.5—13—100	3.4	[358]
		Permalloy II (D) + C	13—13.5—100	5.6	[358]
		Amorphous metal (E) + D + C	17—21—100	21.5	[358]
		Soft iron I (F) + E + D + C	23.8—24.5—100	36.0	[358]
		Soft iron II (G) + F + E + D + C	28.6—30.2—100	52.0	[358]
77.4	2223 (H)	—	2.9—5.9—30	0.98	[361]
	2223 (J)	—	8.67—11.7—30	1.17	[361]
	H + J	—	—	1.7	[361]
		Soft iron (K) (on H + J)	13—20—65	32	[361]
		Soft iron (L) + K (on H + J)	15.55—17.5—65	60	[361]
77.4	2223	—	8.5—11.5—30	1.25	[356]
		Iron	10—12—75	27.5	[356]
77.4	2223	—	13—15.5—141	16	[394]
		Soft iron (5 coaxial tubes)	28.7—29.9—257.9	46	[394]
77.4	2223	—	13.1—15.3—142	15.5	[139, 360]
		Soft iron	36.6—38.2—180	29.5	[360]
		Soft iron	17.5—19.1—180	24.4	[139]
		Soft iron (4 coaxial tubes)	28.7—30.3—180	61.0	[139]
77	2223	—	6—7.6—80	14.04	[353]
		FM-in	4—5—80	18.7	[353]
		FM-out	7.6—8.6—80	27	[353]

Table C3. Summary table reporting the threshold field, B_{lim}, for hybrid configurations combining MgB_2 (SC) with ferromagnetic (FM) shells. The shields are open ('Open': inner radius R_{in}, outer radius R_{out} and height h) or semi-closed tubes ('Semi-closed': inner radius R_{in}, outer radius $R_{out}$and inner depth h) placed in a uniform axial field. B_{lim} is either given by the authors or estimated from the data. The 'Location' column indicates where the field was measured or calculated: at the centre of the tube ('Centre') or close to the inner wall of the closed extremity ('Extremity').

T (K)	SC	FM layer	R_{in}—R_{out}—h (mm)	Shape	Location	B_{lim} (T)	References
25	MgB_2	—	7—10.15—17.5	Open	Centre	0.63	[93, 156]
		Soft iron	11.5—14—10.5	Open	Centre	0.50	[93]
30	MgB_2	—	7—10.15—18.3 +4.2 mm-thick cap	Semi-closed	Extremity	0.94	[93, 156]
		Soft iron	11.5—14—22.5 +2.5 mm-thick cap	Semi-closed	Extremity	1.02	[93]
		Soft iron	11.5—14—26.0 +2.5 mm-thick cap	Semi-closed	Extremity	1.07	[93]

Table C4. Summary table reporting the shielding factor, SF, for hybrid configurations combining MgB_2 (SC) with ferromagnetic shells (FM). The shields are semi-closed tubes (inner radius R_{in}, outer radius R_{out} and inner depth h) placed in a uniform axial field ('Axial') or transverse field ('Transverse'). SF is either given by the authors or estimated from the data in correspondence to the applied field shown in brackets. The 'Location' column indicates where the field was measured or calculated: at the centre of the tube ('Centre') or close to the inner wall of the closed extremity ('Extremity').

T (K)	SC	FM layer	R_{in}—R_{out}—h (mm)	Direction	Shape	Location	SF (B_a (mT))	References
20	MgB_2	—	7.5—10.5—7.5 +3.0 mm-thick cap	Axial	Semi-closed	Extremity	58 (0.1 T) 4.3 (0.8 T)	[354]
		soft iron	11.5—14—10.5 +2.0 mm-thick cap	Axial	Semi-closed	Extremity	45 (0.1 T) 12.5 (0.8 T)	[354]
30	MgB_2	—	7—10.15—18.3 +4.2 mm-thick cap	Axial	Semi-closed	Extremity	30 500 (0.2 T) 5000 (0.95 T[a])	[93]
		Soft iron	11.5—14—22.5 +2.5 mm-thick cap	Axial	Semi-closed	Extremity	22 000 (0.2 T) 8300 (0.95 T)	[93]
		Soft iron	11.5—14—26 +2.5 mm-thick cap	Axial	Semi-closed	Extremity	25 500 (0.2 T) 11 300 (0.95 T)	[93]
30	MgB_2	—	7—10.15—18.3 +4.2 mm-thick cap	Transverse	Semi-closed	Extremity Centre	50 (0.1 T) 10 (0.1 T)	[93]
		Soft iron	11.5—14—22.5 +2.5 mm-thick cap	Transverse	Semi-closed	Extremity Centre	175 (0.1 T) 35 (0.1 T)	[93]
		Soft iron	11.5—14—26 +2.5 mm-thick cap	Transverse	Semi-closed	Extremity Centre	450 (0.1 T) 90 (0.1 T)	[93]

[a] the highest applied field before a flux jump occurrence.

ORCID iDs

Nicolas Rotheudt https://orcid.org/0000-0001-5164-703X
Michela Fracasso https://orcid.org/0000-0002-6339-4188
Philippe Vanderbemden https://orcid.org/0000-0002-1436-7116
Laura Gozzelino https://orcid.org/0000-0002-9204-0792

References

[1] Giunchi G, Bassani E, Cavallin T, Bancone N and Pavese F 2007 *Supercond. Sci. Technol.* **20** L39
[2] Pourrahimi S, Williams J, Punchard W, Tuttle J, DiPirro M, Canavan E and Shirron P 2008 *Cryogenics* **48** 253–7
[3] Wu B, Wang Z, Cheng B, Wang Q, Xu A and Lin Q 2014 *Metrologia* **51** 452
[4] Yu K K *et al* 2014 *Supercond. Sci. Technol.* **27** 105007
[5] Körber R *et al* 2016 *Supercond. Sci. Technol.* **29** 113001
[6] Wang S, Wang S, Yu X, Xu H, Li Y, Jiang H and Sun K 2023 *Supercond. Sci. Technol.* **36** 035001
[7] Delso G and Ziegler S 2009 *Eur. J. Nucl. Med. Mol. Imaging* **36** 86–92
[8] Burigo L N and Oborn B M 2019 *Phys. Med. Biol.* **64** 215015
[9] Mariscotti A 2021 *Energies* **14** 6789
[10] Hartwig V, Sansotta C, Morelli M S, Testagrossa B and Acri G 2022 *Int. J. Environ. Res. Public Health* **19** 7674
[11] Brandl M *et al* 2016 *Rev. Sci. Instrum.* **87** 113103
[12] Hinterberger A, Gerber S and Doser M 2017 *J. Instrum.* **12** T09002
[13] Wei L, Wang G, Li J, Zhang S and Hong G 2021 *J. Instrum.* **16** 04007
[14] He S and Zheng J 2024 *IEEE Trans. Appl. Supercond.* **34** 3602504
[15] Visser L *et al* 2024 Two-stage magnetic shielding for hybrid quantum devices in an adiabatic demagnetization refrigerator *Silicon Quantum Electronics Workshop 2024* (*Davos, Switzerland*, *4th-6th September 2024*) (available at: https://juser.fz-juelich.de/record/1037143)
[16] Battiston R, Burger W J, Calvelli V, Datskov V I, Farinon S and Musenich R 2013 *IEEE Trans. Appl. Supercond.* **23** 4101604
[17] Spillantini P 2010 *Adv. Space Res.* **45** 900–16
[18] Spillantini P, Taccetti F, Papini P and Rossi L 2000 *Nucl. Instrum. Methods Phys. Res.* A **443** 254–63
[19] Spillantini P, Casolino M, Durante M, Mueller-Mellin R, Reitz G, Rossi L, Shurshakov V and Sorbi M 2007 *Radiat. Meas.* **42** 14–23
[20] Ambroglini F, Battiston R and Burger W J 2016 *Front. Oncol.* **6** 97
[21] Lvovsky Y, Stautner E W and Zhang T 2013 *Supercond. Sci. Technol.* **26** 093001
[22] Liang Z, Wang Z and Li P 2017 Analysis of stray field of actively shielded mri magnet *2017 IEEE 5th Int. Symp. on Electromagnetic Compatibility* (EMC) (*Beijing, China*, *28th - 31st October 2017*) (IEEE) pp 1–4
[23] Liang Z 2019 *IEEE Trans. Appl. Supercond.* **29** 4900404
[24] Liang Z 2018 Design of 3T actively shielded MRI superconducting magnet *2018 IEEE Int. Conf. on Applied Superconductivity and Electromagnetic Devices (ASEMD)* (*Tianjin, China*, *15–18 April 2018*) pp 1–2
[25] Wang Y, Wang Q, Wang H, Chen S, Hu X, Liu Y and Liu F 2021 *Supercond. Sci. Technol.* **35** 014001
[26] Parizh M and Stautner W 2021 MRI Magnets *Hanbook of Superconductivity* 2nd edn, vol 3 ed D A Cardwell, D C Larbalestier and A I Braginski (CRC Press) pp 437–92
[27] Iivanainen J, Zetter R, Grön M, Hakkarainen K and Parkkonen L 2019 *Neuroimage* **194** 244–58
[28] Cruciani S, Campi T, Maradei F and Feliziani M 2019 *IEEE Trans. Electromagn. Compat.* **61** 1953–60
[29] Cruciani S, Campi T, Maradei F and Feliziani M 2020 *Energies* **13** 5575
[30] Tong X C 2016 *Advanced Materials and Design for Electromagnetic Interference Shielding* (CRC Press)(https://doi.org/10.1201/9781420073591)
[31] Wang H, Li S, Liu M, Li J and Zhou X 2021 *Macromol. Mater. Eng.* **306** 2100032
[32] Chung D 2020 *Mater. Chem. Phys.* **255** 123587
[33] Jiles D 2015 *Introduction to Magnetism and Magnetic Materials* 3rd edn (CRC Press) (https://doi.org/10.1201/b18948)
[34] Koski A and Wipf S 1996 *IEEE Trans. Magn.* **32** 2663–6
[35] Vant-Hull L L and Mercereau J E 1963 *Rev. Sci. Instrum.* **20** 1238–42
[36] Pavese F 1998 Magnetic shielding *Handbook of Applied Superconductivity* vol 2 ed S Bernd (Institute of Physics Publishing) pp 1461–83
[37] Poole C P, Farach H A, Creswick R J and Prozorov R 2014 *Superconductivity* 3rd edn (Elsevier)
[38] Itoh I, Sasaki T, Minamino S and Shimizu T 1993 *IEEE Trans. Appl. Supercond.* **3** 177–80
[39] Rabbers J J, Oomen M P, Bassani E, Ripamonti G and Giunchi G 2010 *Supercond. Sci. Technol.* **23** 125003
[40] Wéra L, Fagnard J F, Namburi D K, Shi Y, Vanderheyden B and Vanderbemden P 2017 *IEEE Trans. Appl. Supercond* **27** 6800305
[41] Gozzelino L *et al* 2020 *Supercond. Sci. Technol.* **33** 044018
[42] Giunchi G, Barna D, Bajas H, Brunner K, Német A and Petrone C 2018 *IEEE Trans. Appl. Supercond.* **28** 6801705
[43] Barna D, Novák M, Brunner K, Petrone C, Atanasov M G, Feuvrier J and Pascal M A 2019 *IEEE Trans. Appl. Supercond.* **29** 4900108
[44] Dorget R *et al* 2021 *Materials* **14** 2847
[45] Yashchuk V V, Lee S K and Paperno E 2013 Magnetic shielding *Optical Magnetometry* ed Budker D and Jackson Kimball D F (Cambridge University Press) pp 225–48
[46] Prigozhin L and Sokolovsky V 2018 *J. Appl. Phys.* **123** 233901
[47] Chiampi M, Gozzelino L, Manzin A and Zilberti L 2011 *IEEE Trans. Magn.* **47** 4266–9
[48] Ainslie M and Fujishiro H 2019 *Numerical Modelling of Bulk Superconductor Magnetisation* (IOP Publishing)(https://doi.org/10.1088/978-0-7503-1332-2)
[49] Niculescu H, Schmidmeier R, Topolski B and Gielisse P J 1994 *Physica* C **229** 105–12
[50] Denis S, Dusoulier L, Dirickx M, Vanderbemden P, Cloots R, Ausloos M and Vanderheyden B 2007 *Supercond. Sci. Technol.* **20** 192
[51] Hogan K, Fagnard J-F, Wéra L, Vanderheyden B and Vanderbemden P 2018 *Supercond. Sci. Technol.* **31** 015001
[52] Holmes J J 2008 Passive magnetic silencing techniques *Reduction of a Ship's Magnetic Field Signatures* (*Synthesis Lectures on Computational Electromagnetics*) (Springer) pp 7–42
[53] Kleeven W *et al* 2013 The IBA superconducting synchrocyclotron project S2C2 *Proc. Cyclotrons 2013* (available at: https://api.semanticscholar.org/CorpusID:54085432)
[54] Hofman M B M, Kuijer J P A, de Ridder J W, Perk L R and Verdaasdonk R M 2013 *Med. Phys.* **40** 012303
[55] Grohmann K, Hahlbohm H, Lübbig H and Ramin H 1974 *Cryogenics* **14** 499–502
[56] Grohmann K, Hahlbohm H D, Lubbig H and Ramin H 1974 *IEEE Trans. Instrum. Meas.* **23** 261–3

[57] Watanabe T, Watanabe S, Ikeda T, Kase M, Sasaki Y, Kawaguchi T and Katayama T 2004 *Supercond. Sci. Technol.* **17** S450
[58] Arpaia P, Ballarino A, Giunchi G and Montenero G 2014 *J. Instrum.* **9** 04020
[59] Buchman S, Taber M, Lockhart J, Muhlfelder B, Everitt C W F, Turneaure J P and Parkinson B 1996 *Czech. J. Phys.* **46** 2869–70
[60] Bergen A A *et al* 2016 *Rev. Sci. Instrum.* **87** 105109
[61] Kamiya K, Warner B A and DiPirro M J 2001 *Cryogenics* **41** 401–5
[62] Seki Y, Suzuki D, Ogata K and Tsukada K 2003 *Appl. Phys. Lett.* **82** 940–2
[63] Claycomb J R and Miller J H J 1999 *Rev. Sci. Instrum.* **70** 4562–8
[64] Kamiya K, Warner B A, DiPirro M J and Numazawa T 2003 *Physica* B **329–333** 1627–8
[65] Clem J 1983 *IEEE Trans. Magn.* **19** 1278–81
[66] Clem T 1985 *IEEE Trans. Magn.* **21** 606–9
[67] Hoshino K *et al* 1991 *IEEE Trans. Magn.* **27** 2202–5
[68] Horng H-E *et al* 2003 *IEEE Trans. Appl. Supercond.* **13** 381–4
[69] Ohta H *et al* 1999 *IEEE Trans. Appl. Supercond.* **9** 4073–6
[70] Ohta H *et al* 1999 *Supercond. Sci. Technol.* **12** 762
[71] Ohta H, Matsui T and Uchikawa Y 2007 *IEEE Trans. Appl. Supercond.* **17** 730–3
[72] Seki Y, Suzuki D, Ogata K and Tsukada K 2004 *Rev. Sci. Instrum.* **75** 896–9
[73] Hamilton W O 1970 *Rev. Phys. Appl.* **5** 41–48
[74] Miyazoe A, Sekino M, Kiyoshi T and Ohsaki H 2010 *IEEE Trans. Appl. Supercond.* **20** 1557–60
[75] Yanagisawa Y *et al* 2010 *IEEE Trans. Appl. Supercond.* **20** 744–7
[76] Yang D G, Kim K L, Choi Y H, Kwon O J, Park Y J and Lee H G 2013 *Supercond. Sci. Technol.* **26** 105025
[77] Pardo E 2016 *Supercond. Sci. Technol.* **29** 085004
[78] Wang L, Wang Q, Liu J, Wang H, Hu X and Chen P 2017 *IEEE Trans. Appl. Supercond.* **27** 8200106
[79] Barth C *et al* 2019 *Supercond. Sci. Technol.* **32** 075005
[80] Noguchi S, Ueda H, Hahn S, Ishiyama A and Iwasa Y 2019 *Supercond. Sci. Technol.* **32** 045007
[81] Mawatari Y 2018 *Appl. Phys. Express* **12** 013002
[82] Kolb-Bond D *et al* 2021 *Supercond. Sci. Technol.* **34** 095004
[83] Gömöry F, Solovyov M, Šouc J, Navau C, Prat-Camps J and Sanchez A 2012 *Science* **335** 1466–8
[84] Solovyov M *et al* 2017 *IEEE Trans. Appl. Supercond.* **27** 8800204
[85] Capobianco-Hogan K *et al* 2018 *Nucl. Instrum. Methods Phys. Res.* A **877** 149–56
[86] Solovyov M, Šouc J, Kucharovič M and Gömöry F 2021 *IEEE Trans. Appl. Supercond.* **31** 4901205
[87] Souc J, Solovyov M, Gömöry F, Prat-Camps J, Navau C and Sanchez A 2013 *New J. Phys.* **15** 053019
[88] Prat-Camps J, Sanchez A and Navau C 2013 *Supercond. Sci. Technol.* **26** 074001
[89] Narayana S and Sato Y 2012 *Adv. Mater.* **24** 71–74
[90] Zhu J, Jiang W, Liu Y, Yin G, Yuan J, He S and Ma Y 2015 *Nat. Commun.* **6** 8931
[91] Zhou P B, Ma G T, Wang Z T, Gong T Y, Ye C Q and Zhang H 2016 *IEEE Trans. Appl. Supercond.* **26** 0601805
[92] Brialmont S *et al* 2023 *Supercond. Sci. Technol.* **36** 054004
[93] Gozzelino L *et al* 2022 *Supercond. Sci. Technol.* **35** 044002
[94] Wéra L *et al* 2019 *IEEE Trans. Appl. Supercond.* **29** 6801109
[95] Takahata K, Nishijima S, Ohgami M, Okada T, Nakagawa S and Yoshiwa M 1989 *IEEE Trans. Magn.* **25** 1889–92
[96] Fagnard J-F, Dirickx M, Ausloos M, Lousberg G, Vanderheyden B and Vanderbemden P 2009 *Supercond. Sci. Technol.* **22** 105002
[97] Fagnard J-F and Vanderheyden B 2012 Magnetic shielding with bulk high temperature superconductors: factors influencing the magnetic field penetration *Superconductivity: Recent Developments and New Production Technologies* ed M Miryala (Nova Science) (available at: https://shibaura.elsevierpure.com/en/publications/superconductivity-recent-developments-and-new-production-technolo)
[98] Fagnard J F, Vanderheyden B, Pardo E and Vanderbemden P 2019 *Supercond. Sci. Technol.* **32** 074007
[99] Hogan K, Fagnard J-F, Wéra L, Vanderheyden B and Vanderbemden P 2015 *Supercond. Sci. Technol.* **28** 035011
[100] Hogan K 2018 Passive magnetic shielding with bulk high temperature superconductors under a non-uniform magnetic field *PhD Thesis* University of Liége
[101] Kvitkovic J, Burnside K, Zhang M and Pamidi S 2020 *J. Phys.: Conf. Ser.* **1559** 012117
[102] Rotheudt N, Brialmont S, Fagnard J-F, Hlasek T, Plechacek J and Vanderbemden P 2024 *Supercond. Sci. Technol.* **37** 065008
[103] Dewar R L, Monticello D A and Sy W N 1984 *Phys. Fluids* **27** 1723–32
[104] D'haeseleer W D, Hitchon W N G, Callen J D and Shohet J L 1991 *Flux Coordinates and Magnetic Field Structure* (*Scientific Computation*) (Springer) (https://doi.org/10.1007/978-3-642-75595-8)
[105] Hegna C C 2000 *Phys. Plasmas* **7** 3921–8
[106] Kruger S E and Greene J M 2019 *Phys. Plasmas* **26** 082506
[107] Fagnard J-F, Elschner S, Bock J, Dirickx M, Vanderheyden B and Vanderbemden P 2010 *Supercond. Sci. Technol.* **23** 095012
[108] Fagnard J F, Dirickx M, Levin G A, Barnes P N, Vanderheyden B and Vanderbemden P 2010 *J. Appl. Phys.* **108** 013910
[109] Cavallin T, Quarantiello R, Matrone A and Giunchi G 2006 *J. Phys.: Conf. Ser.* **43** 1015
[110] Fagnard J-F, Denis S, Lousberg G, Dirickx M, Ausloos M, Vanderheyden B and Vanderbemden P 2009 *IEEE Trans. Appl. Supercond.* **19** 2905–8
[111] Kvitkovic J, Davis D, Zhang M and Pamidi S 2015 *IEEE Trans. Appl. Supercond.* **25** 8800304
[112] Piekarz H, Hays S, Blowers J, Claypool B and Shiltsev V 2019 *Nucl. Instrum. Methods Phys. Res.* A **943** 162490
[113] Xue W, Huang Z, Xu X, Shen B and Jin Z 2021 *IEEE Trans. Appl. Supercond.* **31** 4902105
[114] Li D, Liu D and Yong H 2022 *Sci. China Technol. Sci.* **65** 115–30
[115] Yang Y *et al* 2022 *Cryogenics* **126** 103524
[116] Liu Q and Kim S 2022 *IEEE Trans. Appl. Supercond.* **32** 4603605
[117] Wang K, Wang Q, Zhou B, Wang L, Zhang Z and Liu J 2023 *Physica* C **615** 1354372
[118] Lu J *et al* 2024 *IEEE Trans. Appl. Supercond.* **34** 4402806
[119] Hämäläinen M, Hari R, Ilmoniemi R J, Knuutila J and Lounasmaa O V 1993 *Rev. Mod. Phys.* **65** 413–97
[120] Nenonen J, Montonen J and Katila T 1996 *Rev. Sci. Instrum.* **67** 2397–405
[121] Seton H, Hutchison J and Bussell D 2005 *Cryogenics* **45** 348–55
[122] Khan S and Cohen D 2013 *Rev. Sci. Instrum.* **84** 056101
[123] Imai K, Matsuba H, Spear P and Fife A 1993 *IEICE Trans. Electron.* **E76-C** 1280–6 (available at: https://globals.ieice.org/en_transactions/electronics/10.1587/e76-c_8_1280/_p)
[124] Lee S-K and Romalis M V 2008 *J. Appl. Phys.* **103** 084904
[125] Miller M, Carroll T, Soulen R, Toth L, Rayne R, Alford N and Saunders C 1993 *Cryogenics* **33** 180–3
[126] Shimbo Y, Niki K, Kabasawa M and Tachikawa K 1994 High-Tc magnetic shields prepared by a low pressure

plasma spray *Advances in Cryogenic Engineering Materials: Volume 40, Part A* (Springer) pp 253–60
[127] Pamidi S, Nguyen D, Zhang G, Knoll D, Trociewitz U and Schwartz J 2007 *IEEE Trans. Appl. Supercond.* **17** 3179–82
[128] Kvitkovic J, Patil P, Pamidi S V and Voccio J 2011 *IEEE Trans. Appl. Supercond.* **21** 1477–80
[129] Tomków Ł, Ciszek M and Chorowski M 2015 *J. Appl. Phys.* **117** 043901
[130] Fang H, Claycomb J, Zhou Y, Putman P, Padmanabhan S, Miller J, Ravi-Chandar K and Salama K 2003 *IEEE Trans. Appl. Supercond.* **13** 3103–5
[131] Chen Q Y, McArdle J L, Werner T R and Lenz J E 1990 *Appl. Phys. Lett.* **57** 2603–5
[132] Claassen J H, Wilson M L, Byers J M and Adrian S 1997 *J. Appl. Phys.* **82** 3028–34
[133] Claassen J H, Osofsky M S, Namburi D K and Vanderbemden P 2015 *IEEE Trans. Appl. Supercond.* **25** 7500204
[134] Yamagishi K, Tsukamoto O, Ogawa J and Miyagi D 2011 *IEEE Trans. Appl. Supercond.* **21** 3320–4
[135] Smirnov A, Dorofeev G, Drobin V, Kulikov E and Malinovski H 2016 *Phys. Part. Nucl. Lett.* **13** 949–53
[136] Bortot L *et al* 2021 *Supercond. Sci. Technol.* **34** 105001
[137] Koike A, Hoshino K, Ohta H, Kotaka H, Sudoh E, Katoh K and Takahara H 1991 *Physica* C **185–189** 2613–4
[138] Matsuba H, Yahara A and Irisawa D 1992 *Supercond. Sci. Technol.* **5** S432
[139] Yasui K, Tarui Y and Itoh M 2006 *J. Phys.: Conf. Ser.* **43** 1393
[140] Hildebrandt A 1970 *Rev. Phys. Appl.* **5** 49–52
[141] Gu C, Chen S, Pang T and Qu T-M 2017 *Appl. Phys. Lett.* **110** 193505
[142] Rotheudt N, Fagnard J-F, Harmeling P and Vanderbemden P 2023 *Cryogenics* **133** 103693
[143] Gozzelino L, Minetti B, Gerbaldo R, Ghigo G, Laviano F, Agostino A and Mezzetti E 2011 *IEEE Trans. Appl. Supercond.* **21** 3146–9
[144] Itoh M, Ohyama T, Minemoto T, Numata K and Hoshino K 1992 *J. Phys. D: Appl. Phys.* **25** 1630
[145] Dbeyssi A, Froelich B, Espi M C M, Maas F, Capozza L, Noll O, Wang Y and Lin D 2023 *Nucl. Instrum. Methods Phys. Res.* A **1050** 168087
[146] Lousberg G P, Fagnard J-F, Chaud X, Ausloos M, Vanderbemden P and Vanderheyden B 2010 *Supercond. Sci. Technol.* **24** 035008
[147] Nagasaki Y, Solovyov M and Gömöry F 2018 *IEEE Trans. Appl. Supercond.* **28** 6601905
[148] Cabrera B 1975 The use of superconducting shields for generating ultra low magnetic field regions and several related experiments *PhD Thesis* Standford University
[149] Caputo J-G *et al* 2013 *J. Appl. Phys.* **114** 233913
[150] Bean C P 1964 *Rev. Mod. Phys.* **36** 31–39
[151] Kim Y B, Hempstead C F and Strnad A R 1962 *Phys. Rev. Lett.* **9** 306–9
[152] Qin M, Wang X, Liu H K and Dou S 2002 *Phys. Rev.* B **65** 132508
[153] Fujishiro H, Naito T and Yoshida T 2014 *Supercond. Sci. Technol.* **27** 065019
[154] Ainslie M D and Fujishiro H 2015 *Supercond. Sci. Technol.* **28** 053002
[155] Barna D *et al* 2019 *IEEE Trans. Appl. Supercond.* **29** 4101310
[156] Gozzelino L *et al* 2019 *Supercond. Sci. Technol.* **32** 034004
[157] Anderson P W 1962 *Phys. Rev. Lett.* **9** 309–11
[158] Brandt E H 1996 *Phys. Rev.* B **54** 4246–64
[159] Brandt E H 1998 *Phys. Rev.* B **58** 6506–22
[160] Denis S, Dirickx M, Vanderbemden P, Ausloos M and Vanderheyden B 2007 *Supercond. Sci. Technol.* **20** 418
[161] Solovyov M and Gömöry F 2019 *Supercond. Sci. Technol.* **32** 115001
[162] Campbell A M 2007 *Supercond. Sci. Technol.* **20** 292–5
[163] Fracasso M *et al* 2022 *Materials* **15** 667
[164] Sirois F, Grilli F and Morandi A 2019 *IEEE Trans. Appl. Supercond.* **29** 8000110
[165] Trillaud F, Dos Santos G and Goncalves Sotelo G 2021 *Materials* **14** 1892
[166] Claycomb J R 2016 Magnetic shields *Encyclopedia of Applied Physics* (Wiley) pp 1–32
[167] Mager A 1970 *IEEE Trans. Magn.* **6** 67–75
[168] Bondarenko S, Vinogradov S, Gogadze G, Perepelkin S and Sheremet V 1974 *Sov. Phys. Tech. Phys.* **19** 824–8
[169] Landau L D 1938 *Nature* **141** 688
[170] Sumner T 1987 *J. Phys. D: Appl. Phys.* **20** 692–6
[171] Ginzburg V L 1962 *Sov. Phys. - JETP* **15** 207–9
[172] Lung-Tao H and Zharkov G F 1963 *Sov. Phys. - JETP* **17** 1426–31
[173] Wills A P 1899 *Phys. Rev.* I **9** 193–213
[174] Thomas A K 1968 *IEEE Trans. Electromagn. Compat.* **EMC-10** 142–52
[175] Bidinosti C P and Martin J W 2014 *AIP Adv.* **4** 047135
[176] Mikheenko P and Kuzovlev Y 1993 *Physica* C **204** 229–36
[177] Clem J R and Sanchez A 1994 *Phys. Rev.* B **50** 9355–62
[178] Mawatari Y, Sawa A and Obara H 1996 *Physica* C **258** 121–8
[179] Feng Z 1985 *IEEE Trans. Magn.* **21** 993–6
[180] Chen D and Goldfarb R B 1989 *J. Appl. Phys.* **66** 2489–500
[181] Zhilichev Y 1997 *IEEE Trans. Appl. Supercond.* **7** 3874–9
[182] Kato Y, Hanawaka M and Yamafuji K 1976 *Jpn. J. Appl. Phys.* **15** 695
[183] Carr J W 2001 *AC Loss and Macroscopic Theory of Superconductors* (CRC Press) (https://doi.org/10.1201/9781482264760)
[184] Osborn J A 1945 *Phys. Rev.* **67** 351–7
[185] Mawatari Y 2011 *Phys. Rev.* B **83** 134512
[186] Brandt E H 1997 *Physica* C **282-287** 343–6
[187] Navau C *et al* 2005 *Phys. Rev.* B **71** 214507
[188] Prigozhin L and Sokolovsky V 2018 *Supercond. Sci. Technol.* **31** 055018
[189] Prigozhin L and Sokolovsky V 2023 *IEEE Trans. Appl. Supercond.* **33** 6601310
[190] Stavrev S *et al* 2002 *IEEE Trans. Magn.* **38** 849–52
[191] Bossavit A and Verite J 1983 *IEEE Trans. Magn.* **19** 2465–70
[192] Shen B, Grilli F and Coombs T 2020 *IEEE Access* **8** 100403–14
[193] Campbell A 2011 *J. Supercond. Novel Magn.* **24** 27–33
[194] Gömöry F *et al* 2009 *Supercond. Sci. Technol.* **22** 034017
[195] Yang P, Fagnard J-F, Vanderbemden P and Yang W 2019 *Supercond. Sci. Technol.* **32** 115015
[196] Wéra L, Fagnard J F, Hogan K, Vanderheyden B and Vanderbemden P 2016 Magnetic shielding with bulk high temperature superconductors: improvement of the shielded volume in hollow cylinders *Superconductivity: Applications Today and Tomorrow* ed M Muralidhar (Nova Science) pp 95–114 (available at: https://novapublishers.com/shop/superconductivity-applications-today-and-tomorrow/)
[197] Gozzelino L, Gerbaldo R, Ghigo G, Laviano F, Truccato M and Agostino A 2016 *Supercond. Sci. Technol.* **29** 034004
[198] Lousberg G P, Ausloos M, Geuzaine C, Dular P, Vanderbemden P and Vanderheyden B 2009 *Supercond. Sci. Technol.* **22** 055005
[199] Gömöry F, Solovyov M and Šouc J 2015 *Supercond. Sci. Technol.* **28** 044001
[200] Arsenault A, Sirois F and Grilli F 2021 *IEEE Trans. Appl. Supercond.* **31** 6800111
[201] Douine B, Male G, Lubin T, Mezani S, Leveque J and Berger K 2014 *J. Supercond. Nov. Magn.* **27** 903–7

[202] Wu Y, Zhang G, Wu Y, Zhang D and Jing L 2023 *IEEE Trans. Appl. Supercond.* **33** 8800205
[203] Sirois F, Cave J R and Basile-Bellavance Y 2007 *IEEE Trans. Appl. Supercond.* **17** 3652–5
[204] Bortot L *et al* 2020 *IEEE Trans. Appl. Supercond.* **30** 4900911
[205] Dular J, Geuzaine C and Vanderheyden B 2020 *IEEE Trans. Appl. Supercond.* **30** 8200113
[206] Brambilla R, Grilli F, Martini L, Bocchi M and Angeli G 2018 *IEEE Trans. Appl. Supercond.* **28** 5207511
[207] Dular P, Remacle J-F, Henrotte F, Genon A and Legros W 1997 *IEEE Trans. Magn.* **33** 1302–5
[208] Berrospe-Juarez E, Zermeño V M, Trillaud F and Grilli F 2019 *Supercond. Sci. Technol.* **32** 065003
[209] Berrospe-Juarez E, Trillaud F, Zermeño V M and Grilli F 2021 *Supercond. Sci. Technol.* **34** 044002
[210] Stenvall A and Tarhasaari T 2010 *Supercond. Sci. Technol.* **23** 075010
[211] Pratap S and Hearn C S 2015 *IEEE Trans. Appl. Supercond.* **25** 5203910
[212] Dular J, Brialmont S, Vanderbemden P, Geuzaine C and Vanderheyden B 2024 *IEEE Trans. Appl. Supercond.* **34** 4903507
[213] Zhang H, Zhang M and Yuan W 2017 *Supercond. Sci. Technol.* **30** 024005
[214] Liang F, Venuturumilli S, Zhang H, Zhang M, Kvitkovic J, Pamidi S, Wang Y and Yuan W 2017 *J. Appl. Phys.* **122** 043903
[215] Wang J, Lin H, Huang Y and Sun X 2011 *IEEE Trans. Magn.* **47** 1378–81
[216] Dular J, Berger K, Geuzaine C and Vanderheyden B 2022 *IEEE Trans. Magn.* **58** 8205204
[217] Niyonzima I, Sabariego R, Dular P and Geuzaine C 2012 *IEEE Trans. Magn.* **48** 587–90
[218] Gyselinck J and Dular P 2004 *IEEE Trans. Magn.* **40** 856–9
[219] Wipf S L 1967 *Phys. Rev.* **161** 404–16
[220] Swartz P S and Bean C P 1968 *J. Appl. Phys* **39** 4991–8
[221] Murai K, Hori J, Fujii Y, Shaver J and Kozlowski G 2005 *Cryogenics* **45** 415–20
[222] Moseley D A, Matthews G A B, Zhou D, Cientanni V, Tsui Y, Ainslie M D, Speller S and Durrell J H 2021 *Supercond. Sci. Technol.* **34** 085018
[223] Gubser D, Wolf S, Francavilla T, Claassen J and Das B 1985 *IEEE Trans. Magn.* **21** 320–3
[224] Giunchi G, Turrioni D, Kashikhin V, Nguyen H and Barzi E 2016 *IEEE Trans. Appl. Supercond.* **26** 8801005
[225] Moseley D A, Wilkinson D P, Mousavi T, Dennis A R, Speller S and Durrell J H 2022 *Supercond. Sci. Technol.* **35** 085003
[226] Murakami M 1993 *Appl. Supercond.* **1** 1157–73
[227] Bean C P 1962 *Phys. Rev. Lett.* **8** 250–3
[228] Mints R 1996 *Phys. Rev.* B **53** 12311–7
[229] Fracasso M *et al* 2023 *Supercond. Sci. Technol.* **36** 044001
[230] Zhou Y-H and Yang X 2006 *Phys. Rev.* B **74** 054507
[231] Xia J, Li M and Zhou Y 2017 *Supercond. Sci. Technol.* **30** 075004
[232] Zhang W, Xia J, Yong H and Zhou Y 2020 *AIP Adv.* **10** 025021
[233] Jing Z 2022 *Supercond. Sci. Technol.* **35** 054006
[234] Fujishiro H, Mochizuki H, Naito T, Ainslie M D and Giunchi G 2016 *Supercond. Sci. Technol.* **29** 034006
[235] Cientanni V, Ainslie M D, Fujishiro H and Takahashi K 2021 *Supercond. Sci. Technol.* **34** 114003
[236] Wang L, Wu H and Yong H 2025 *Int. J. Thermal Sci.* **209** 109524
[237] Cientanni V and Ainslie M D 2023 *Supercond. Sci. Technol.* **36** 025007
[238] Van der Biest O O and Vandeperre L J 1999 *Annu. Rev. Mater. Res.* **29** 327–52
[239] Pavese F, Bergadano E, Bianco M, Ferri D, Giraudi D and Vanolo M 1996 Progress in fabrication of large magnetic shields by using extended YBCO thick films sprayed on stainless steel with the HVOF technique *Advances in Cryogenic Engineering Materials* vol 42, ed L T Summers (Springer) pp 917–22
[240] Hemmes H *et al* 1994 Plasma sprayed high-Tc layers for magnetic shielding *Advances in Cryogenic Engineering Materials* vol 40, ed R P Reed, F R Fickett, L T Summers and M Stieg (Springer) pp 271–80
[241] Hatsukade Y, Hayashi K, Takemoto M and Tanaka S 2009 *Supercond. Sci. Technol.* **22** 114010
[242] Johnson D, Opie D, Schone H, Lanagan M and Stevens J 1996 *IEEE Trans. Appl. Supercond.* **6** 50–54
[243] Omura A, Kotani K, Yasu K and Itoh M 2006 *J. Phys. Chem. Solids* **67** 43–46
[244] Itoh E, Hotta Y, Itoh M, Munser N, Pleva J, Jaszczuk W and Altenburg H 2001 *IEEE Trans. Appl. Supercond.* **11** 2394–7
[245] Lousberg G P *et al* 2009 *Supercond. Sci. Technol.* **22** 125026
[246] Zhang Z, Matsumoto S, Teranishi R and Kiyoshi T 2012 *Phys. Proc.* **27** 180–3
[247] Wang J and Sayer M 1993 *IEEE Trans. Appl. Supercond.* **3** 185–8
[248] Karthikeyan J, Paithankar A S, Chaddah P and Sreekumar K P 1991 *Supercond. Sci. Technol.* **4** 250–6
[249] Okada T, Takahata K, Nishijima S, Yoshida S and Hanasaka T 1989 *IEEE Trans. Magn.* **25** 2270–2
[250] Terao Y, Sekino M, Ohsaki H, Teshima H and Morita M 2011 *IEEE Trans. Appl. Supercond.* **21** 1584–7
[251] Masson P, Netter D, Leveque J and Rezzoug A 2001 *IEEE Trans. Appl. Supercond.* **11** 2248–51
[252] CAN Superconductors (available at: https://bit.ly/CANSuperconductor) (Accessed 6 February 2025)
[253] Sarkar A K, Maartense I, Peterson T and Kumar B 1989 *J. Appl. Phys.* **66** 3717–22
[254] Fagnard J-F, Elschner S, Hobl A, Bock J, Vanderheyden B and Vanderbemden P 2012 *Supercond. Sci. Technol.* **25** 104006
[255] Irisawa D, Imai K, Shintomi K, Yahara A and Matsubara H 2019 *Electr. Eng. Japan* **207** 3–14
[256] Ichikawa M and Okazaki M 1995 *IEEE Trans. Appl. Supercond.* **5** 1067–70
[257] Gupta R *et al* 2019 *IEEE Trans. Appl. Supercond.* **29** 4002104
[258] Plechacek V *et al* 1995 *IEEE Trans. Appl. Supercond.* **5** 528–31
[259] Vanderbemden P *et al* 2007 *Phys. Rev.* B **75** 174515
[260] Nishikubo T, Endo H and Itoh M 2009 *IEEE Trans. Appl. Supercond.* **19** 2245–8
[261] Haseyama S, Fujinaka N, Yoshizawa S and Nakane H 2001 *Physica* C **354** 437–40
[262] Zhang Z, MacManus-Driscoll J, Suo H and Wang Q 2022 *Superconductivity* **3** 100015
[263] Giunchi G 2003 *Int. J. Mod. Phys.* B **17** 453–60
[264] Giunchi G, Bassani E, Hassel J, Helistö P and Penttilä J 2010 *AIP Conf. Proc.* **1218** 1636–40
[265] Xing Y, Bernstein P, Muralidhar M and Noudem J 2023 *Supercond. Sci. Technol.* **36** 115005
[266] Guo Z *et al* 2018 *Supercond. Sci. Technol.* **31** 065005
[267] Guo Z *et al* 2018 *Physica* C **551** 28–32
[268] Cai X *et al* 2019 *IEEE Trans. Appl. Supercond.* **29** 1200104
[269] Kvitkovic J, Patel S and Pamidi S 2017 *IEEE Trans. Appl. Supercond.* **27** 4700705
[270] Doinaki A *et al* 2023 *J. Instrum.* **18** C10011
[271] Kvitkovic J, Pamidi S and Voccio J 2009 *Supercond. Sci. Technol.* **22** 125009

[272] Kvitkovic J, Voccio J and Pamidi S V 2009 *IEEE Trans. Appl. Supercond.* **19** 3577–80
[273] Kvitkovic J, Hatwar R and Pamidi S 2016 *IEEE Trans. Appl. Supercond.* **26** 9000505
[274] Solovyov M *et al* 2016 *IEEE Trans. Appl. Supercond.* **26** 0500206
[275] Kvitkovic J, Davis D, Zhang M and Pamidi S 2013 *IEEE Trans. Appl. Supercond.* **23** 8200605
[276] Hatwar R, Kvitkovic J, Herman C and Pamidi S 2015 *IOP Conf. Ser: Mater. Sci. Eng.* **102** 012012
[277] Patel A *et al* 2018 *Supercond. Sci. Technol.* **31** 09LT01
[278] Matsumoto S, Kiyoshi T and Uchida A 2011 *IEEE Trans. Appl. Supercond.* **21** 2283–6
[279] Kvitkovic J, Patel S, Zhang M, Zhang Z, Peetz J, Marney A and Pamidi S 2018 *IEEE Trans. Appl. Supercond.* **28** 9001705
[280] Álvarez A, Rivera B, Pérez B and Suárez P 2023 *IEEE Access* **11** 22835–42
[281] Tomków Ł, Kulikov E, Kozłowski K and Drobin V 2019 *J. Appl. Phys.* **126** 083903
[282] Kostrov E, Demikhov E, Bagdinov A, Demikhov T, Lysenko V and Tysyachnykh Y 2016 *IEEE Trans. Appl. Supercond.* **26** 0601305
[283] Maher E, Abell J S, Chakalova R I, Cheung Y L, Button T W and Tixador P 2004 *Supercond. Sci. Technol.* **17** 1440
[284] Kvitkovic J, Pamidi S V, Graber L, Chiocchio T, Steurer M and Usoskin A 2014 *IEEE Trans. Appl. Supercond.* **24** 5600604
[285] Tomków Ł, Ciszek M and Chorowski M 2016 *IEEE Trans. Appl. Supercond.* **26** 0602204
[286] Huang D, Shang H, Xie B, Zou Q, Dong H, Wang K, Zhang L, Gu H and Ding F 2022 *Supercond. Sci. Technol.* **35** 075004
[287] Huang D, Dong H, Wang T, Gu H and Ding F 2024 *Supercond. Sci. Technol.* **37** 085024
[288] Levin G A, Barnes P N, Murphy J, Brunke L, Long J D, Horwath J and Turgut Z 2008 *Appl. Phys. Lett.* **93** 062504
[289] Lee H-G, Kim J-G, Lee S-W, Kim W-S, Lee S-W, Choi K-D, Hong G-W and Ko T-K 2006 *Physica* C **445-448** 1099–102
[290] Wéra L, Fagnard J F, Levin G A, Vanderheyden B and Vanderbemden P 2015 *Supercond. Sci. Technol.* **28** 074001
[291] Wéra L, Fagnard J F, Levin G A, Vanderheyden B and Vanderbemden P 2013 *IEEE Trans. Appl. Supercond.* **23** 8200504
[292] Sheng J, Zhang M, Wang Y, Li X, Patel J and Yuan W 2017 *Supercond. Sci. Technol.* **30** 094002
[293] Zheng Y, Wang Y, Li J and Jin Z 2017 *AIP Adv.* **7** 095218
[294] Ali M Z, Zheng J, Huber F, Zhang Z, Yuan W and Zhang M 2020 *Supercond. Sci. Technol.* **33** 04LT01
[295] Zhao C, Shi J, Sheng J and Chen W 2022 *Crystals* **12** 1438
[296] Qiu D *et al* 2017 *IEEE Trans. Appl. Supercond.* **27** 4601605
[297] Gu C, Lai L, Chen S, Qu T and Yue Y 2019 *IEEE Trans. Appl. Supercond.* **29** 4602904
[298] Chi C *et al* 2020 *Supercond. Sci. Technol.* **33** 095001
[299] Peng Y *et al* 2021 *J. Supercond. Nov. Magn.* **34** 2493–501
[300] Patel A, Hahn S, Voccio J, Baskys A, Hopkins S C and Glowacki B A 2017 *Supercond. Sci. Technol.* **30** 024007
[301] Hahn S, Voccio J, Bermond S, Park D-K, Bascuñan J, Kim S-B, Masaru T and Iwasa Y 2011 *IEEE Trans. Appl. Supercond.* **21** 1632–5
[302] Claassen J H and Thieme C L H 2008 *Supercond. Sci. Technol.* **21** 105003
[303] Miyagi D, Yunoki Y, Umabuchi M, Takahashi N and Tsukamoto O 2008 *Physica* C **468** 1743–6
[304] Brialmont S, Fagnard J F, Vanderheyden B, Mazaleyrat F, Hahn S, Patel A and Vanderbemden P 2022 *IEEE Trans. Appl. Supercond.* **32** 6602710
[305] Funaki K and Yamafuji K 1982 *Jpn. J. Appl. Phys.* **21** 299–304
[306] Vanderbemden P, Dorbolo S, Hari-Babu N, Ntatsis A, Cardwell D and Campbell A 2003 *IEEE Trans. Appl. Supercond.* **13** 3746–9
[307] Campbell A, Baghdadi M, Patel A, Zhou D, Huang K Y, Shi Y and Coombs T 2017 *Supercond. Sci. Technol.* **30** 034005
[308] Yamagishi K, Tsukamoto O and Ogawa J 2009 *IEEE Trans. Appl. Supercond.* **19** 3561–4
[309] Yamagishi K, Ogawa J and Tsukamoto O 2014 *J. Phys.: Conf. Ser.* **507** 032060
[310] Yamagishi K, Ogawa J and Tsukamoto O 2015 *IEEE Trans. Appl. Supercond.* **25** 5201905
[311] Liao H, Dennis A R, Yuan W and Zhang M 2023 *J. Appl. Phys.* **134** 083902
[312] Liao H, Yuan W, Zhang Z and Zhang M 2023 *J. Appl. Phys.* **133** 023902
[313] Shi J, Li X and Sheng J 2022 *IEEE Trans. Appl. Supercond.* **32** 3600605
[314] Brialmont S, Fagnard J F, Fracasso M, Laura G, Yang P, Yang W and Vanderbemden P 2023 Screening of the stray magnetic field of a large bore superconducting magnet *16th European Conf. on Applied Superconductivity (EUCAS 2023)* (*Bologna, Italy*, *3rd - 7th September 2023*)
[315] Rotheudt N, Fagnard J-F, Hlasek T, Plechacek J and Vanderbemden P 2025 *Supercond. Sci. Technol.* **38** 025012
[316] Ouellet J L *et al* 2019 *Phys. Rev. Lett.* **122** 121802
[317] Salemi C P *et al* 2021 *Phys. Rev. Lett.* **127** 081801
[318] Cabrera B and Van Kann F 1978 *Acta Astron.* **5** 125–30
[319] Iwashita Y, Kuriyama Y, Tongu H and Fuwa Y 2022 *IEEE Trans. Appl. Supercond.* **32** 3500404
[320] European Commission 2015 Delegated Directive (EU) 2015/863 of 31 March 2015 Restriction of Hazardous Substances in Electrical and Electronic Equipment (RoHS) (available at: https://eur-lex.europa.eu/legal-content/EN/TXT/?uri=CELEX:32015L0863)
[321] Ouellet J L *et al* 2019 *Phys. Rev.* D **99** 052012
[322] Hogan K, Vanderbemden P, Vanderheyden B, Radovinsky A and Minervini J V 2021 Design of a superconducting magnetic shield closed on both ends for a high-sensitivity particle detector *7th Int. Workshop on Numerical Modelling of High Temperature Superconductors* (*Virtual (Nancy, France*, *22nd–23rd June 2021*) (available at: https://hal.science/hal-03295730v1/file/Hogan_etal_HTS_mod_2020.pdf)
[323] Prozorov R, Zarea M and Sauls J A 2022 *Phys. Rev.* B **106** L180505
[324] Karasik V and Shebalin I Y 1970 *Sov. Phys. - JETP* **30** 1068–75
[325] Kamiya K, Warner B A and Numazawa T 2004 *IEEE Trans. Appl. Supercond.* **14** 1042–5
[326] Muething K, Edwards D, Feder J, Gully W and Scholz H 1982 *Rev. Sci. Instrum.* **53** 485–90
[327] Sinokita K, Toda R and Sasaki Y 2009 *J. Phys.: Conf. Ser.* **150** 012041
[328] Seo K, Nishijima S, Katagiri K and Okada T 1991 *IEEE Trans. Magn.* **27** 1877–80
[329] Okada T, Takahata K, Nishijima S, Nakagawa S and Yoshiwa M 1988 *IEEE Trans. Magn.* **24** 895–8
[330] Seo K, Nishijima S, Okada T and Katagiri K 1991 *Cryogenics* **31** 524–7
[331] Banno N 2023 *Superconductivity* **6** 100047
[332] Frankel D 1979 *IEEE Trans. Magn.* **15** 1349–53
[333] Zheng B, Xie W, Liu Y, Zhu X, Ming X, Zhang Y and Wen H H 2024 *IEEE Trans. Appl. Supercond.* **34** 8200910
[334] Benaroya R and Mogensen H 1966 *J. Appl. Phys.* **37** 2162–6

[335] Lorant S S 1972 Superconducting shields for magnetic flux exclusion and field shaping *4th International Conference on Magnet Technology (MT-4)* (*Upton, NY, USA, 19th–22nd September 1972*) vol eConf C720919 ed Y Winterbottom (Brookhaven National Laboratory) p 227 (available at: https://inspirehep.net/literature/73466)
[336] Novosel N *et al* 2012 *Supercond. Sci. Technol.* **25** 095018
[337] Huang J and Wang H 2017 *Supercond. Sci. Technol.* **30** 114004
[338] Eley S, Glatz A and Willa R 2021 *J. Appl. Phys.* **130** 050901
[339] Villegas J, Savel'ev S, Nori F, Gonzalez E, Anguita J, Garcia R and Vicent J 2003 *Science* **302** 1188–91
[340] Gozzelino L, Laviano F, Przyslupski P, Tsarou A, Wisniewski A, Botta D, Gerbaldo R and Ghigo G 2006 *Supercond. Sci. Technol.* **19** S50
[341] Vlasko-Vlasov V, Colauto F, Buzdin A I, Rosenmann D, Benseman T and Kwok W-K 2017 *Phys. Rev.* B **95** 144504
[342] Vojenčiak M, Šouc J and Gömöry F 2011 *Supercond. Sci. Technol.* **24** 075001
[343] Ainslie M D 2019 *Supercond. Sci. Technol.* **32** 030501
[344] Krüger P, Grilli F, Vojenčiak M, Zermeno V M, Demencik E and Farinon S 2013 *Appl. Phys. Lett.* **102** 202601
[345] Kapolka M and Ruiz H 2022 *Sci. Rep.* **12** 7030
[346] Philippe M *et al* 2015 *Supercond. Sci. Technol.* **28** 095008
[347] Li R, Fang J, Liao X, Wang Y, Wu Y, Wang Z, Zan Y and Wang X 2023 *IEEE Trans. Appl. Supercond.* **33** 6801206
[348] Fracasso M, Gerbaldo R, Ghigo G, Torsello D, Xing Y, Bernstein P, Noudem J and Gozzelino L 2024 *Materials* **17** 1201
[349] Philippe M P, Fagnard J F, Wéra L, Morita M, Nariki S, Teshima H, Caps H, Vanderheyden B and Vanderbemden P 2016 *J. Phys.: Conf. Ser.* **695** 012003
[350] Prat-Camps J, Navau C and Sanchez A 2014 *Appl. Phys. Lett.* **105** 234101
[351] Zhou P B, Ma G T, Yang C, Queval L, Mei G M, Liu K, Qian H Y and Liu K 2017 *IEEE Trans. Appl. Supercond.* **27** 0601105
[352] Navau C, Mach-Batlle R, Parra A, Prat-Camps J, Laut S, Del-Valle N and Sanchez A 2017 *Sci. Rep.* **7** 44762
[353] Lousberg G P, Fagnard J-F, Ausloos M, Vanderbemden P and Vanderheyden B 2010 *IEEE Trans. Appl. Supercond.* **20** 33–41
[354] Gozzelino L, Agostino A, Gerbaldo R, Ghigo G and Laviano F 2012 *Supercond. Sci. Technol.* **25** 115013
[355] Ohyama T, Minemoto T, Itoh M and Hoshino K 1993 *IEEE Trans. Magn.* **29** 3583–5
[356] Itoh M, Ohyama T, Hoshino K, Ishigaki H and Minemoto T 1993 *IEEE Trans. Appl. Supercond.* **3** 181–4
[357] Itoh M, Ohyama T, Mori K and Minemoto T 1995 *IEEE Trans. Electr. Inf. Syst.* **115** 696–701
[358] Mori K, Minemoto T and Itoh M 1997 *IEEE Trans. Appl. Supercond.* **7** 378–81
[359] Itoh M, Mori K and Minemoto T 1996 *IEEE Trans. Magn.* **32** 2605–8
[360] Omura A, Oka M, Mori K and Itoh M 2003 *Physica* C **386** 506–11
[361] Itoh M, Ohyama T, Mori K and Minemoto T 1994 *Cryogenics* **34** 817–20
[362] Gozzelino L, Gerbaldo R, Ghigo G, Laviano F and Truccato M 2017 *J. Supercond. Novel Magn.* **30** 749–56
[363] Xue C, Cao K W, He T, Wei C, Liu W and Ge J Y 2024 arXiv:2403.06389
[364] Miniussi A R *et al* 2019 *J. Low Temp. Phys.* **194** 433–42
[365] Wood B and Pendry J 2007 *J. Phys.: Condens. Matter* **19** 076208
[366] Magnus F *et al* 2008 *Nat. Mater.* **7** 295–7
[367] Navau C, Chen D-X, Sanchez A and Del-Valle N 2009 *Appl. Phys. Lett.* **94** 242501
[368] Mawatari Y 2013 *Supercond. Sci. Technol.* **26** 074005
[369] Sanchez A, Navau C, Prat-Camps J and Chen D-X 2011 *New J. Phys.* **13** 093034
[370] Navau C, Prat-Camps J and Sanchez A 2011 arXiv:1112.2847
[371] Yampolskii S and Genenko Y 2014 *Appl. Phys. Lett.* **104** 033501
[372] Yampolskii S and Genenko Y 2014 *Appl. Phys. Lett.* **104** 143504
[373] Solovyov M, Šouc J and Gömöry F 2015 *IEEE Trans. Appl. Supercond.* **25** 8800705
[374] Šouc J, Solovyov M and Gömöry F 2016 *Appl. Phys. Lett.* **109** 033507
[375] Kucharovič M, Gömöry F and Solovyov M 2024 *IEEE Trans. Appl. Supercond.* **34** 8200404
[376] Müller R, Fuchs G, Grahl A and Köhler A 1993 *Supercond. Sci. Technol.* **6** 225–32
[377] Chandra R *et al* 1991 *IEEE Trans. Magn.* **27** 2210–3
[378] Symko O G, Yeh W J, Zheng D J and Kulkarni S 1989 *J. Appl. Phys.* **65** 2142–4
[379] Wang J, Li J, Yang W and Zhou L 1991 *IEEE Trans. Magn.* **27** 1029–32
[380] Purpura J and Clem T 1989 *IEEE Trans. Magn.* **25** 2506–10
[381] Tjukanov E *et al* 1987 *Phys. Rev.* B **36** 7244–7
[382] Willis J, McHenry M, Maley M and Sheinberg H 1989 *IEEE Trans. Magn.* **25** 2502–5
[383] Hurben M, Symko O, Yeh W, Kulkarni S and Novak M 1991 *IEEE Trans. Magn.* **27** 1874–6
[384] Grenci G, Denis S, Dusoulier L, Pavese F and Penazzi N 2006 *Supercond. Sci. Technol.* **19** 249
[385] Denis S *et al* 2006 *J. Phys.: Conf. Ser.* **43** 509–12
[386] Closset R *et al* 2014 *Mater. Lett.* **119** 154–6
[387] Pavese F, Bianco M, Andreone D, Cresta R and Rellecati P 1992 *Physica* C **204** 1–7
[388] Kumar N D, Closset R, Wera L, Cloots R, Vanderbemden P and Vertruyen B 2015 *Supercond. Sci. Technol.* **28** 015007
[389] Sasaki T, Tanaka M, Morita M, Miyamoto K M K and Hashimoto M H M 1992 *Jpn. J. Appl. Phys.* **31** 1026
[390] Yang P T, Yang W M and Chen J L 2017 *Supercond. Sci. Technol.* **30** 085003
[391] Itoh M, Pavese F, Mori K, Vanolo M and Minemoto T 1996 *J. Magn. Soc. Japan* **20** 289–92
[392] Çelebi S, Gencer A and Öztürk A 1997 *J. Alloys Compd.* **257** 14–18
[393] He A, Hua P, Zhang J, Fu X and Zhou Y 1997 *Physica* C **282-287** 2635–6
[394] Horikawa Y, Omura A, Mori K and Itoh M 2001 *IEEE Trans. Appl. Supercond.* **11** 2387–90